Study on Solution-Processable Polypyrrole-Based Conducting Polymers

by

Haoyu Fu

A thesis
presented to the University of Waterloo
in fulfilment of the
thesis requirement for the degree of
Master of Applied Science
in
Chemical Engineering

Waterloo, Ontario, Canada, 2022

Author's Declaration

I hereby declare that I am the sole author of this thesis. This is a true copy of the thesis, including any required final revisions, as accepted by my examiners. I understand that my thesis may be made electronically available to the public.

Abstract

Due to the adjustable conductivity, cost-effective synthesis, and easy device fabrication, conducting polymers have wide-ranging applications in numerous areas, including sensors, solar cells, supercapacitors, and electrodes. Among conducting polymers, polypyrrole (PPy) has attracted lots of attention because of its high conductivity, biocompatibility, and mass producibility. However, PPy is insoluble in most solvents, which lowers its processability and limits its application. In the past few decades, many works by researchers around the world have been done to improve the solubility of PPy. Unfortunately, the two major strategies, including doping with large contour ions and introducing an alkyl sidechain to the PPy backbone, were found to significantly decrease the conductivity of PPy by several orders of magnitude. For the doping method, the restricted dopant options limit the conductivity of PPy, whereas the alkyl sidechains twist the polymer structure thus influencing the conductivity. As a result, new methods need to be explored to improve the solubility of PPy without sacrificing its electrical properties.

In this work, two strategies were applied to address this problem. The first is to introduce an alkyl carbamate sidechain to the PPy backbone; the carbamate sidechain can solubilize the polymer, while allowing thermal removal at mild temperatures. Thus, after solution processing, the obtained polymer film can be thermally annealed to remove the sidechain, thereby recovering the PPy structure and conductivity. The second one is to introduce an alkoxy sidechain at the N position of the PPy backbone. This sidechain has less steric hindrance than the alkyl sidechain. Therefore, the PPy with the alkoxy sidechain was expected to have a more planar backbone compared to the alkyl chain-substituted counterpart and as such was expected to have higher conductivity.

We first designed, synthesized, and characterized poly(2-ethylhexyl 1H-pyrrole-1-carboxylate) (PEPC), with a 2-ethylhexyl carbamate chain substituted at the N position of PPy. Different synthetic routes were explored and optimized, including organometallic polymerization and oxidative polymerization. The desired polymer was successfully

synthesized and was soluble in various organic solvents, including acetone, dichloromethane, and chloroform. Polymer films in a thickness of 50-60 nm could be deposited from the PEPC chloroform solution on a SiO_2/Si substrate, which satisfies requirements for sensor applications. [1] However, the 2-ethylhexyl carbamate sidechain could not be completely removed by thermal annealing and acid cleavage due to the primary structure of ethylhexyl aliphatic chain of the carbamate being reluctant to undergo decomposition. This led to a low conductivity of the PEPC thin films. In the future, a carbamate sidechain with a different secondary or tertiary structure may be applied, allowing easy removal of the sidechain and restoration of the PPy structure.

Poly[1-((2-ethylhexyl)oxy)-1H-pyrrole] (PEOP) with a 2-(ethylhexyl)oxy sidechain at the N position of PPy was designed, and its synthesis was explored. Due to the difficulties in the synthesizing and purifying the monomer, 1-((2-ethylhexyl)oxy)-1H-pyrrole, the desired PEOP was not obtained. However, it was found that the 2-(ethylhexyl)oxy sidechain can undergo a thermolysis process under milder temperatures than the alkyl carbamate sidechain, as evidenced by FTIR and TGA results. Therefore, the thermal instability of 2-(ethylhexyl)oxy and other alkoxy sidechains on nitrogen may allow the development of other polymers that require the sidechains to be thermally removable at mild temperatures. In addition, new synthetic approaches can be explored in the future to obtain a more structurally defined PEOP.

Acknowledgements

I want to thank my supervisor, Prof. Yuning Li, for welcoming me to his lab and allowing me to complete this project. Besides the immeasurable help he gave me in research, he also taught me to plan thoroughly, observe carefully, record vividly, and work wisely which are helpful not only for my experiments, but also for my future career and daily life. What I learned from him are not only skills in the laboratory, but also critical and independent thinking and, most importantly, the principle of never making an easy conclusion before enough evidence is obtained. He treats scientific research with a strict attitude, which also influenced me about how to become a real researcher. I was a beginner in research when I just came to this lab, and I may still be now, but what I learned here will undoubtedly benefit my future life.

I would like to thank my committee members, Prof. Michael Tam and Prof. Xianshe Feng, for their valuable time in reviewing this work and participating in my oral examination.

I would like to especially thank my lab members, Dr. Jenner Ngai and Yi Yuan, for all their guidance and help throughout the whole research process. They were not only my lab mates but also my mentors, patiently teaching me invaluable experimental skills and techniques including synthesis, characterization, and device fabrication. I could not have finished this work without their guidance and helps.

I am very thankful to my lab member and reliable partner, Scott Flynn, for all his help in my research, coursework, and lab duties. He is so enthusiastic and kind, helping me solve many of the problems that I had met in my research. We discussed, studied, and worked together so much, and his support was always there to encourage me no matter the obstacle I faced.

I would like to thank my lab members, Dr. Sungjae Jeon, Dr. Xiguang Gao, Daniel Afzal, John Polena, Zhe Huang, Yonglin Wang, and Andrew Stella, for all their valuable help in different aspects of my experiments.

I would also like to especially thank Dr. Jiaxin Xu for helping me with material characterization and for all the encouragement she gave me for my research and day-to-day life. She always gave me a hand when I needed help and provided me with numerous useful suggestions when I had difficulties. I was incredibly fortunate that I could be guided and helped by her, and for that I am incredibly grateful.

I would like to thank Gaili Cao and Zhuizhui Fan for their help in FTIR spectroscopy.

I would like to thank Dr. Fangyan Sun and Jun Wang for their many assists in my experiments.

Also, I would like to recognize all my other lab members in the PEML group, including Prof. Ali Reza, Dr. Zhong Ma, Dr. Samala Venkateswarlu, Dr. Ravinder Singh, Naixin Zhao, Yaoyao Li, Fangqing Ge, Guoliang Zhang, Merlan Nurzhanov, Yunsheng Jiang, Zhaoyi Yin, and Yvonne Zhong, for helping me with experiments and analysis. I would like to acknowledge them as well as other group members during my time in graduate school, for their support and friendship over these last two years.

In addition, I would like to especially thank my friend Julia Solonenka for all her support in my research and day-to-day life.

Lastly, I would like to extend a thank you to my parents and my friend Mengting Wang for their support, concern, understanding, encouragement, acceptance, and company to me. Without them, I would not have been able to complete this work.

Table of Contents

List of Figures

List of Tables

List of Abbreviations and Symbols

APS: Ammonium persulfate

BPY: 2-2'Bipyridine

COD: 1,5-Cyclooctadiene

CV: Cyclic voltammetry

DBSA：4-Dodecylbenzenesulfonic

DFT: Density-functional theory

DMAP: 4-Dimethylaminopyridine

DMSO: Dimethyl sulfoxide

E_g: Band gap

E_{HOMO}: HOMO energy level

E_{LUMO}: LUMO energy level

F4TCNQ: 2,3,5,6-Tetrafluoro-7,7,8,8-tetracyanoquinodimethane

FTIR: Fourier-transform infrared spectroscopy

HOMO: Highest occupied molecular orbital

IP: In-plane

ITO: Indium tin oxide

LUMO: Lowest unoccupied molecular orbital

M_n: Number-average molecular weight

M_w: Weight-average molecular weight

NaDBSA: Dodecylbenzene sulfonic acid sodium salt

NaDEHS: Di(2-ethylhexyl) sulfosuccinic acid sodium salt

NMP: N-Methyl-2-pyrrolidone

NMR: Nuclear magnetic resonance

NBS: N-Bromosuccinimide

OOP: Out-of-plane

OTFT: Organic thin film transistor

PEG: Polyethylene glycol

PEOP: Poly[1-((2-ethylhexyl)oxy)-1H-pyrrole]

PEPC: Poly(2-ethylhexyl 1H-pyrrole-1-carboxylate)

PPP: Poly(p-phenylene)

PPy: Polypyrrole

PPh_3: Triphenylphosphine

t-BOC: tert-Butyloxycarbonyl

TEA: Triethylamine

$TEABF_4$: Tetraethylammonium tetrafluoroborate

TGA: Thermogravimetric analysis

TLC: Thin layer chromatography

UV-Vis-NIR: Ultraviolet-visible-near infrared

XRD: X-ray diffraction

λ_{max}: Wavelength of incident light with maximum absorption

λ_{onset}: Onset wavelength of incident light

Other abbreviations and symbols are defined in the text.

Chapter 1. Introduction

1.1. Overview of Conducting Polymers

1.1.1. Structures of Conducting Polymers

The concept of conducting polymers (CP) originated in the mid-1970s when polyacetylene, the first polymer with the property of high electrical conductivity, was synthesized by Shirakawa [2]. Conducting polymers are polymers that can generate and propagate charge carriers along their backbone [3]. CP have attracted much interest in the past few decades due to their advantageous nature: adjustable conductivity via oxidation and/or reduction, clearly defined majority carrier types, easy cycling between conductive and insulating states, cost-effective synthesis, and good production scalability.

Conducting polymers are insulators in the pure state, and they become conductive when treated with an oxidizing or reducing agent [3]. They usually have polyconjugated structures, repeatedly alternating single and multiple bonds. Several examples of conducting polymer structures are shown in **Figure 1.1.**

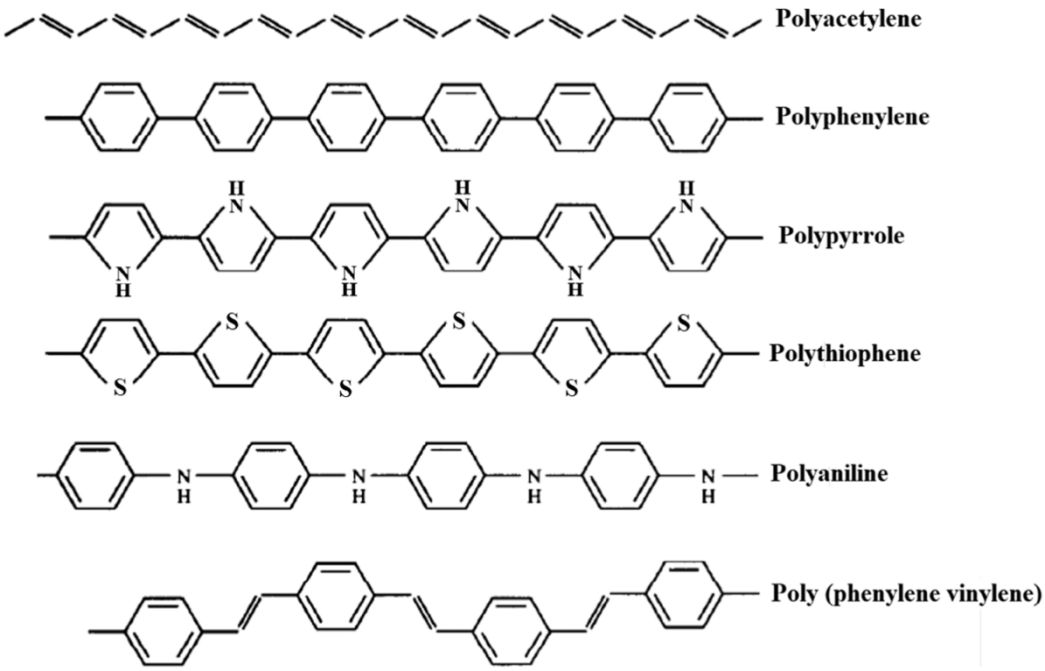

Figure 1.1. Examples of Conducting Polymers [3].

The quasi-infinite π system that extends through a significant number of repeating monomer units is the fundamental structure characteristic of all conjugated conducting polymers

(**Figure 1.1**) [4]. This structure provides directional conductivity to the material. In addition, the extended π system allows the conjugated polymer to be easily oxidized or reduced, making it possible to achieve adjustable electrical properties with high precision.

1.1.2. Conducting Mechanism

The electronic structure of a material determines its electrical conductivity [5]. Based on the energy band theory, the valence electrons are contained within the valence band of a material, defining their lowest energy states [4]. A valance band electron must obtain enough energy to be excited to the conduction band to achieve conductivity. The energy difference between the valance band and the conduction band is the band gap of a material. For an intrinsic conductor, the valence band and the conduction band are overlapped; thus, the electrons can move and travel freely within the conduction band. In contrast, semiconductors and insulators have an energy gap between the valence and conduction bands. A semiconductor has a small band gap, thus, the electrons can be excited to the conduction band by gaining energy to achieve conductivity, whereas the energy gap for an insulator is too large for an electron to cross- therefore, it is non-conductive.

From a chemistry perspective, molecular orbital theory is used to explain the conductivity of conducting polymer. It is necessary for a polymer to have a set of overlapped molecular orbitals to provide carrier mobility along the polymer chain [4]. Conjugated polymers have an extended p-orbital system along the polymer backbone, formed from the overlapping p-orbitals of each repeating unit, allowing electrons to cross the whole backbone. Each carbon atom in the conjugated bond of the conducting polymer has one unpaired electron from the π bond. π Electrons can delocalize along the continuously overlapped p_z-orbitals of the polymer backbone. This electron delocalization paves the way for the intramolecular charge transport.

Polyacetylene is used as an example to demonstrate the concepts of delocalization and the resulting conductivity [5]. As shown in **Figure 1.2**, conjugated single and double bonds exist along the polymer backbone. Both single and double bond contain localized σ-bonds, whereas localized π-bond only exists in the double bond. Due to overlapping p_z orbitals in the π-bonds, the π-bond between the first and second carbon atoms can transfer to the position between the

second and third carbon atoms. Similarly, the next π-bond can transfer to the carbon atom next to it, and so on. This process is called delocalization, and it can occur through the whole polymer backbone due to the repeating conjugated bonding along the backbone.

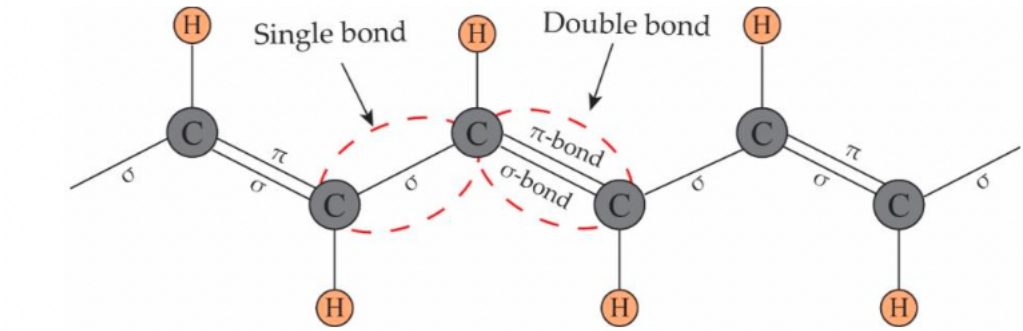

Figure 1.2 Illustration of Conjugated Structure of Polyacetylene [5].

However, conjugated bonds and delocalization cannot provide high conductivity (metallic conductivity) [5]. Doping is a commonly used method to improve the conductivity of a conjugated polymer. By oxidation or reduction of the polymer by a dopant, a charge carrier (e.g., polaron, bipolaron, soliton) will be created, allowing the charge to flow through the polymer chain. This will be discussed in the next section.

1.1.3. Doping

Doping is the oxidation or reduction process of a polymer to create positive or negative charge carriers respectively, which can raise the polymer's conductivity [6]. Different doping methods have been applied to CPs to improve their conductivity [5]. By taking advantage of doping, the semiconductor or insulator CP can change its conductivity to a metallic conducting regime (10^0 to 10^4 S/cm). A small amount of doping agent (typically less than 10 percent by mass) can usually lead to a dramatic change in the electrical properties of a conjugated polymer, and through the de-doping process, the original polymer can be recovered without degradation. Though doping is also a common technique used in inorganic semiconductor materials such as silicon, the doping mechanism for organic polymers is different from that for inorganic semiconductors. From a chemistry perspective, the doping process is a redox reaction between the polymer and the dopant, which involves charge transfer and formation of charge carriers [5,7]. Unlike doping in inorganic semiconductors where

dopants simply add electrons to the semiconductor or create holes in the semiconductor, the dopants for polymers add and withdraw electrons to the polymer backbone at the same time in the form of the oxidation-reduction reaction [5]. This can be explained using molecular orbital theory- the electrons from the highest occupied molecular orbital (HOMO) of the valence band are extracted by oxidation or transferred to the lower unoccupied molecular orbital (LUMO) of the conduction band by reduction. During the oxidation/ reduction process, charge carriers in the form of polarons, bipolarons, or solitons are formed in the polymer. Based on the bond structure of the polymer ground state, CPs can be classified into two types: degenerate and non-degenerate CPs. Degenerate CPs have two identical ground state geometry structures, whereas non-degenerate CPs have two different ground state structures with different ground state energy. In degenerate CPs, solitons are the charge carriers, while polarons and bipolarons are known to be the charge carriers in non-degenerate CPs. The flow of these charge carriers creates the current and conductivity. The terminology for the oxidative doping process is p-type doping, in which the electron from the HOMO of the polymer moves to the dopant by oxidation, leaving a hole in the polymer backbone. In contrast, the terminology for reductive doping is n-type doping, in which the electron from dopant is transferred to the LUMO of the polymer, making the polymer backbone more electron-rich. Therefore, the charge carrier density of CPs can be adjusted by doping, and thus the conductivity is tunable.

Figure 1.3 illustrates n-type and p-type doping using polythiophene as an example. Positive polarons/bipolarons are formed through p-type doping, whereas negative polarons/bipolarons are formed through n-type doping. These charge carriers can delocalize over polymer chains, enhancing the polymer's electrical conductivity.

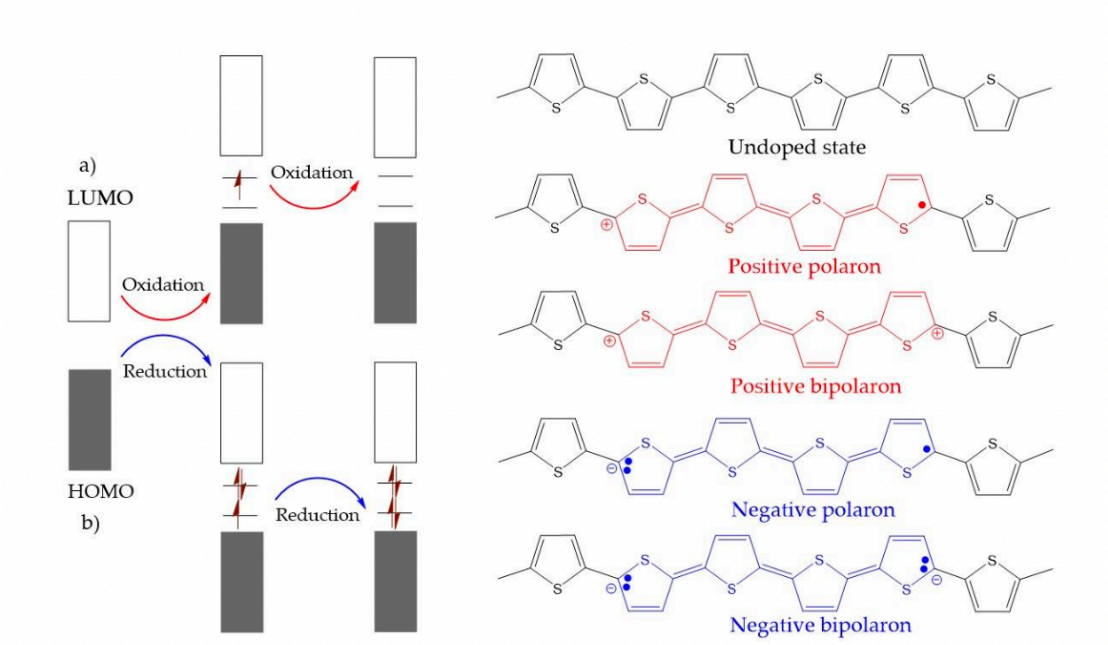

Figure 1.3. (a) Positive doping (p-type) and **(b)** negative doping (n-type) of conjugate polymers [5].

Trans-polyacetylene is a representative conjugated polymer with degenerate ground states or more than one ground states [5]. The doping mechanism of degenerate conjugated polymers is slightly different from that of non-degenerated ones **(Figure 1.4.)**. In the doping process in a degenerate conjugated polymer, oxidation of the polymer will first generate polarons and bipolarons. However, due to the two identical energy ground states, the charged carriers are not bonded to each other by a higher energy bonding configuration. Instead, they can freely separate along the polymer chain. These charged defects can form domain walls and separate the polymer into two geometric structures (A and B phases) with identical energy. These defects are called solitons, and they can be neutral. Positive and negative solitons can form through oxidation or reduction by a dopant, and they have no unpaired spin (S). The regions of single-charged solitons can overlap in the polymer backbone. Therefore, a soliton band is formed by the interaction of the solitons. The soliton band is between the HOMO and the LUMO of the polymer, and the band is more expansive as the doping level is higher. Polarons and solitons are both charge carriers and enhance the conductivity of a conjugated polymer.

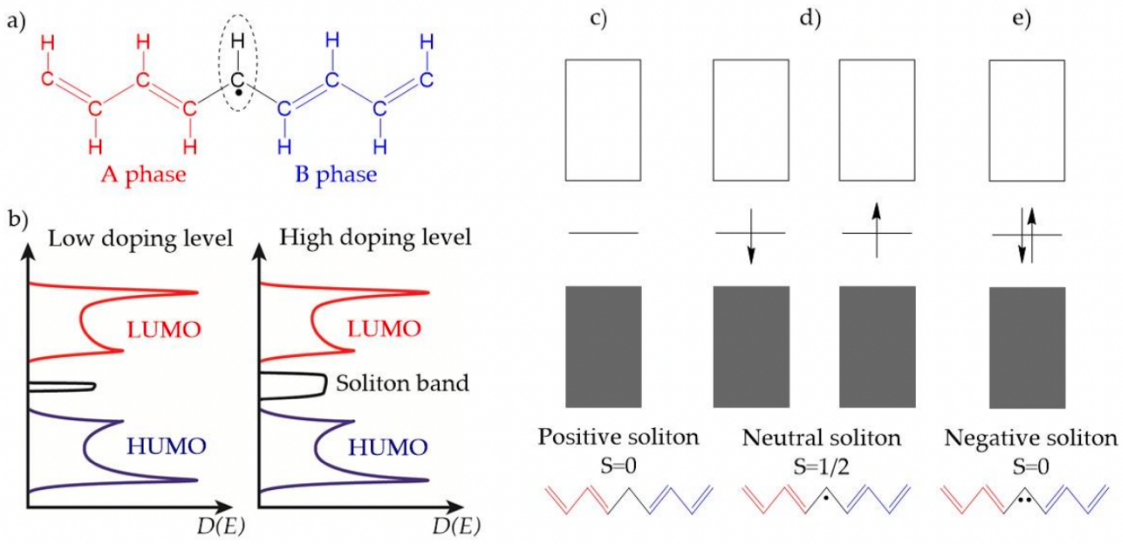

Figure 1.4. **(a)** Graph depicting the geometric structure of a neutral soliton **(b)** Energy level of a soliton band in a low (left) and high (right) doping level; trans-polyacetylene band structure with **(c)** a positive soliton; **(d)** a neutral soliton; and **(e)** a negative soliton [5].

1.2. Polypyrrole

Polypyrrole (PPy) is one of the earliest developed CPs, which was first obtained by chemical oxidation of pyrrole in 1916 [8]. It was in the form of black powder and was called pyrrole black. It was not characterized due to its insolubility until 1979, when an improved electrochemical technique was used to prepare free-standing PPy films. The structure of PPy is illustrated in **Figure 1.5**.

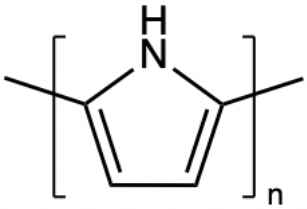

Figure 1.5. Structure of Polypyrrole.

In the past few decades, polypyrrole has attracted particular interest due to its unique properties, including high conductivity, ease of mass preparation, good mechanical properties, and electroactivity in organic electrolyte and aqueous solutions [3,4]. Besides, in recent years, conducting polymers have played an increasingly important role in biomedical engineering.

For example, CPs have been used to achieve communication between artificial devices and neuronal networks, organs, and tissues (**Figure 1.6**) [9]**.** PPy is especially well known for its non-toxicity and good biocompatibility, which makes it an excellent candidate for biomedical applications (**Figure 1.7**) [10].

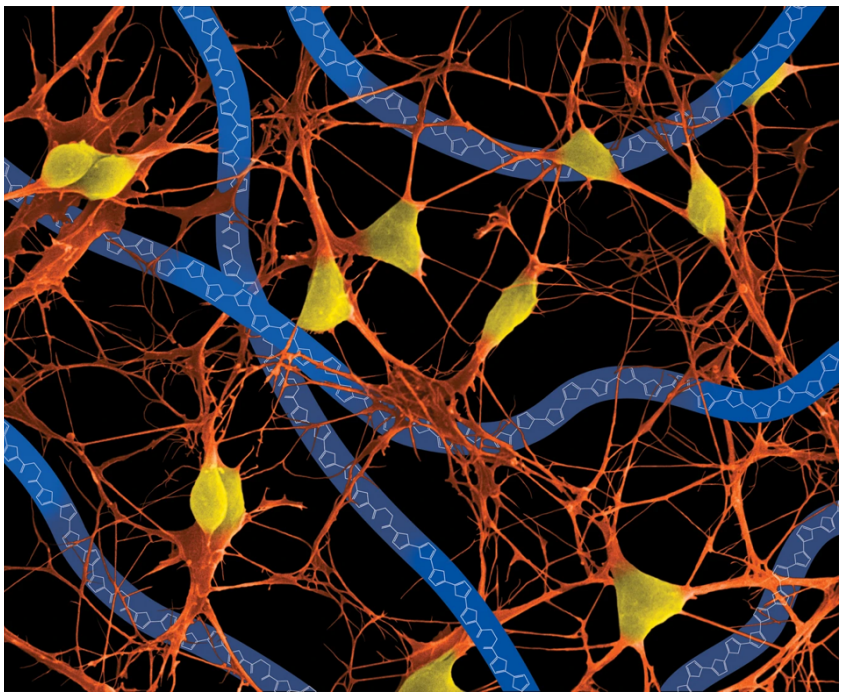

Figure 1.6. Conjugated polymer chains interpenetrating a neuronal network, establishing a functional connection [9].

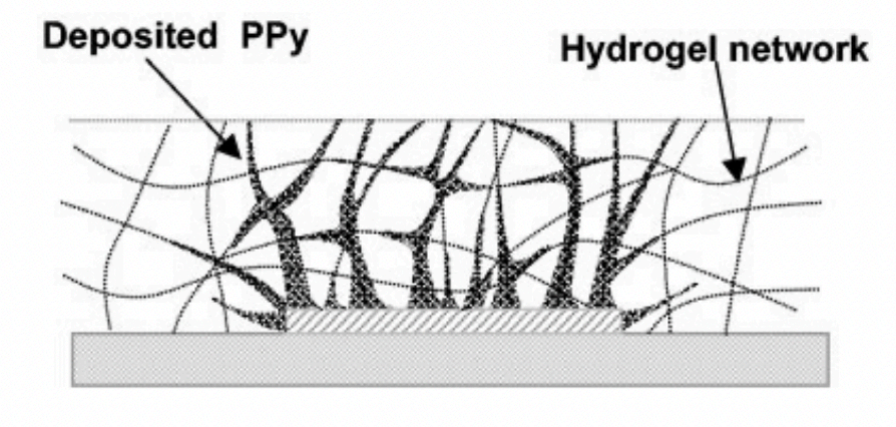

Figure 1.7. An application of PPy in tissue engineering, which polypyrrole grown in hydrogel scaffolds coated on neural prosthetic devices [10].

In addition, PPy has one of the highest conductivities of all the CPs- up to 380 S/cm [3]. With these excellent properties, PPy has a wide range of applications, including supercapacitors, electrodes, gas sensors, biosensors, drug delivery, tissue engineering, anticorrosion coatings, actuators, protective clothing, adsorbents for removal of heavy metals, dyes, chromatographic stationary phases, lightweight batteries, and membrane separation [3,4]. Some applications of different forms of PPy are illustrated in **Figure 1.8**.

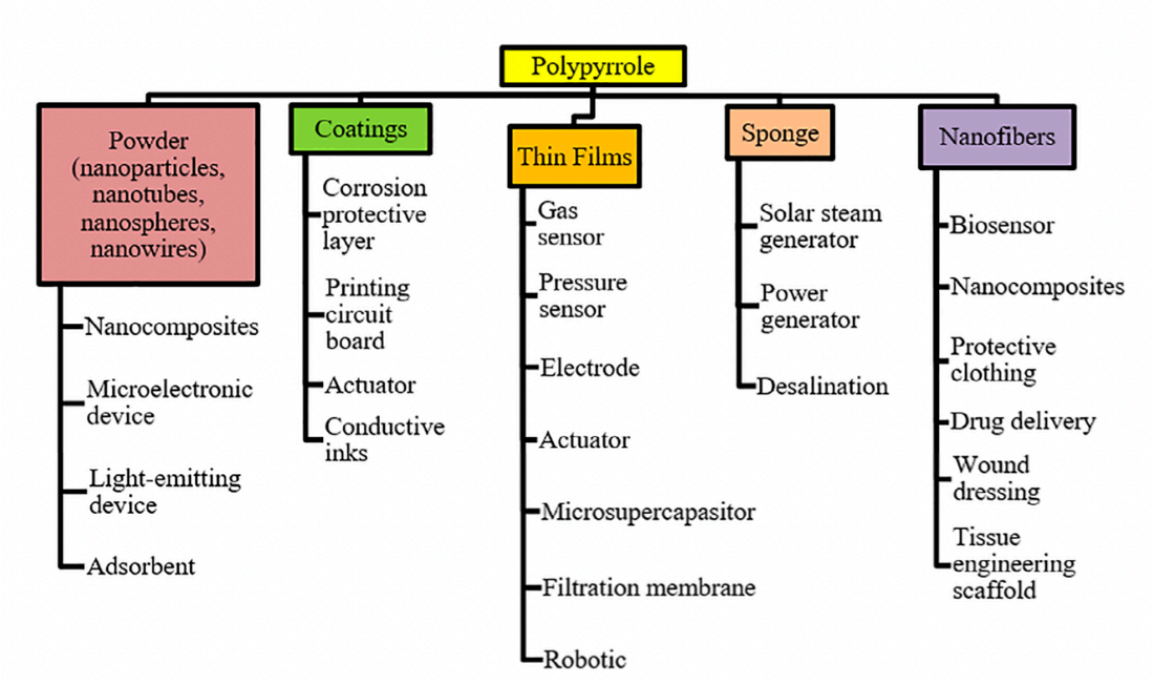

Figure 1.8. Summary of PPy applications [3].

Polypyrrole (PPy) is a representative polymer that undergoes p-type doping [5]. **Figure 1.9 (a) –(d)** illustrates the band structure of polypyrrole in different doping levels. In the undoped state, the band gap of PPy is approximately 3.16 eV. The large bandgap of undoped polypyrrole makes it an insulator. In the lightly doped PPy represented as a hexamer in **Figure 1.9 (b)**, a π-electron is removed from the neutral PPy chain by oxidation by the dopant. In addition, the structure of PPy also changes from benzenoid to quinoid to generate a polaron. A higher doping level leads to further oxidation of PPy (**Figure 1.9 (c)**), resulting in a second electron removal from the PPy chain and generation of a doubly charged bipolaron. In this process, the structure deformation from benzenoid to quinoid is enhanced. Further increases in doping level will continue to oxidize the PPy chain and finally lead to overlap

between bipolarons, resulting in the formation of two narrow bipolaronic bands. The energy gap between the two bipolaronic bands will define the new band gap of PPy, which is decreased to 1.46 eV from 3.16 eV of the undoped state. HCl, p-TSA, and $FeCl_3$ are common ionic dopants for PPy [3]. Furthermore, molecular dopants such as 2,3,5,6-tetrafluoro-7,7,8,8-tetracyanoquinodimethane (F4TCNQ) are also good candidates for p-type doping [11].

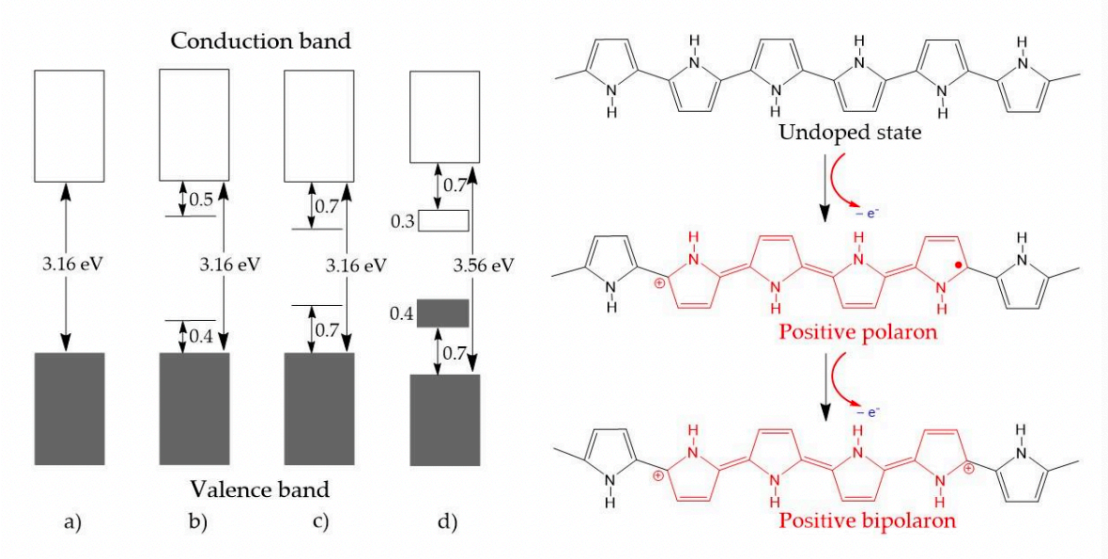

Figure 1.9. band structure of polypyrrole in **(a)** undoped state, **(b)** lightly doped state, **(c)** medium doped state and **(d)** high doped state. **(e)** Polypyrrole structure change after doping and the formation of polaron and bipolaron [5].

1.3. Problem Statement and Objectives

1.3.1. Solubility and Conductivity of Polypyrrole

Although polypyrrole has the advantages mentioned above, its poor solution processability is a drawback in some applications. Whether synthesized by chemical or electrochemical means, polypyrrole is insoluble in most solvents [12] .However, many applications of conducting polymers such as biosensors require high solution processability. PPy is a good candidate for an organic thin film transistor (OTFT)-type biosensor due to its good biocompatibility. Printing technology is one of the most favored methods to fabricate OTFT-based biosensors due to its simple fabrication process, low cost, capability to integrate with rigid and flexible substrates, and capability of mass production [13]. Printing technology for OTFT device

fabrication, as represented by inkjet printing and screen printing, requires the material to be soluble in a particular solvent. Thus, the poor solubility or processability of PPy and the poor has, in fact, become the most critical factor that limit its large-scale application [12].

The strong interchain interaction, long chain conjugation structure, and the cross-linking of polypyrrole chains lead to the insolubility of PPy [14]. Many studies have attempted to address this issue in the past few decades. Up to now, the most common strategies aimed at increasing the solubility of PPy can be classified into two types: (1) doping with large molecular size counter ions and (2) introducing sidechains to the nitrogen or β positions of the pyrrole ring [14]. However, both strategies lead to a dramatic decrease in the electrical conductivity of doped polypyrrole.

Many studies have been conducted to increase the solubility of PPy by doping. Lee et al. studied the synthesis of a soluble PPy using ammonium persulfate (APS) as an oxidant and dodecylbenzene sulfonic acid (DBSA) as a dopant. The conductivity of the resulting PPy ranged from 10^{-5} to 10^{0} S/cm [15]. Later, Song et al. studied the doping of PPy with DBSA to make it soluble in organic polar solvents, including m-cresol, DMSO, NMP, chloroform, chlorobenzene, and tetrachloromethane [16]. The conductivity of the doped PPy they obtained was between 10^{-2} and 10^{0} S/cm. Oh et al. studied doping PPy with di(2-ethylhexyl) sulfosuccinate dopant anions to make the doped PPy soluble in DMSO, DMF, and m-cresol, with conductivities ranging from ~10^{-3} to 3 S/cm [17]. Lim et al. reported that PPy doped with dodecylbenzenesulfonate (DBS) sodium salt (NaDBSA), synthesized with APS as oxidant and poly(ethylene glycol) (PEG) as an additive, was soluble in some organic solvents (N-NMP and m-cresol), with the highest conductivity of 1.02 S/cm [18]. Lee et al. reported that PPy doped with DBSA and co-doped with tetraethylammonium tetrafluoroborate (TEABF4) was soluble in m-cresol, NMP, and solublein chloroform [19]. The highest conductivity they obtained was 1.18 S/cm. Most recently in 2018, John et al. reported polypyrrole doped with di(2-ethylhexyl) sulfosuccinic acid sodium salt (NaDEHS) and dodecylbenzene sulfonic acid sodium salt (NaDBSA) that is soluble in NMP m-cresol 1,2-dichloromethane and chloroform, with the highest conductivity of the order of 10^{-1} S/cm [20].

On the other hand, many researchers also studied the introduction of the alkyl sidechain to the polypyrrole backbone to make it soluble. Some soluble polypyrroles with alkyl sidechain substitution on the nitrogen have been developed (**Figure 1.10 left**). Kou et al. reported poly(N-methylpyrrole) and poly(N-Ethyl pyrrole) with conductivities in the 10^{-2} and 10^{-3} S/cm orders, respectively [21]. Aradilla et al. reported poly[N-(2-cyanoethyl)pyrrole] with a conductivity of 10^{-3} S/cm [22]. Massoumi et al. reported poly(N-ethyl pyrrole), poly(N-butyl pyrrole), poly(N-octyl pyrrole), and copolymers (poly(N-alkylpyrrole-co-pyrrole) using pyrrole and N-ethyl pyrrole, N-butyl pyrrole or N-octyl pyrrole [23]. They only reported conductivity of one homopolymer, poly(N-ethyl pyrrole), with a value in the 10^{-5} order of S/cm. The copolymers had a conductivity ranging in orders from 10^{-5} to 10^{-1} S/cm. Other pyrrole substituents, such as N-phenyl-substituted pyrrole and its derivatives, were used as co-monomers with pyrrole to synthesize some poly(N-substituted pyrrole-co-pyrrole) [24]. It was found that even in the presence of 10% of the substituted pyrrole in the copolymer resulted in a dramatic drop in the conductivity by six orders of magnitude [25].

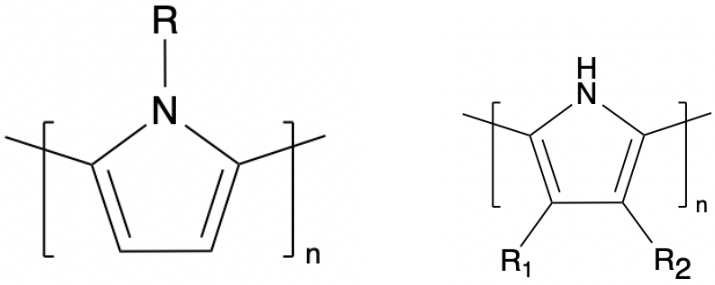

Figure 1.10. Structure of N-substituted PPy (**left**) and β-substituted PPy (**right**).

Substitution on the β-position of the pyrrole ring (**Figure 1.10. right**) has also been extensively studied to increase the solubility of PPy. A series of poly(3-alkylpyrrole) with an alkyl chain length from 4 to 12 carbon atoms were synthesized by Fotizik et al., which were soluble in chloroform [26]. They obtained conductivity of the polypyrrole derivatives ranging from 10^{-1} to 10^{0} S/cm. Zotti et al. reported a series 3,4-disubstituted polypyrrole, with the conductivities in order of 10^{-4} to 10^{-3} S/cm [27]. The methods to make soluble PPy and the corresponding conductivities were summarized in **Table 1.1**.

Table 1.1. Summary of the Methods Making Soluble PPy and the Corresponding Conductivity

Method to Increase Solubility	Conductivity(S/cm)	References
Dopes with DBSA	10^{-5} - 10^{0}	15
Doped with di(2-ethylhexyl) sulfosuccinate	10^{-3} - 3	17
Doped with NaDBSA with PEG as additive	1.02	18
Doped with DBSA and TEABF4	1.18	19
Doped with NaDMEHS and NaDBSA	10^{-1}	20
Introducing N-alkyl Chain	10^{-5} -10^{-1}	21, 23
Introducing beta-alkyl Chain	10^{-4} to 10^{0}	26,27
Note: PPy can achieve a conductivity up to 380 S/cm [3].		

The low conductivity of soluble PPy can be attributed to the following reasons. The conductivity of polypyrrole is highly dependent on the dopant type [3]. To make the PPy soluble, only limited dopants can be chosen, which limits the conductivity of polypyrrole. On the other hand, the sidechain of conjugated polymer can influence the doping mechanism and efficiency, long-range order, polymer packing, and morphology of polymer [28]. The relative fraction of active material on the conjugated polymer film will be reduced by the alkyl sidechain. Sidechains are also detrimental to π-π intermolecular interactions, thus affecting the electrical conductivity of the polymer. In substituted polypyrrole specifically, the bulky size of the alkyl sidechain can lead to a lack of planarity, increasing chain separation of the polymer and resulting in a lower conductivity than the non-substituted polypyrrole [29]. The twisted structure of substituted polypyrrole was also confirmed by Massoumi et al., who stated that the lower conductivity of N-alkyl substituted polypyrroles may result from stereochemistry, since the N-alkyl substituted polypyrrole lacked planar structure due to the

steric van der Waals repulsion interactions from alkyl groups [23]. In addition, the long alkyl chain also reduced the conjugation length of the polymer backbone, which led to a decrease in the concentration of charge carriers. These factors explain the lower conductivity of the longer alkyl chain-substituted polypyrrole.

From the previous results discussed above, it is clear that either doping with a large counter ion or introducing a sidechain to the pyrrole backbone will inevitably result in a dramatic drop in the electrical conductivity of polypyrrole. To the best of our knowledge, no soluble polypyrrole has been synthesized without compromising the electrical conductivity. Thus, to address this problem, a novel soluble polypyrrole needs to be designed to achieve both good solubility and electrical performance.

1.3.2. Approaches and Methodology

1.3.2.1 Carbamate Sidechain

Carbamate is one of the essential amine protecting groups, which can be easily introduced through reactions between an amino group with chloroformates or different derivatives of carbonic acid (**Figure 1.11 a**) [30]. Different methods can be applied to remove the carbamate-protecting group, including β-elimination, metal-assisted nucleophilic capture, hydrogenolysis, and protonolysis. Removal of alkyl carbamate chains by thermal decomposition under mild temperatures (100-250 ℃) is a well-known method, with the removal of *tert*-butyloxycarbonyl (t-BOC) group (**Figure 1.11 b**) as the best example [1,31,32]. Alkyl carbamate sidechains have been applied as thermally removable sidechains for some π-conjugated polymers (**Figure 1.12**) [1,32,33].

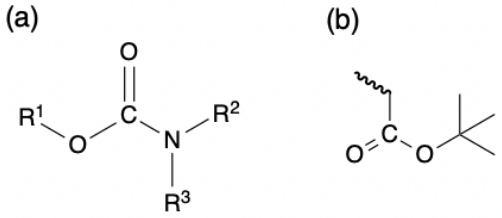

Figure 1.11. (a) Chemical Structure of Carbamate groups and **(b)** *tert*-butyloxycarbonyl (t-BOC) groups.

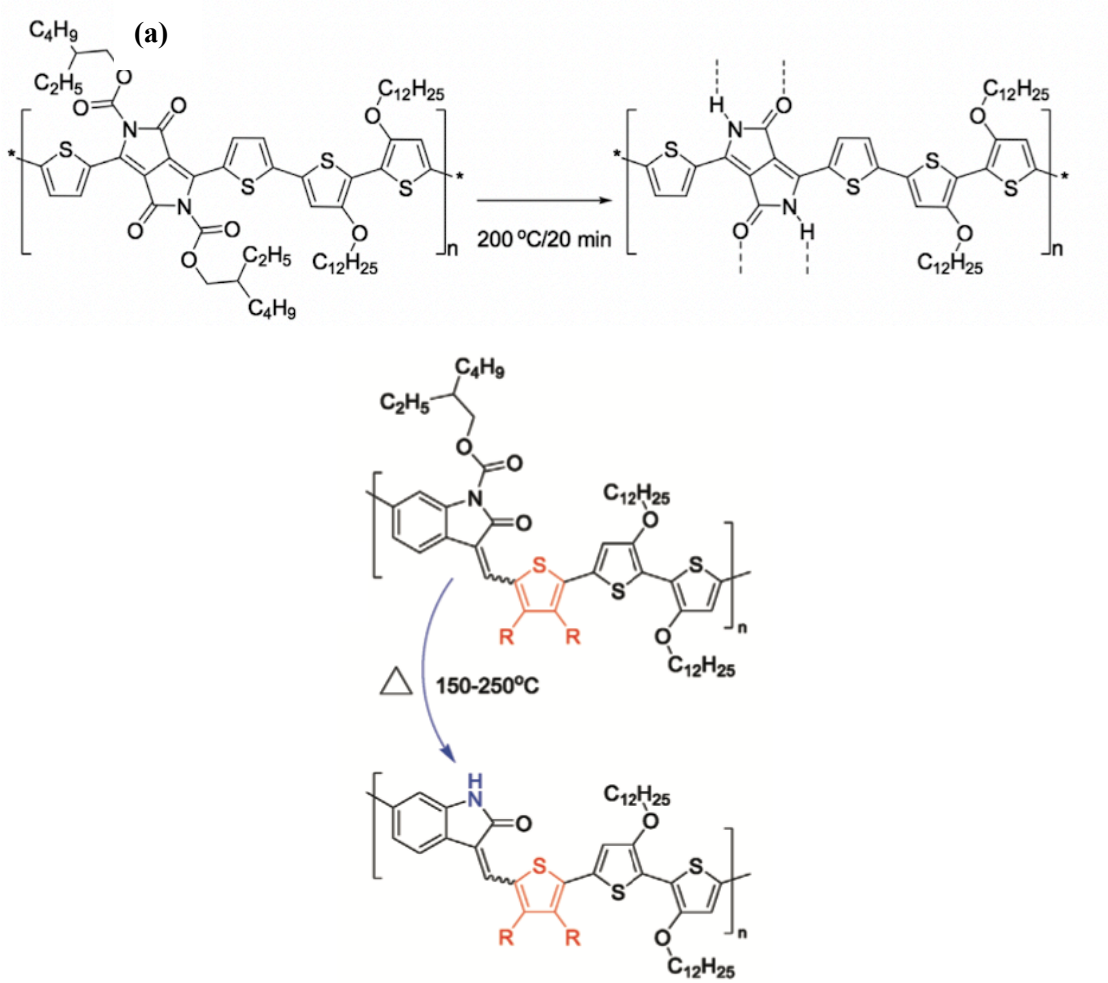

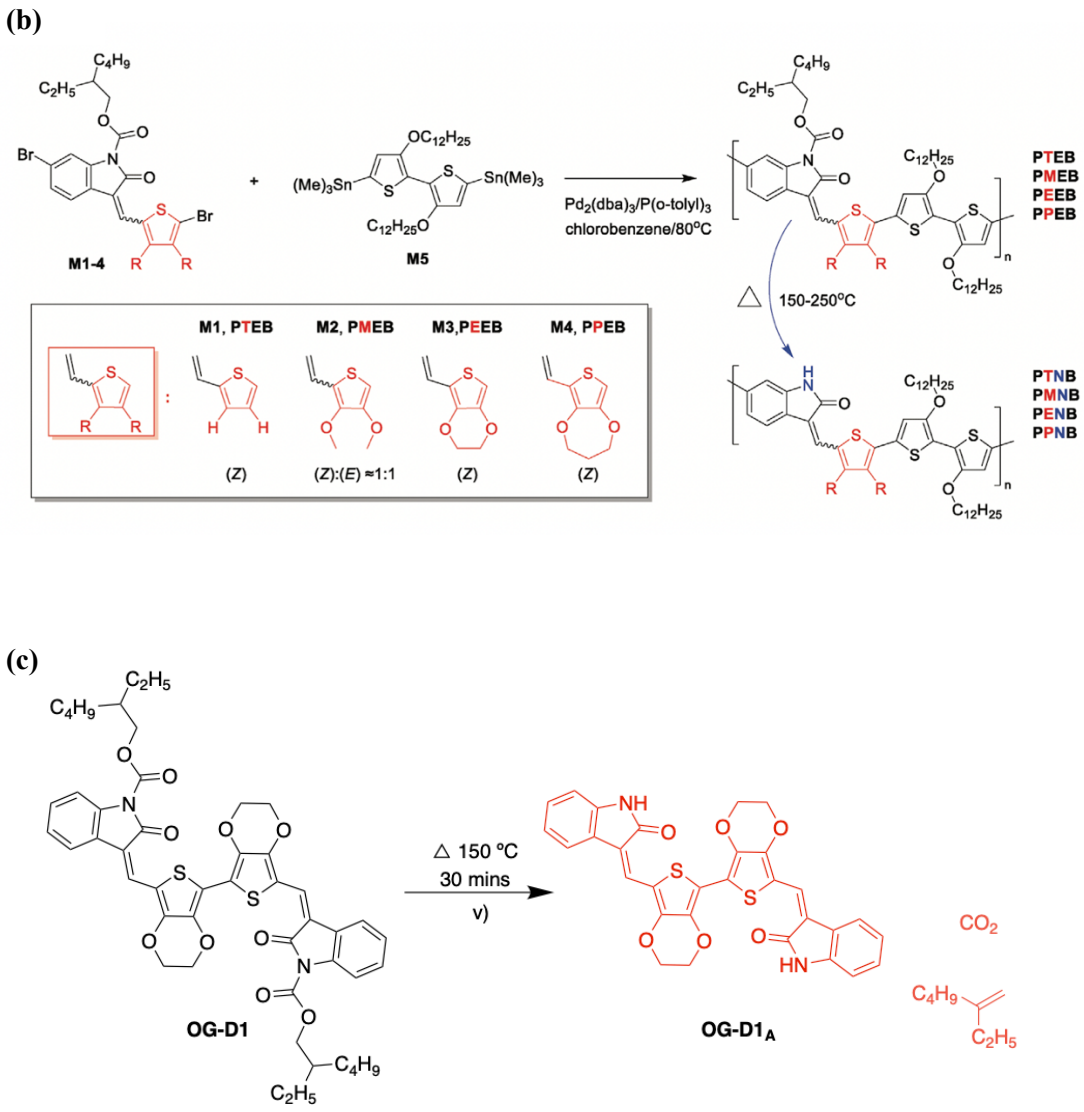

Figure 1.12. Examples of using alkyl carbamate sidechains on polymers and thermal removal of the carbamate sidechain [1,32,33].

Alkyl carbamate sidechain thermal decomposition may involve McLafferty-like rearrangement and hydrolysis [1]. During the thermal decomposition process, carbon dioxide, alkene, and alcohol may form. The thermolysis mechanism is shown in **Scheme 1.1** using t-BOC-pyrrole as an example [31].

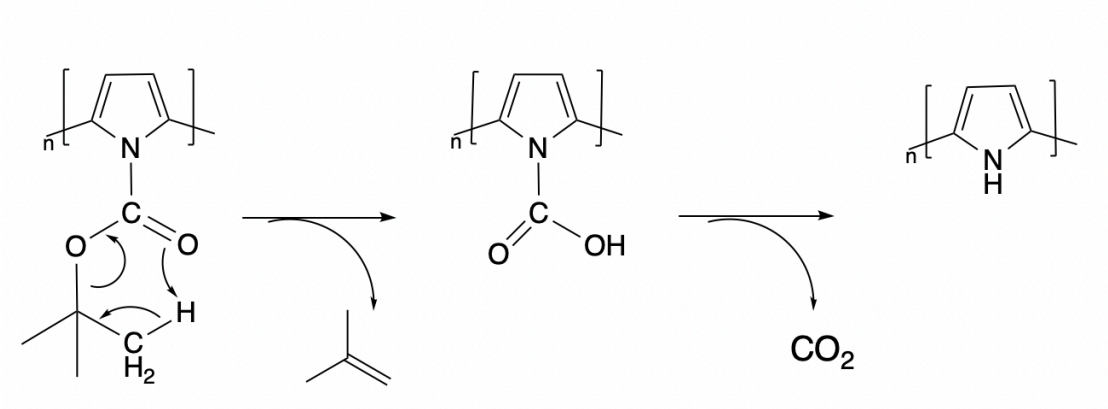

Scheme 1.1. Mechanism of t-BOC group thermal decomposition [31].

In addition, the alkyl carbamate sidechain can also be removed through protonation [30]. The sensitivity of alkyl carbamate to acidic condition may provide another way to remove it. However, it is also a concern for the polymer synthesis because any acidic conditions would need to be avoided to prevent cleavage of the carbamate groups during polymerization.

1.3.2.2 Alkoxy Sidechain

Compared to the alkyl chain, the alkoxy chain starts with an oxygen atom, which is smaller than the corresponding methylene (CH_2) moiety of the alkyl chain (**Figure 1.13**). Thus, the steric hindrance from the alkoxy chain is lower than that of the alkyl chain. As a result, compared to the polymer with an alkyl sidechain, the polymer with an alkoxy chain can have a more planar structure, leading to higher electrical conductivity. Alkoxy sidechains have been used for some other conjugated polymers by our research group [34–37].This will be discussed in more detail in Chapter 3.

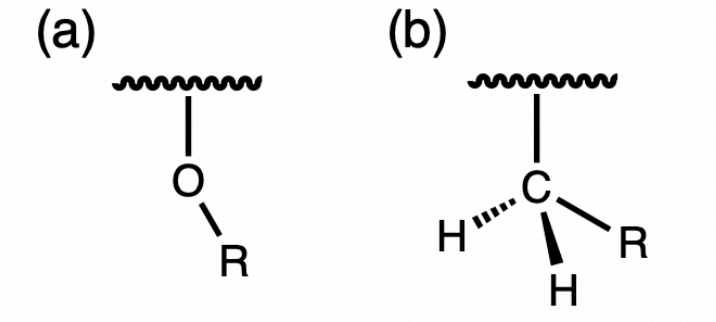

Figure 1.13 (a) Structure of alkoxy chain and **(b)** Structure of alkyl chain, which has a larger steric hindrance than the alkoxy chain.

1.3.2.3 Methodologies

We proposed two strategies to address the problem stated in section 1.3.1 that the polypyrrole cannot achieve high conductivity and goo dsolubility at the sae time. The first strategy is introducing a carbamate sidechain to the polypyrrole to form an N-alkyl carbamate substituted polypyrrole. The long alkyl part of the alkyl carbamate chain can increase polypyrrole's solubility, making it more processable for many applications. In addition, this sidechain can be thermally removed after the device fabrication to recover the original polypyrrole. The negative influence of the sidechain on the polymer's electrical performance can be eliminated by removing sidechains, which has been used as a strategy to optimize the conductivity of conjugated polymer [28].

A polymer, poly(2-ethylhexyl 1H-pyrrole-1-carboxylate) (PEPC), was designed to demonstrate this strategy. The structure of PEPC before and after the removal of the carbamate sidechain is shown in **Figure 1.14.**

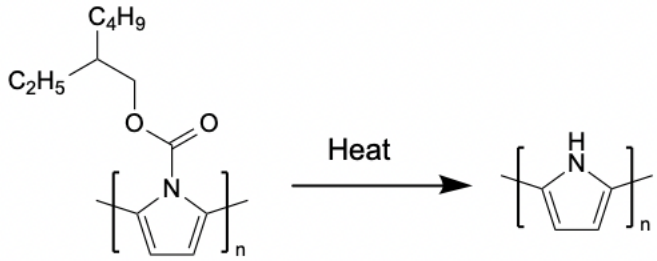

Figure 1.14 Structure of PEPC before and after thermally removal of the carbamate sidechain.

The second strategy is to use a less sterically hindered alkoxy chain instead of an alkyl chain on the nitrogen atom of pyrrole to make a more planar polymer backbone to increase the electrical conductivity (See Chapter 3). At the same time, the long alkyl part of the alkoxy chain can increase the solubility of PPy.

A polymer, poly[1-((2-ethylhexyl)oxy)-1H-pyrrole] (PEOP), was designed to demonstrate this strategy (**Figure 1.15**).

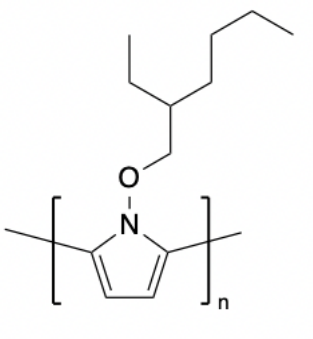

Figure 1.15. Structure of PEOP.

1.4. Thesis Summary

In this work, two novel polypyrrole-based polymers were designed and studied, aiming to address the previously stated issues: increasing the solubility of polypyrrole without sacrificing its conductivity.

In chapter 1, problem statements and the methodology to address the problem is proposed.

In chapter 2, experiment methods, including synthesis methods and characterization methods are introduced and discussed.

In chapter 3, the synthesis of PEPC by different synthetic routes is discussed. Characterization results of the PEPC by TGA, FTIR, CV, UV-Vis-NIR spectroscopy, and XRD are reported. The conductivity values of PEPC thin film, doped with different dopants, are measured and summarized.

In chapter 4, the synthesis of PEOP is explored. The product obtained is characterized by TGA, FTIR, and XRD. The conductivity values of the obtained product thin films are measured.

In chapter 5, the thesis findings are summarized to make conclusions. Future work based on the results of this thesis is proposed.

Chapter 2. Experimental Methods

2.1.Polymer Synthesis Through Organometallic Polycondensation

2.1.1. Introduction

Since the first π-conjugated conductive polymer, polyacetylene, was developed by Heeger, MacDiarmid, and Shirakawa in 1977, developing new synthetic methods for π-conjugated polymers has received lots of attention [38]. Polyacetylene is usually synthesized via the addition polymerization of acetylene. However, many other synthetic approaches to π-conjugated polymers have been developed and optimized since. Among them, organometallic polycondensation between organohalides (Ar_1–X) and organometallic compounds (Ar_2–M) is considered to be one of the most effective methods to form the π-conjugated polymer because they are usually composed of electron-withdrawing olefin and aromatic monomeric units, and a polymer constituted of electron-accepting monomeric units and with well-defined bonds between the monomeric units can be formed via the Csp^2- Csp^2 bond formation during organometallic polycondensation [38,39,40].

Polypyrrole, as a well-known π-conjugated conducting polymer, is mainly synthesized via chemical or electrochemical oxidative polymerization [3]. The first polypyrrole powder was made in 1916 by pyrrole monomer chemical oxidation, and in 1968, the first polypyrrole film was synthesized via electrochemical oxidation of pyrrole monomer [41]. However, the polypyrrole synthesized via chemical or electrochemical oxidative polymerization has a backbone that is not only constituted by α-α bonded pyrrole monomers, but also some α-β coupling and β-β coupling (**Figure 2.1**) [3]. These “mislinkages” in the polypyrrole backbone are detrimental to the electrical conductivity of polypyrrole, because α-β coupling and β-β coupling limit the effective conjugation length of polypyrrole [31].

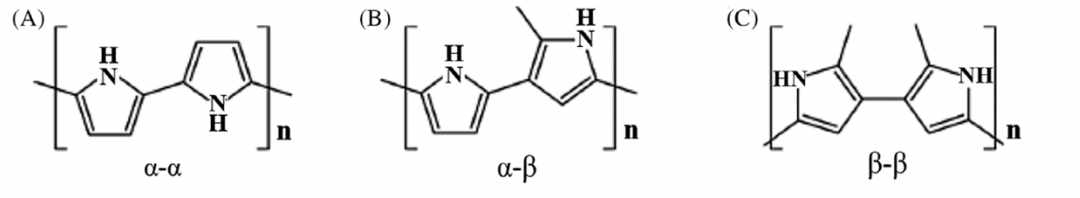

Figure 2.1. Possible Monomer Coupling Structures in Polypyrrole Backbone. (A) $\alpha - \alpha$ coupling. (B) $\alpha - \beta$ coupling and (C) $\beta - \beta$ coupling [3].

To eliminate these structural defects, organometallic polymerization can be applied to the synthesis of polypyrrole and its derivatives, because it allows precise growth of the polymer to form a well-defined α-α coupled polypyrrole backbone. The five most commonly used organometallic aryl-aryl coupling methods in the synthesis of conjugated polymers involving pyrrole are Kumada, Suzuki, Negishi, Stille, and Yamamoto couplings. In the following sections, these five organometallic coupling methods will be discussed.

2.1.2. Synthetic Methods Analysis and Choice

2.1.2.1. Kumada Coupling

The Kumada coupling is a cross-coupling reaction between Grignard reagents (organomagnesium compounds) and aryl halides catalyzed by a nickel or palladium complex, which was first reported independently by Corriu et al. and Kumada et al. in 1972 (Scheme 2.1) [39]. Nickel catalysts are less expensive than palladium catalysts and therefore more widely used in Kumada coupling reactions. Among all the nickel complex catalysts, [1,3-Bis(diphenylphosphino)propane]dichloronickel(II) ($NiCl_2$(dppb) is the most efficient for Kumada coupling [42,43].

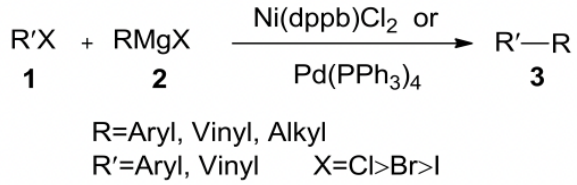

Scheme 2.1. Kumada Coupling [44].

The proposed mechanism of the Kumada coupling reaction cycle consists of four steps, as shown in **Figure 2.2**. In the first step, the dihalodiphosphinenickel (II) complex **1** reacts with two equivalents of the Grignard reagent, and the nickel(0) complex (**2**) is formed [45]. The nickel (0) complex works as the active catalyst for the following steps in the reaction cycle. In the second step, oxidative addition occurs between **2** and the organohalide compound to form the halo(organo)nickel (II) complex **3** [39]. In the third step, a new nickel (II) complex **4** formed through the transmetalation reaction between **3** and the Grignard reagent, with MgX_2 as a by-product. The fourth step is a reductive elimination reaction of complex **4** to give Ar^1–Ar^2 as the coupled product. Simultaneously, the $L_2Ni(0)$ complex is regenerated as the catalyst to complete the catalytic cycle [46].

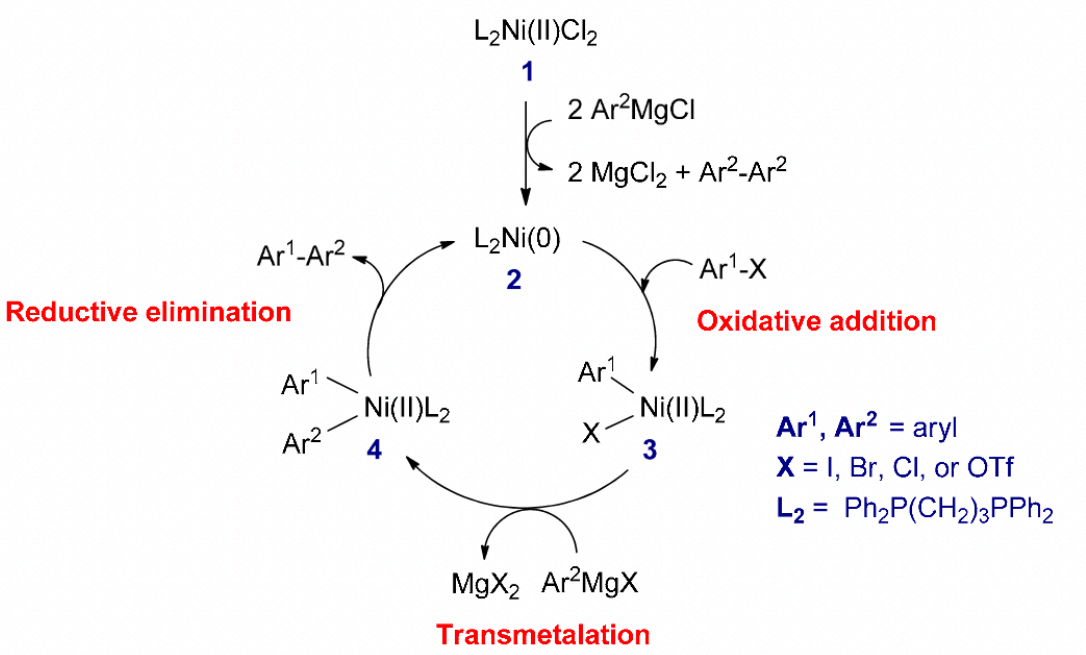

Figure 2.2. Catalytic cycle of Kumada Coupling [39].

There are several examples of the application of the Kumada coupling to polymerization involving pyrrole derivatives. In 2008, Yokozawa's group synthesized poly(N-hexylpyrrole) through Kumada coupling (**Scheme 2.2 upper**) [47]. By applying 1 mol% of $Ni(dppe)Cl_2$ with an additional 1 mol% dppe, a polymer with a Mn of 1.43×10^4 and a polydispersity (PDI = M_w/M_n) of 1.11 was obtained [47]. A year later, poly(N-dodecylpyrrole) was synthesized by Stefan et al. through Kumada coupling in a similar way. By using a Li salt (LiCl) and a Ni

complex catalyst, a polymer with M_n =11900 and PDI = 1.4 could be obtained (**Scheme 2.2 lower**) [48].

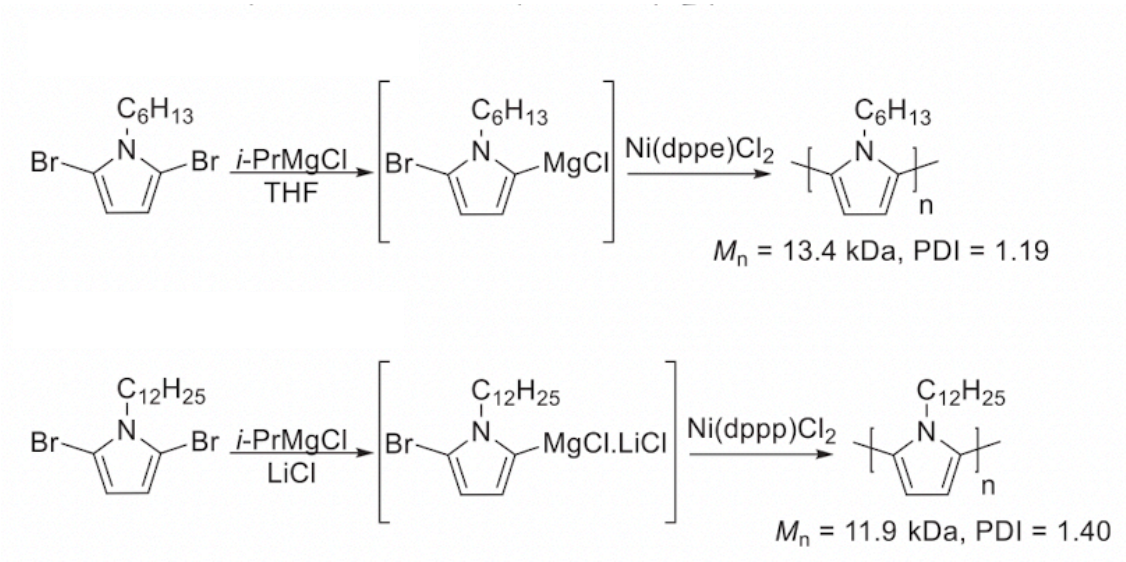

Scheme 2.2. Examples of Kumada coupling in synthesis of polypyrrole derivatives [49].

Although Kumada coupling has been successful in the synthesis of numerous conjugated polymers including polypyrrole derivative, it is not a suitable method to synthesize our PEPC. In monomeric 2-ethylhexyl 2,5-dibromo-1H-pyrrole-1-carboxylate **(a)**, due to the more electron-withdrawing property of the carbamate sidechain than the bromine atom, the most electron deficient part in the monomer is not the α-carbon of the pyrrole ring but the carbon that is double bonded with oxygen in the sidechain. Thus, when the Grignard reagent reacts with the monomer molecule, the formation of the Ar-Mg-X intermediate, which will involve the first and the third step in the catalytic cycle through the Br-Mg exchange reaction, will be severely affected by the competitive nucleophilic addition side reaction occurring at the carbonyl group [50]. **Scheme 2.3** illustrates the mechanism of the nucleophilic addition of Grignard reagent to the carbonyl group. Without the Ar-Mg-X intermediate, the Kumada coupling cannot occur.

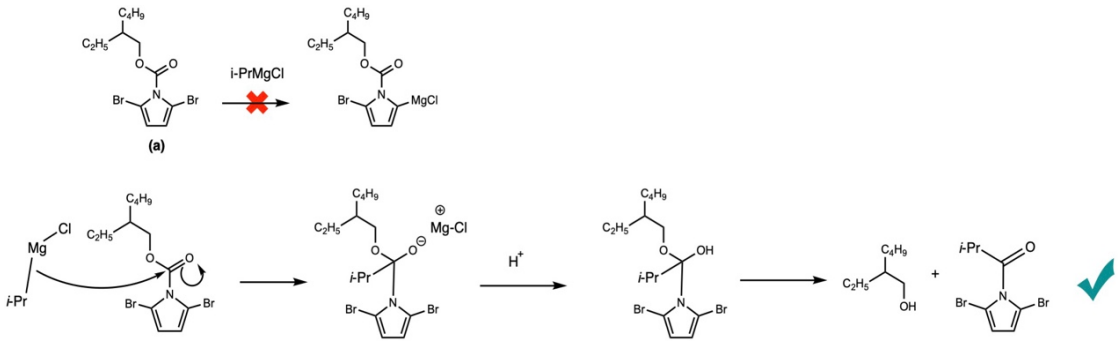

Scheme 2.3. Magnesium Halogen Exchange (upper part) is hard to occur due to the nucleophilic addition of the Grignard reagent to the carbonyl group (lower part).

2.1.2.2. Negishi Coupling

In 1982, cross-coupling reactions between organozinc derivatives and organohalides catalyzed by Ni or Pd were first discovered by Negishi and his colleagues [51]. **Scheme 2.4** represent a generalized Negishi coupling reaction.

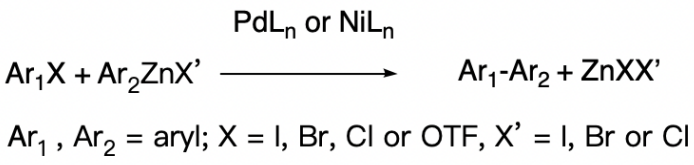

Scheme 2.4. Negishi Cross Coupling Reactions [39].

While there are many examples of Negishi coupling being used in the synthesis of small molecules, Negishi coupling is not very commonly used in the synthesis of polymers [52]. One example of the application of Negishi coupling to the synthesis of pyrrole compounds is the arylation of N-methyl-2-(chlorozincio)pyrrole with some aryl iodides catalyzed by a Pd complex (**Scheme 2.5**) [31,53]. Moreover, Negishi coupling has the same issue as Kumada coupling in that the halogen-metal exchange reaction has a possibility of not occurring due to competitive side reactions between the carbonyl group and organozinc compound, which would effectively destroy the carbamate sidechain. Thus, Negishi Coupling is also not suitable for the synthesis of our target PEPC.

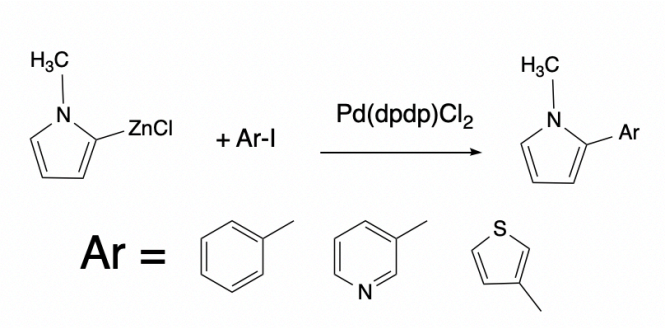

Scheme 2.5. Examples of synthesis of pyrrole derivatives through Negishi coupling [53].

2.1.2.3. Stille Coupling

Stille coupling is a reaction between organic electrophiles and organostannanes in the presence of a palladium catalyst, which results in the formation of a carbon-carbon single bond (**Scheme 2.6**) [54]. It is one of the most widely used and effective synthetic methods to generate Sp^2-Sp^2 carbon-carbon bonds because Stille coupling occurs under neutral conditions [39,52]. Furthermore, the organotin reagents can be simply prepared and are also stable to moisture and air, making Stille coupling a useful generic coupling reaction for synthesizing conjugated conducting polymers [39]. In 1976, Eaborn discovered that the preparation of aryltin compounds could be achieved using bis(tributyltin) catalyzed via palladium complexes [55]. A year later, Kosugi reported the first C-C bond formation between acyl chlorides and organostannanes through Pd-catalyzed cross-coupling [56]. In the mid-1980s, Stille and his colleagues described a standard method of Pd-catalyzed cross-coupling reactions with organostannanes involved, and thus the reaction was named after him [57,58,59].

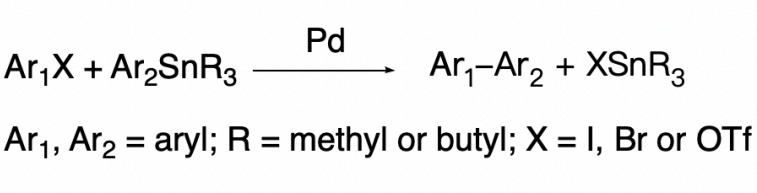

Scheme 2.6. Stille Coupling Reaction [39].

With an electron-rich ditin compound and an electron-deficient difunctional electrophile involved, Stille coupling has been applied to synthesizing numerous conjugated polymers with high molecular weights since the 1980s. The general form of a Stille polycondensation is shown in **Scheme 2.7**.

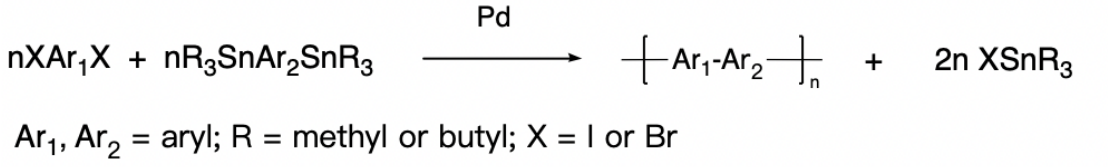

Scheme 2.7. Stille Polycondensation [39].

The mechanism of Stille coupling is complex, and may vary depending on the reaction conditions such as ligands, catalysts, additives, and solvents [54]. The generally accepted catalytic cycle involves four major steps, which are oxidative addition, transmetalation, trans to cis isomerization, and reductive elimination. The catalyst for a Stille reaction is a Pd(0) complex. It can come either from a Pd(0) compound such as $Pd(PPh_3)_4$, which enters the catalytic cycle directly, or from a Pd(II) precursor such as $Pd(OAc)_2$, which is reduced by the organostannane compound before entering the catalytic cycle. The first step of the cycle is the oxidative addition between the organic electrophile Ar^1-X and the Pd(0) catalyst. For sp^2 carbon-X, it is believed that the electrophile Ar-X and the active $Pd(0)L_2$ will form a three-center transition state of *cis*-[Pd(II)ArXL_2] as a kinetic product, followed by isomerization to form *trans*-[Pd(II)ArXL_2] as a thermodynamically stable product [54,60]. This process is illustrated in **Scheme 2.8**.

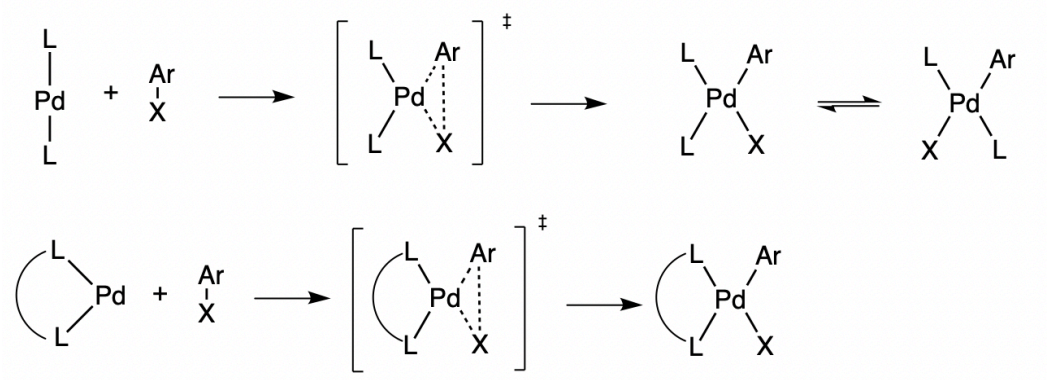

Scheme 2.8. Isomerization of the transmetalation step [54].

The transmetalation step of the Stille reaction is different from other Pd-catalyzed cross-coupling reactions. Through the interaction between the organostannane and the Pd center, the Sn-C bond is broken to form a Pd-C bond. Espinet and Echavarren pointed out that the transmetalation step can undergo two possible pathways, the cyclic pathway and the open pathway [60]. The cyclic pathway is associative, in which a trigonal bipyramidal trans-

$Ar^1Pd(II)L_2X$ intermediate undergoes a substitution of L for Ar^2 via transition state (TS1), where X and Ar^2 are bonded to Pd and Sn, respectively. After $XSnR_3$ is eliminated, a T-shaped cis-$Ar^1Ar^2Pd(II)L$ complex is formed. Reductive elimination occurs at this complex resulting in the formation of the final product Ar^1-Ar^2 and the active $Pd(0)L_2$ complex that reenters the catalytic cycle [61]. The open pathway is favoured in highly polar solvents because a dissociative substitution of ligand or solvent at the T-shaped intermediate, trans-$Ar^1Pd(II)L_2X$, occurs rapidly due to unavailability of bridging ligands [62]. Through the transition state TS2, solvent (S) or ligand (L) substitutes X in the intermediate to form a cis- and trans-$Pd(II)Ar^1Ar^2$ complex competitively [63]. The final product, Ar^1-Ar^2, forms after reductive elimination. The cyclic and open transition states are illustrated in **Scheme 2.9**. The catalytic cycle is shown in **Figure 2.3**.

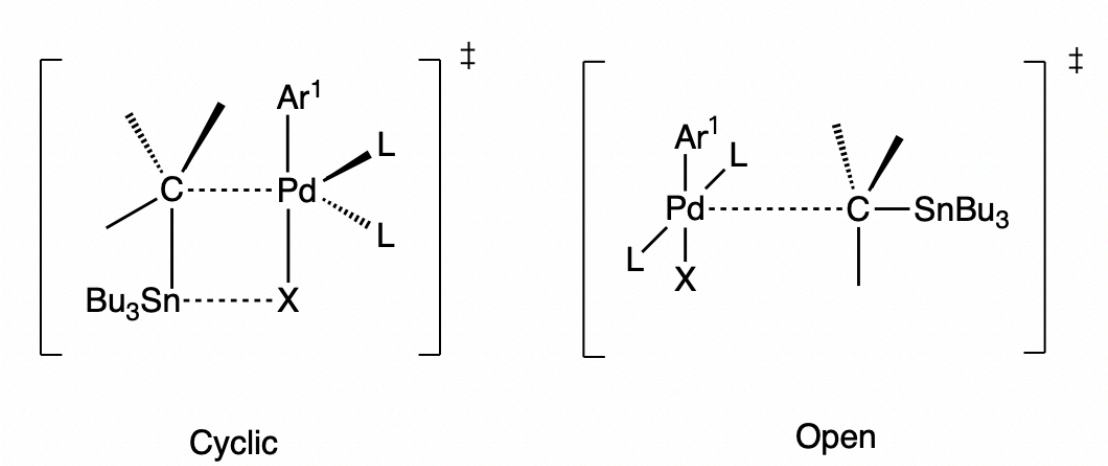

Scheme 2.9 Cyclic and Open structure of the transition state [60].

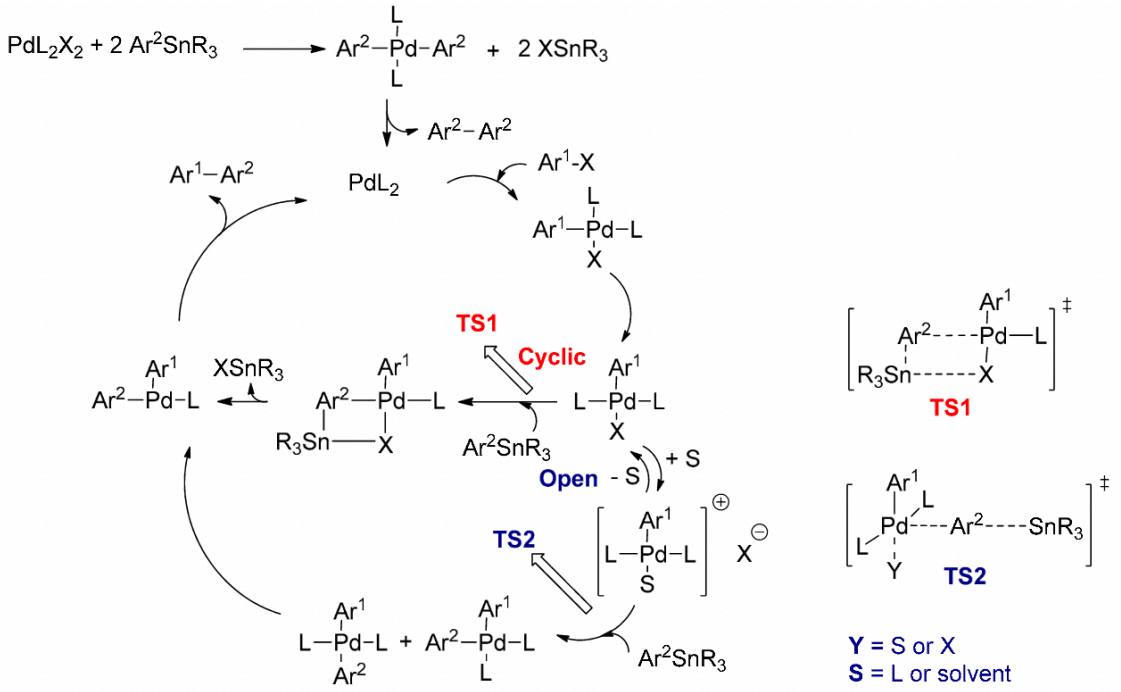

Figure 2.3. Catalytic cycles for Stille coupling via cyclic or open pathways [39].

Although Stille polycondensation is a widely used method for conjugate polymer synthesis, only a few examples of it with pyrrole monomers are reported. Martina, Schluter, and Weger were able to synthesize N-t-BOC protected oligo(pyrrole-2,5-diyls) by Pd(0)$(PPh)_3$-catalyzed Stille reactions between N-t-BOC-2-trimethylstannyl-pyrrole and α-α dibrominated oligopyrroles (**Scheme 2.10**) [64]. However, only a low molecular weight product with about nine repeating units was obtained.

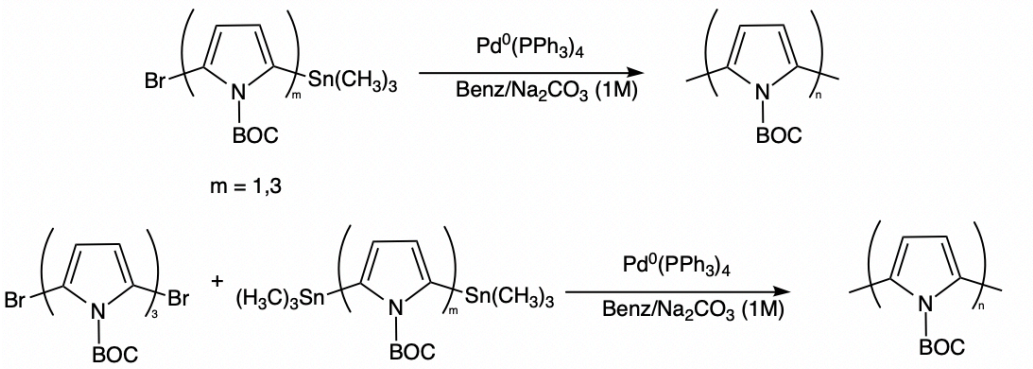

Scheme 2.10. N-t-BOC protected oligo(pyrrole-2,5-diyl) synthesized via Stille coupling [31].

Groenendaal and Lambertus conducted a detailed study on the application of Stille coupling to synthesize well-defined oligopyrroles. They synthesized a series of oligomers with N-t-BOC pyrroles as repeating units terminated with phenyl groups (**Scheme 2.11**). The maximum number of N-t-BOC pyrrole repeating units they obtained was four, and as the number of repeating units increased, the reaction yield decreased dramatically (**Figure 2.4**) (**Table 2.1**) [31].

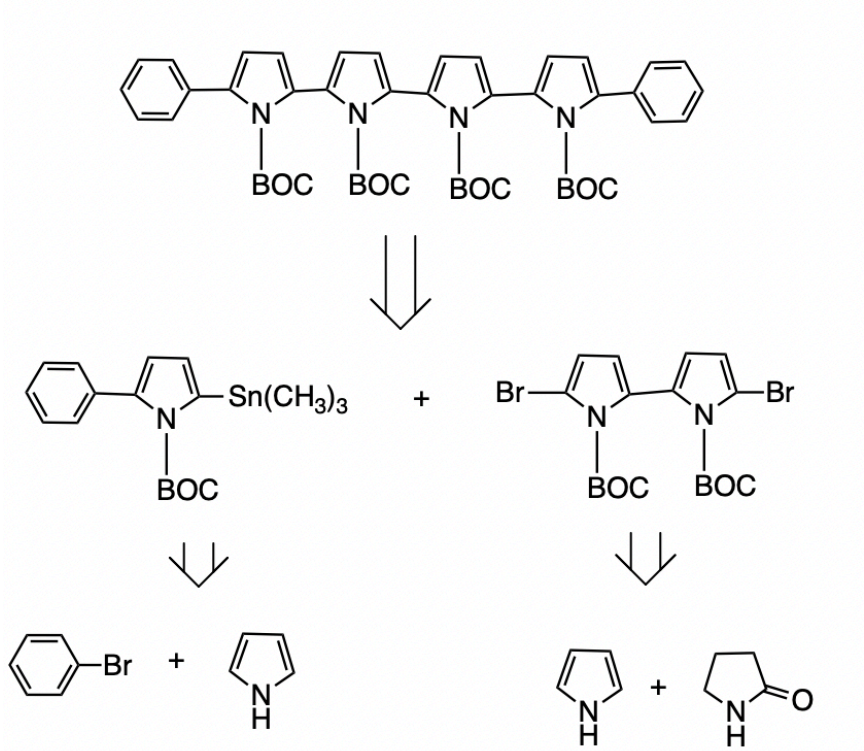

Scheme 2.11. An example of the retrosynthesis route of oligomers with N-t-BOC pyrrole repeating units terminated with phenyl groups [31].

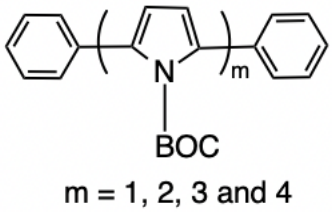

Figure 2.4. Structure of the oligomer with N-t-BOC pyrroles as repeating units and terminated with phenyl groups [31].

Table 2.1. Summary of the Yield of Corresponding Oligomer [31]

Number of Repeating Units	Product Structure	Yield (%)
1	Ph-p-Ph	79
2	Ph-p-p-Ph	54
3	Ph-p-p-p-Ph	43
4	Ph-p-p-p-p-Ph	39

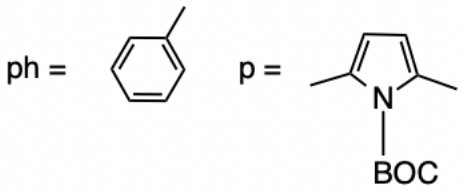

They analyzed the causes for the low yields of longer chain products and came to the following conclusions [31]:

1. Destannylation of organostannanes

   N-t-BOC-protected pyrrolystannanes more easily undergo protolysis compared to other hetero arylstannanes. This protolysis process, also called destannlyation, is due to the high electron-rich property of the pyrrole ring. As a result, for pyrrolystannanes, the protic condition is harmful. However, as a compromise, a slight excess of organostannane is needed in this reaction because an aqueous basic condition is necessary to neutralize HBr generated in the process of $(CH_3)_3SnX$ hydrolysis. In contrast, destannlyation barely occurs for arylstannanes with lower electron density.

2. Deprotection of N-t-BOC-pyrrole derivatives

   The t-BOC sidechain is sensitive to acidic conditions. During the reaction, trace acid may form due to the hydrolysis of trimethylstannyl halide. This trace acid can cleave the t-BOC group, which is harmful to synthesizing the desired product. The necessary long duration of heat for the Stille reaction is also harmful to the t-BOC sidechain since it is heat labile. According to their experimental data, deprotection of the N-t-BOC group is unavoidable even under optimized reaction conditions because of thermolysis.

3. Methyl shift

During the Stille reaction of N-t-BOC pyrrole organostaanes, the bromo group on the pyrrole bromide would always be replaced by a methyl group from the trimethylstannyl substituent on the pyrrole ring. This phenomenon is the so-called “methyl shift” and was first discovered by Martina et al. when they synthesized similar N-t-BOC-protected polypyrroles using the Stille reaction. This methyl shift severely influences the chain growth, since without the halogen substituent on the pyrrole ring, the Stille reaction will not continue because the oxidative substitution step in the catalytic cycle cannot occur. As a result, a high-repeating unit number is hard to obtain.

4. Homo-coupling of organostannanes

   Instead of proceeding to a Stille reaction, the arylstannanes can undergo homo-coupling. This phenomenon was also studied and summarized by Kang et al. [65]. Homo-coupling of organostannanes more easily occurs in electron-rich moieties such as pyrrolstannanes. According to Groenendaal and Lambertus, the governing factor of this homo-coupling reaction is the electron density on the aromatic nucleus, as they found that the less electron-rich monothienylstannanes only undergo a Stille reaction. Homo-coupling is also harmful to chain growth since without the tin substituent, the Stille reaction cannot proceed because the transmetalation step in the catalytic cycle is prevented, stopping the chain growth.

   The monomer used in this project has a similar structure to the N-t-BOC-protected pyrrole they studied for the Stille coupling reaction. The only difference is that our project's 2-ethylhexyl carbamate protecting group has a longer alkyl chain than the t-BOC group. The sensitivity of the sidechain to acidic conditions and heat and the electron-rich property of the pyrrole ring can run into similar issues they had encountered in Stille coupling. Based on the four reasons stated above, Stille polycondensation may not be an attractive choice for our project.

2.1.2.4. Suzuki Coupling

In 1979, Akira Suzuki and his colleagues first described a coupling reaction between an organoboron reagent and an organic electrophile such as a halide or triflate catalyzed by a palladium complex to form a C-C bond (**Scheme 2.14**) [66].

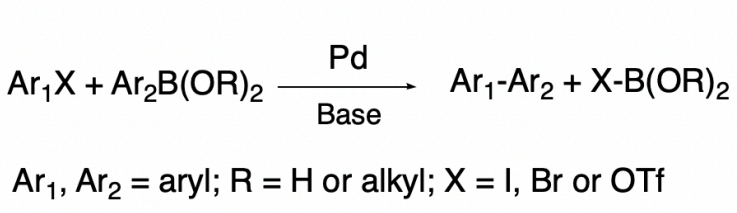

Scheme 2.12. Suzuki coupling

Suzuki coupling has been used to synthesize different types of conjugated polymers. There are two different ways to achieve Suzuki polycondensation in a step-growth polymerization mechanism: the AA/BB approach and the AB approach. AA/BB approach is always used for synthesizing copolymers, whereas the AB approach is applied to homopolymer synthesis (**Scheme 2.13**) [67]. In the AA/BB approach, one of the monomers has two boronic acid or ester substituents, and another is substituted with two halogens. In the AB approach, only one type of monomer is involved, where one side of the monomer is substituted by boric acid or ester, and another side of the monomer has a halide substituent.

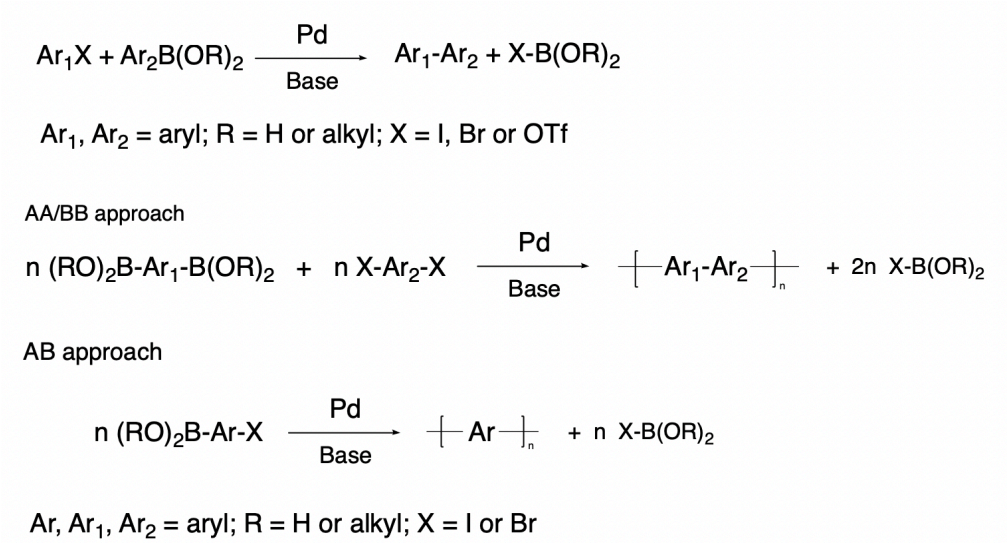

Scheme 2.13. Suzuki Polycondensation

Martina et al. studied both the AA/BB and AB approach of Suzuki polycondensation in synthesizing N-t-BOC-protected oligopyrroles. For the AA/BB approach, they started with tert-butyl 2,5-dibromo-1H-pyrrole-1-carboxylate (2) and (1-(tert-butoxycarbonyl)-1H-pyrrol-

2-yl)boronic acid (5) (**Scheme 2.14**). However, they only obtained brominated dimer (6) in a meager yield (around 10%) and trimer (7) in trace amounts due to unavoidable deboronification of compound (5) (**Scheme 2.15**) [68].

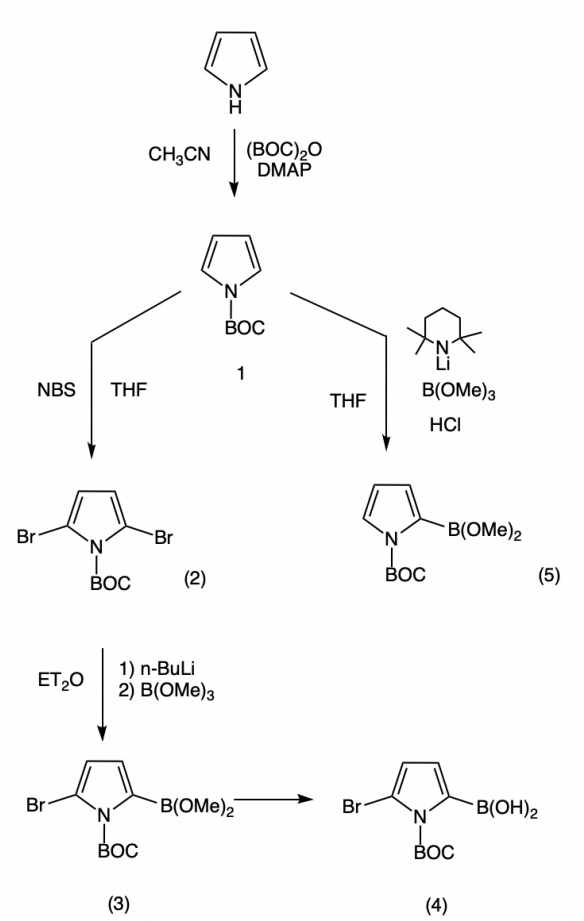

Scheme 2.14

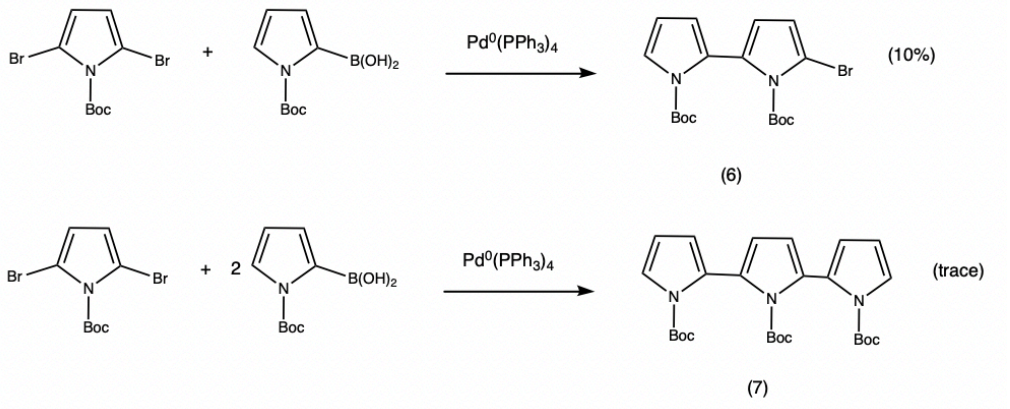

Scheme 2.15. Suzuki polycondensation AA/BB approach for N-t-BOC protected oligopyrroles

For the AB approach, they started with tert-butyl 2-bromo-5-(dimethoxyboraneyl)-1H-pyrrole-1-carboxylate (3) due to the instability of the boronic acid (4) (Scheme 2.16). They stated that oligomers up to the pentamer were formed. However, the yield was lower than 5% with respect to the monomer [68]. This was also due to the deboronification side reaction.

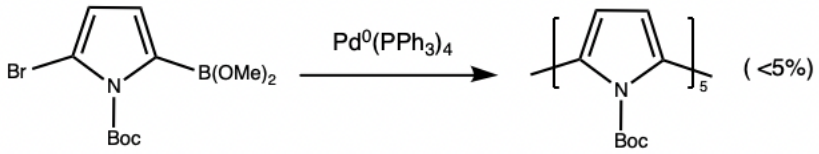

Scheme 2.16. AB approach of Suzuki polycondensation for synthesis of N-t-BOC protected oligopyrroles

The monomer structure used in this project is similar to the monomer that Martina and his colleagues studied. It was predicted that the yield and the degree of polymerization will be low due to the deboronification that will occur using the Suzuki polycondensation method. Thus, Suzuki polycondensation also appears to be unfavourable for this project.

2.1.2.5. Yamamoto Coupling

Yamamoto coupling refers to a dehalogenation-based carbon-carbon coupling reaction of aryl halides catalyzed using an Ni(0) complex (**Scheme 2.17**). Since the 1970s, the Yamamoto group has utilized nickel complexes to conduct a series of Yamamoto coupling reactions to synthesize various conjugated polymers [38]. The monomers for Yamamoto polycondensations are usually dihaloaromatic compounds, and $Ni(COD)_2$ is the most commonly used Ni(0) complex, in which 1,5-cyclooctadiene (COD) acts as a neutral ligand to make the nickel effective as a catalyst (**Figure 2.5**). 2,2'-Bipyridine (bpy) is also used as a complementary ligand to form Ni(COD)(bpy) to facilitate the reaction. In some cases, the $Ni(0)L_m$ complex can be formed in situ by reducing a Ni(II) compound with a reducing agent, such as zinc (**Scheme 2.18**) [38].

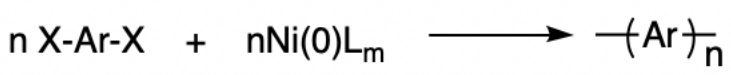

Scheme 2.17

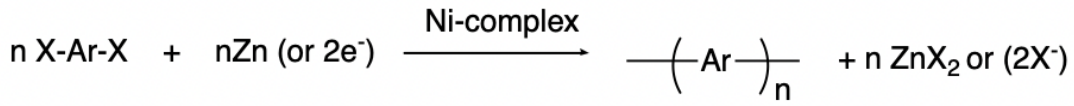

Scheme 2.18

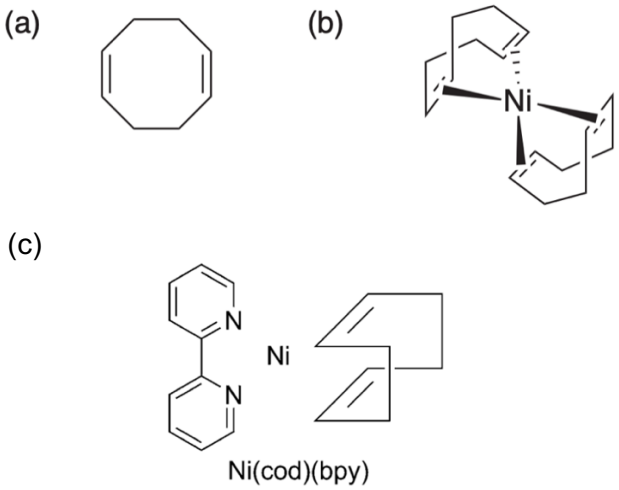

Figure 2.5. Structure of **(a)** COD, **(b)** $Ni(COD)_2$ and **(c)** Ni(COD)(bpy) [52].

The mechanism of Yamamoto coupling involves oxidative addition, disproportionation, and reductive elimination. It is slightly different from other metal-catalyzed C-C coupling reactions because it does not have a transmetalation step. **Scheme 2.19** shows the steps of a typical Yamamoto coupling reaction in the presence of bpy. The first step is the formation of the active nickel complex catalyst Ni(COD)(bpy). Then, oxidative addition between a halogenated monomer (ArX) and the nickel complex occurs as the second step to form an intermediate 1 (ArNi(II)). The third step is disproportionation, which involves two intermediate 1 complexes to form $Ni(II)Ar_2$ and $Ni(II)X_2$. In this step, $Ni(II)X_2$ is reduced, and $Ni(II)Ar_2$ is oxidized since the disproportionation is a redox reaction in which the net oxidation state is not changed [52]. The last step is reductive elimination. The Ar-Ar bond is

formed in this step, and the Ni(II) is reduced to Ni(0). If the starting material is dihalogenated, the coupling can keep proceeding via the polycondensation reaction and form a polymer. The whole catalytic cycle using halogen-substituted benzene as an example is shown in **Figure 2.6**.

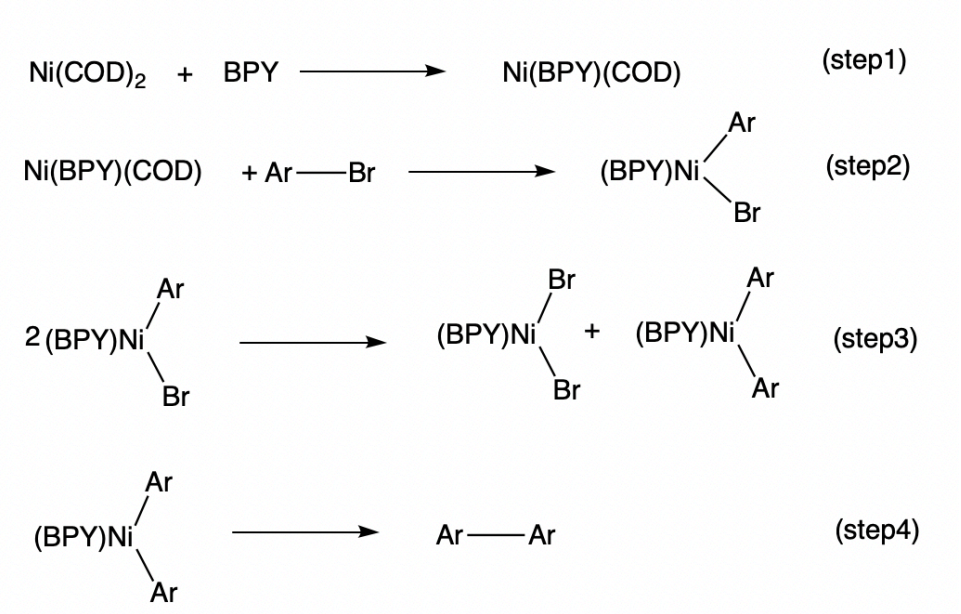

Scheme 2.19.

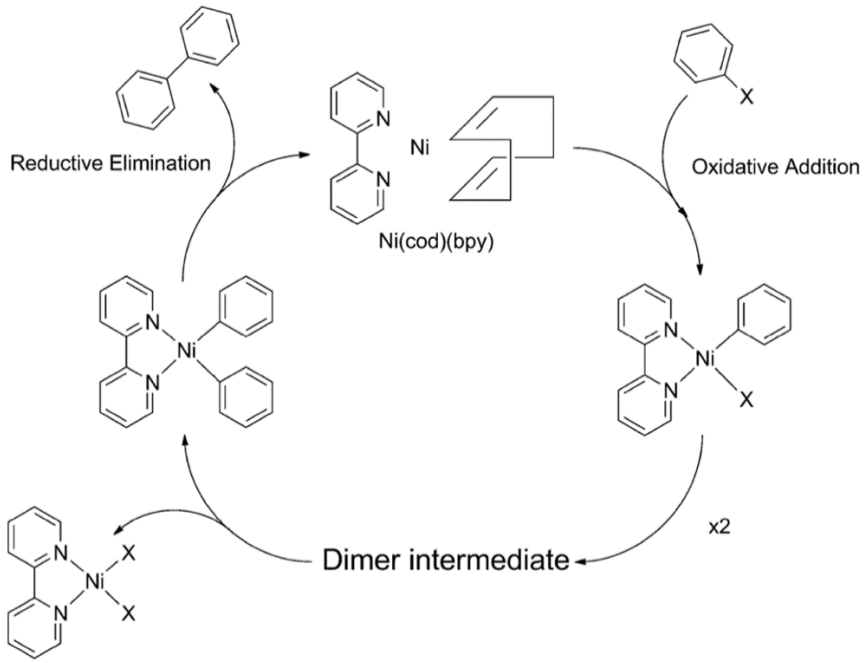

Figure 2.6. Catalytic Cycle of Yamamoto coupling of two halogen substituted benzene, where X is halogen atom [69].

Yamamoto coupling can be used to synthesize a homopolymer or a copolymer by using one or more than one monomer, respectively [52]. In Yamamoto coupling, half of the nickel is consumed as Ni(II)X_2. Thus, the nickel complex is not only a catalyst strictly, and the amount of nickel used is crucial for the polycondensation duration because the remaining half of the Ni(0) is maintained in the next reaction step, and so on [52]. It has been discovered that for many Yamamoto polycondensations, the rate-limiting factor is usually the polymer solubility [52]. For many polymers synthesized via Yamamoto polycondensation, their solubility must be high to achieve a large molecular weight. For example, for the synthesis of poly(p-phenylene) (PPP), a solubilizing sidechain greatly increases the degree of polymerization compared to PPP without any sidechains [52].

Numerous conjugated polymers have been synthesized through Yamamoto polycondensation, including poly(p-phenylene) (PPP) [70] ; poly(m-phenylene) (PMP) [71] ; poly(pyridine-2,5-diyl) [72] ; poly(alkyl pyridine-2,5-diyl) [73] ; and poly(pyrimidine-2,5-diyl) [74]. Polypyrrole and its derivatives were also successfully synthesized with this method [75]. Structures of these example polymers synthesized by Yamamoto polycondensation are shown in **Figure 2.7**.

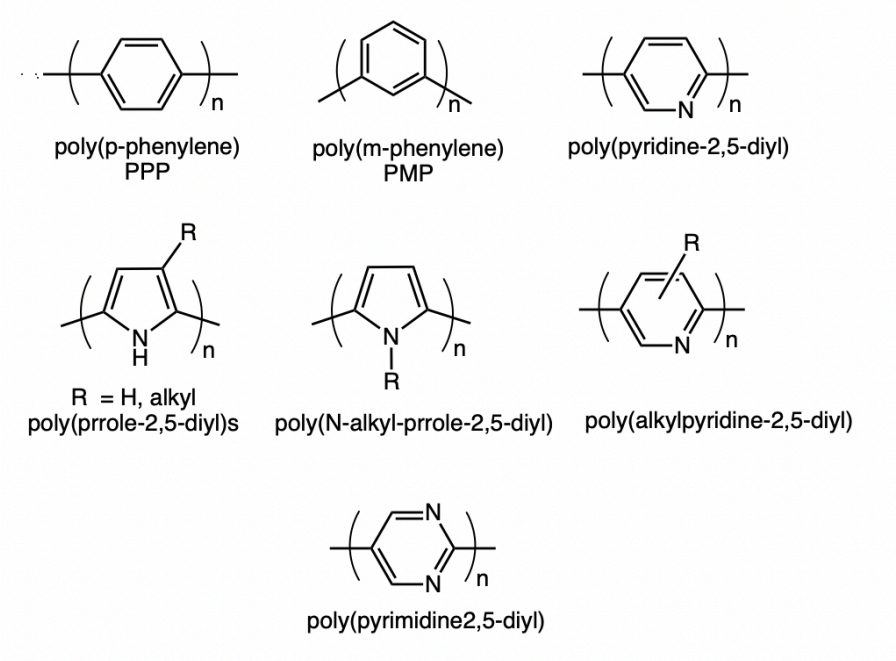

Figure 2.7. Examples of polymers synthesized via Yamamoto polycondensation.

Unlike the aforementioned metal-catalyzed polycondensation methods, Yamamoto polycondensation has a unique advantage for our project: it does not involve a transmetalation step. As a result, there is no need for an organo-metal compound as a monomer. As stated previously, for the Kumada, Negishi, Stille, and Suzuki polycondensation methods, the formation of the organo-metal monomer is harmful to the carbamate sidechain for various reasons, and all of them have some issues with the continuation of polymerization, which makes these methods not ideal for this project. Yamamoto polycondensation overcomes this drawback because it can proceed directly with the dihaloaromatic monomer. Furthermore, the reaction conditions are milder than other organometallic polycondensations since the nickel used is zero-valent, and no acidic conditions are created in the process, unlike the Stille reaction where acidic conditions would be created due to the hydrolysis of $Sn(Me)_3$ [31].

In addition, Yamamoto et al. have successfully synthesized N-Boc-protected poly(3-heptylpyrole) PPr(3-Hep; N-BOC) with a molecular weight of $M_n = 9640$ **(Scheme 2.20)** [76] . They also studied the synthesis of poly(tert-butyl 1H-pyrrole-1-carboxylate) (PPr(N-BOC)) using the same method used for the synthesis of N-Boc-protected poly(3-heptylpyrole). However, they only obtained an oligomer with five subunits (**Scheme 2.21**) [76].

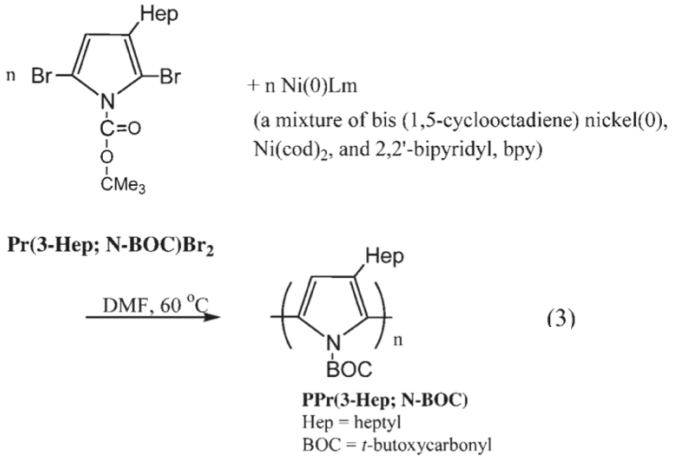

Scheme 2.20 [76].

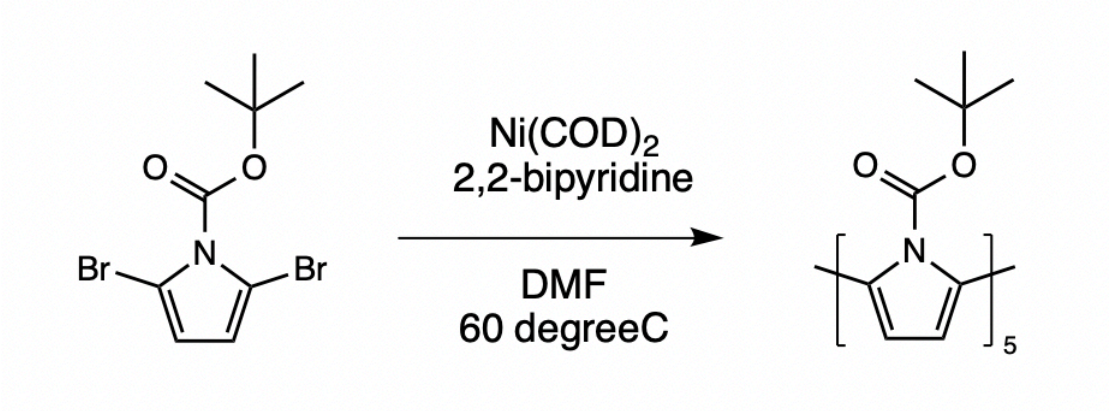

Scheme 2.21. Pentamer of N-BOC-Pyrrole Synthesized by Yamamoto Group

Though Yamamoto only obtained an oligo(tert-butyl 1H-pyrrole-1-carboxylate) through Yamamoto polycondensation, it still inspired our research. Because as mentioned above, the solubility of the polymer can be a crucial factor in the degree of polymerization. Compared with Yamamoto's research, our project will use a longer carbamate sidechain in our monomer which is expected to improve the solubility of the resultant polymer (**Figure 1.14**). Comparing the two different polymers of Yamamoto's research, the one with the heptyl group on the 3-position of pyrrole ring has a much higher degree of polymerization, which could be further evidence for the influence of solubility on the degree of polymerization since the heptyl group significantly increased the solubility of the polymer. With this knowledge in mind, we hypothesized that we could achieve a greater degree of polymerization by using Yamamoto's approach.

Thus, with all the benefits of Yamamoto polycondensation stated above, we chose to explore Yamamoto polycondensation as the method for synthesizing PEPC.

2.1.3. Conclusion

Through the above critical analysis, it can be concluded that among all the organometallic polycondensation methods, Yamamoto polycondensation is the most favourable method for our project.

2.2. Polymer Synthesis Through Oxidative Polymerization

As a well-studied conducting polymer, polypyrrole has been synthesized through many different methods in the past few decades. Among them, oxidative polymerization is one of the oldest methods to afford polypyrrole. Chemically oxidative polymerization of polypyrrole is the most preferred method because it is easily processible, cost-effective, fast, convenient, and scalable [77]. In fact, oxidative polymerization has also been utilized to synthesize numerous different π-conjugated polymers and can be applied in different forms, including chemically, electrochemically, or by utilizing ultrasonic waves [77].

Polypyrrole can be synthesized through chemically oxidative polymerization of pyrrole monomers in organic solvents or aqueous solutions by applying different oxidizing agents, including ferric chloride ($FeCl_3$) and ammonium persulfate (APS) [77,78]. Generally, chemical oxidative polymerization of polypyrrole starts with the preparation of the monomer solution and oxidizing agent solution, followed by mixing them to initiate polymerization. **Figure 2.8** shows the flow chart of the general procedure of synthesis of polypyrrole through chemical oxidative polymerization.

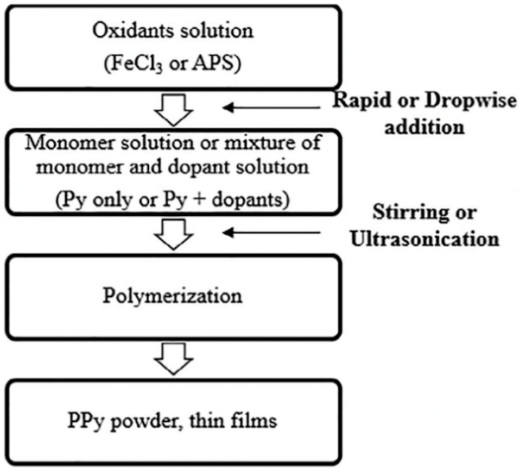

Figure 2.8. Flowchart of the process of synthesizing PPy by oxidative polymerization [3].

A generally accepted mechanism for the oxidative polymerization of polypyrrole is shown in **Figure 2.9**. Three steps are involved in this mechanism, which are oxidation, deprotonation, and crosslinking reactions [79]. In the first step, radical cations are formed through the oxidation

of the pyrrole monomer. Subsequently, deprotonation occurs between these radical cations to form soluble bipyrroles. The third step is propagation, in which oxidation occurs to bipyrroles again to form the oligomers and radical cations. Higher oligomers, and finally, an extended conjugated polymer forms through the continuous coupling reaction between the oligomers. Polymerization proceeds by repeating the propagation step until the polymer is insoluble and the polypyrrole precipitates through the liquid medium [12].

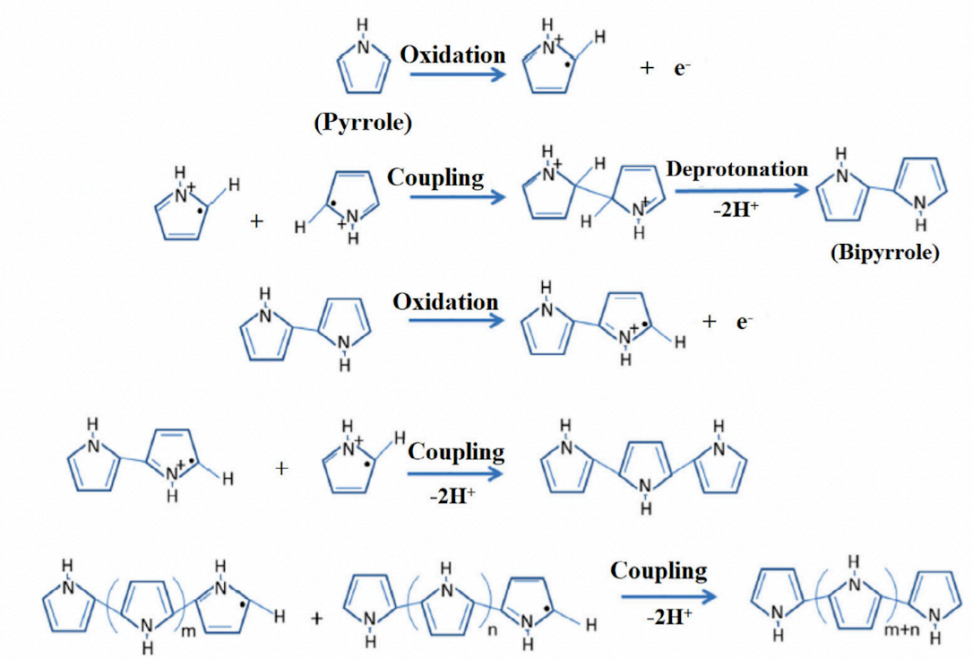

Figure 2.9 Mechanism of oxidative polymerization of polypyrrole [3].

However, in a recent study, Tan et al. proposed a different mechanism wherein ferric chloride was used as the oxidizing agent. In this mechanism, after the radical cation is formed, it can also react with a neutral monomer to form a bipyrrole radical cation [79]. The bipyrrole radical cation will be further oxidated and deprotonated to afford a bipyrrole dimer. The re-initiation will occur to the dimer, and it will be oxidized to form a radical cation again. This process will propagate and finally form the polypyrrole. This mechanism is shown in **Figure 2.10**.

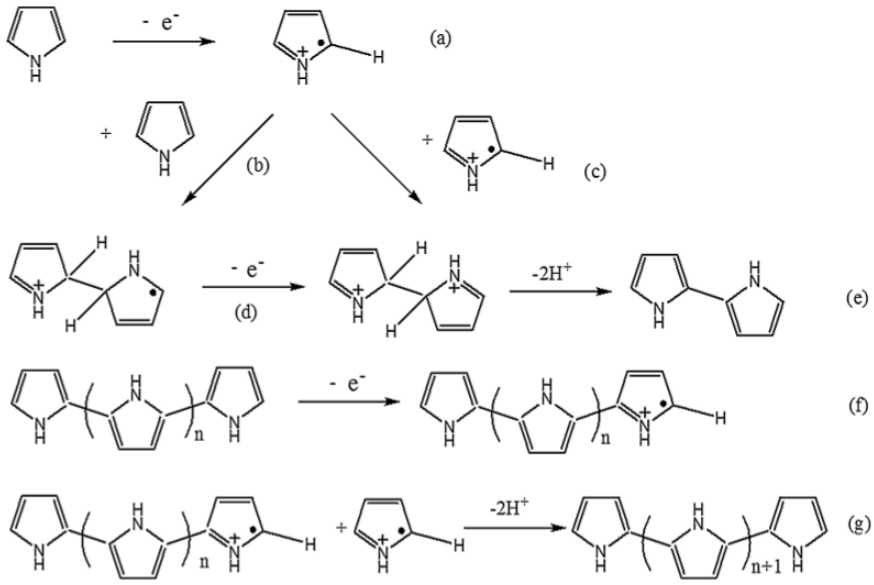

Figure 2.10. Mechanism of oxidative polymerization of pyrrole proposed by Tan et. al. [79].

2.3. Characterization Methods

2.3.1. Nuclear Magnetic Resonance (NMR)

NMR is a technique used to determine the molecular structure of a chemical by measuring the interaction of nuclear spins under a strong magnetic field [80]. Some nuclei exist in specific nuclear spin states when exposed to an external magnetic field. Under an external magnetic field, hydrogen nuclei ^{1}H and carbon nuclei ^{13}C possess magnetic moments that produce a specific resonance frequency recorded as a chemical shift (δ). The transitions between spin states to specific nuclei and their chemical environment can be observed through NMR. As a result, the composition of atomic groups can be determined from the chemical shift of NMR spectra, in which the signal intensity shows the ratios.

2.3.2. Ultraviolet-visible-Near Infrared Spectroscopy (UV-VIS-NIR)

Light transmittance of a sample is measured by UV-VIS-NIR spectroscopy and is converted to absorbance according to the equation: A= -log(T) [81]. In UV-VIS-NIR spectroscopy, absorption is performed in the wavelength range of 200 nm and 3000 nm, referred to as partial ultraviolet, entire visible regions, and near-infrared regions, respectively. There are two main applications of UV-VIS-NIR spectroscopy: qualitatively determining a functional group of a chemical and quantitively determining the absorption coefficient to be used for

other calculations. For conducting polymer, the ground states electrons can gain energy by absorbing light to transfer to the excited state. This property can be used to determine the band gap of a conducting polymer, which corresponds to the HOMO-LUMO gap. By using the onset wavelength (λ_{onset}), the optical band gap E_g can be calculated according to the following equation:

$$E_g(eV) = hc/\lambda_{onset}$$

where h is Planck's constant and c is the speed of light, $2.998\times 10^3 m/s$.

2.3.3. Cyclic Voltammetry (CV)

CV is a useful and standard electrochemical method to study the reduction and oxidation process of a polymer [82]. When a voltage is applied to an active redox solution or a material on the electrode and switches back and forth to form a cycle, the current change is measured and recorded as a CV diagram. For conducting polymer, the oxidation process corresponds to the extraction of electrons from the HOMO of a polymer, whereas the reduction process is accompanied by the injection of electrons into the LUMO of a polymer. Thus, by using CV measurement, the redox potentials of a polymer sample can be determined and can be converted to the E_{HOMO} according to the following equation:

$$E_{HOMO} = -e\left[E_{ox}^{onset} - E_{\frac{FC}{FC^+}}\right] - 4.8eV$$

where e is the elementary charge and $E_{\frac{FC}{FC^+}}$ is the measured E_{ox}^{onset} of ferrocene from the same CV device.

2.3.4 Fourier Transform Infrared (FTIR)

FTIR refers to the Fourier transform infrared, which is a more rapid technique of infrared spectroscopy [83]. When IR radiation emitted from a glowing balck-body source passes through a sample, only a partial of the radiation passes through the sample (is transmitted), and some of the radiation with specific frequencies is absorbed by the sample. FTIR spectroscopy records the radiation that passes through the sample. The covalent bonds of a molecule can selectively absorb radiation of specific wavelengths to change its vibrational energy. Different bonds and functional groups absorb different wavenumber radiation. Therefore, different

molecules have different transmittance patterns, and the recorded FTIR spectra are different. The spectra can be applied to distinguish different functional groups and different molecules. Compared with traditional IR spectroscopy, FTIR has three unique advantages: not destroying the sample, faster, and more precise and sensitive.

2.3.5 Thermogravimetric Analysis (TGA)

TGA is a thermal analysis technique that measures a sample's weight changes versus a changing temperature in a constant heating rate or versus time at an unchanged temperature in a specific atmosphere (for example, air or nitrogen) [84]. The weight changes of a sample for TGA are related to their chemical and physical properties. Therefore, using TGA, a conducting polymer's thermal properties can be determined. TGA can also be combined with a mass spectrometer of FTIR further to evaluate a sample's volatile and thermal decomposition.

2.3.6 X-ray Diffraction (XRD)

XRD is a method to investigate the crystal structure of the materials. XRD takes advantage of the intensities change of the x-ray beam caused by interference when monochromatic x-rays scatter from a substance to study the substance's crystal structure and atomic spacing [85]. The intensity changes follow Bragg's law, and the intensities are recorded as XRD peaks. Bragg's law is shown in the following equation:

$$n\lambda = 2dsin\theta$$

where λ is the wavelength of X-ray beam, d is the distance of lattice planes and θ is the incident angle of beam.

Chapter 3. Synthesis and Characterization of PEPC

3.1. Introduction

As mentioned in Section 1.3, polymer PEPC is designed to address the problem that polypyrrole cannot achieve high conductivity and good solubility at the same time. PEPC with the 2-ethylhexyl carbamate sidechain is expected to achieve good solubility due to the long alkyl sidechain and high conductivity by removing the carbamate sidechain [1,14,32]. To the best of our knowledge, no N-substituted carbamate polypyrrole has ever been synthesized, achieving both high conductivity and good solubility. In this work, synthesizing PEPC with Yamamoto polycondensation and oxidative polymerization was studied, and the obtained PEPC was fully characterized. The PEPC synthesized through oxidative polymerization had good solubility in various organic solvents. However, the conductivity of the PEPC thin film was poor due to the carbamate sidechain could not be totally removed.

3.2. Synthesis of Poly(2-ethylhexyl 1H-pyrrole-1-carboxylate) (PEPC) through Yamamoto Polycondensation

3.2.1. Introduction

Scheme 3.1 illustrated the approaches A and B of the synthesis route of Poly(2-ethylhexyl 1H-pyrrole-1-carboxylate) (PEPC) through Yamamoto polycondensation. The synthetic routes with NMR data of each step are listed in Chapter 3.2.4.

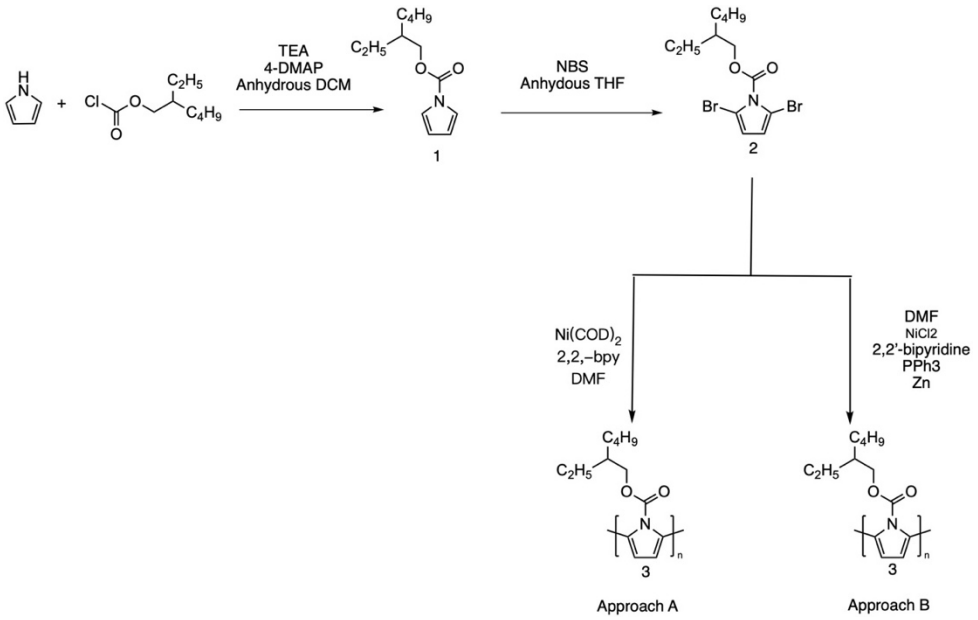

Scheme 3.1

Briefly, in the first step, commercially available pyrrole and 2-ethylhexyl chloroformate were used as the starting material to synthesize 2-ethylhexyl 1H-pyrrole-1-carboxylate 1, with 4-Dimethylaminopyridine (4-DMAP) as catalyst and triethylamine (TEA) as the base. This step aimed to add the carbamate sidechain to pyrrole, not only to improve the solubility of the monomer and resultant polymer, but also to stabilize the following dibromo product. Early research has shown that the unsubstituted dibromo pyrrole or dichloro pyrrole is very unstable and cannot be isolated after synthesis due to rapid decomposition [86]. In contrast, the N-substituted dibromo pyrrole is more stable compared to its unsubstituted counterpart. We found that Compound 2 can be stably stored under -20 ℃ for at least several weeks without decomposition. Compound 1 is also stable and can be stored at room temperature for at least several days and under -20 ℃ for months. An important note is that when we synthesized Compound 1, around 10% of the yield consisted of the side product, bis-(2-ethylhexyl)carbonate; it would unavoidably form, and it could not be separated through column chromatography. However, this side product did not influence the next bromination step since it will not react with N-bromosuccinimide (NBS), the bromination reagent. Compound 1 was then used as the starting material to synthesize 2-ethylhexyl 2,5-dibromo-1H-pyrrole-1-carboxylate (Compound 2) via a bromination reaction with NBS. Compound 2 is the dibromo monomer that was used for Yamamoto polycondensation.

Two approaches of Yamamoto polycondensation were used to synthesize PEPC (polymer 3). For approach A, a commonly used catalyst for Yamamoto polycondensation, $Ni(COD)_2$, was attempted, and 2,2-bipyridine (2,2-bpy) was used as the ligand. For approach B, the nickel(0) catalyst was formed in situ through the reduction of $Ni(II)Cl_2$ by zinc. 2,2-bpy and triphenylphosphine (PPh_3) were used as the ligands.

3.2.2. Result and Discussion

Polymerization using approach A was conducted under N_2 atmosphere with heating at 60 ℃ for 48 hours. During the whole course of the reaction of 48 hours, the reaction mixture was transparent and non-viscous, indicating no high molecular weight polymer formed. After the reaction proceeded for 24 hours, green precipitation showed up in the bottom of the vial, indicating nickel (II) bromide formed. After 48 hours, the reaction was stopped and cooled to room temperature. The reaction mixture was poured into methanol, stirred, and filtered. Only a trace amount of filter residue was left. Most products were soluble in methanol which was further evidence that high molecular weight polymer was not obtained.

Polymerization using approach B was conducted under N_2 atmosphere, heated at 80℃ through an oil bath, and was monitored with thin layer chromatography (TLC) after 24, 48, 72, and 96 hours, respectively. Starting material Compound 2 existed during the whole course of 96 hours of the reaction, confirmed by TLC, indicating the polymerization did not complete thoroughly. In addition, the TLC did not show a significant difference after 24, 48, 72, and 96 hours by using the same concentration and amount of sample, indicating the reaction may have stopped before 24 hours. After 96 hours, the reaction was stopped and cooled to room temperature. Part of the reaction mixture was poured into methanol as a test trial and filtrated, and the filter residue was not soluble in acetone, hexane, and chloroform and was soluble in aqueous HCl solution indicating most parts of the filter residue was zinc powder added as reducing agent. The remaining part of the reaction mixture was then poured into chloroform, filtered, and the filtrate was washed with water. The organic phase was collected, and the solvent was removed by rotary evaporation to yield yellow-brown oil. The oil was soluble in methanol, indicating it was not a high molecular weight polymer. Since it

was not the desired polymer, further characterization was not conducted due to the limited time.

As previously mentioned, the solubility of the monomer and the polymer is a crucial factor in a successful Yamamoto polycondensation. In this project, a longer carbamate chain was used to increase the solubility, but no high molecular weight polymer was obtained. Compared with the oligomer of (PPr(N-BOC) with five repeating units synthesized by Yamamoto and his colleague, it can be found that under the same conditions, higher solubility was not the most important factor to obtain the desired high molecular weight polymer in our project.

In the above-mentioned Yamamoto polycondensations of Compound 2, there were signs indicating some reactions occurred. However, the polymerization did not proceed to the end to form a high molecular weight polymer. In approach A, the green nickel (II) complex formed, indicating that an oxidative addition step occurred since the nickel added at the beginning of the reaction was zero-valent. Based on this observation, one possible reason for the polymerization not proceeding could be attributed to the competition between the cleavage of the Br-C bond and the cleavage of the CO-O bond following different routes of oxidative addition, respectively. Specifically, oxidative addition can not only occur through the cleavage of the bromine-pyrrole bond and formation of the pyrrole α-carbon-nickel-bromine bond but also can occur through the cleavage of the C-O bond of the carbamate chain and formation of O-Ni-CO bond (**Scheme 3.2**). It is well known that oxidative addition can occur between C-OY and $Ni(0)L_m$ [40]. In fact, Yamamoto and his colleagues studied two different types of ester carbonyl group addition to Ni(0) complexes, and the type of reaction depended on the carbonyl group employed and the ligand coordinated to nickel (**Scheme 3.3**) [87].

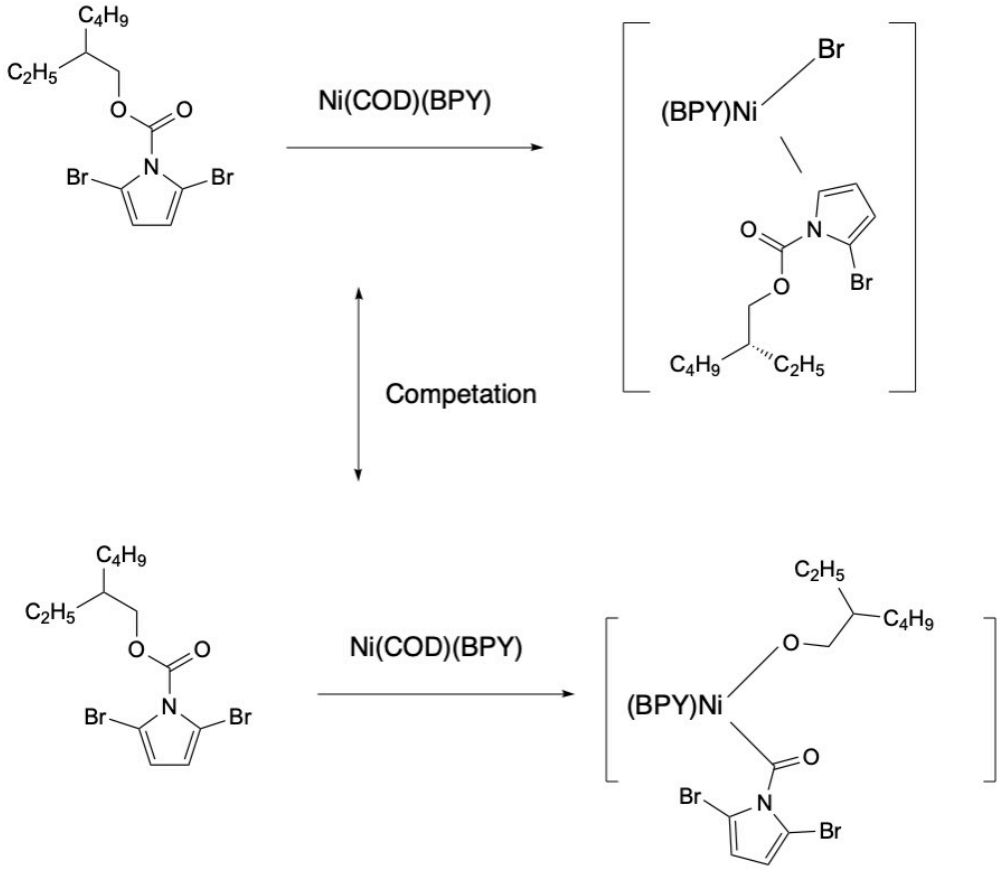

Scheme 3.2. Possible competition reactions and the different oxidative addition.

Scheme 3.3. Two types of nickel catalyst ester carbonyl group cleavage [88].

According to Yamamoto et al., when bpy is used as the ligand, type A oxidative addition will occur [88]. They used phenyl propionate as an example to study the whole process. The first step involved the cleavage of the C_2H_5CO-OC_6H_5 bond, which is the oxidative addition to form nickel complex 1, followed by decarbonylation to release a carbon monoxide to afford nickel complex 2. Then, two Complex 1 and two carbon monoxide ligands are involved in a disproportionation reaction to finally form the $Ni(OC_6H_5)_2$ complex (**Scheme 3.4**) [87] .

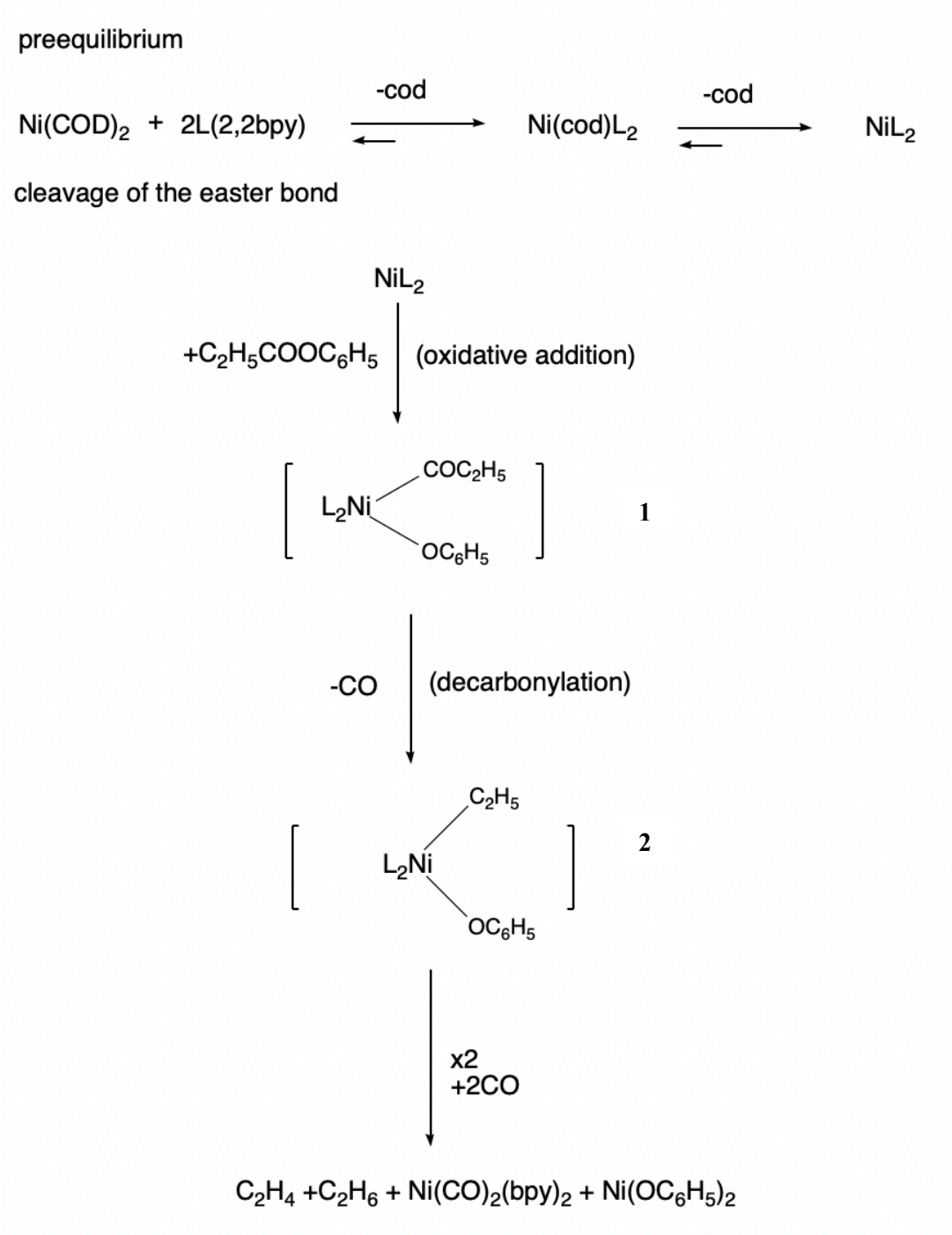

Scheme 3.4 [87].

In addition, it has been confirmed that nitrogen atoms can form an N-Ni bond with Ni(II) complexes to form a new complex [89]. With this knowledge in mind, one possible reaction pathway may be proposed, as shown in **Scheme 3.5**. In the preequilibrium, $Ni(cod)_2$ releases two cod and combines with two bpy to form an NiL_2 complex. The first step starts with the cleavage of the CO-O bond of the carbamate group and an oxidative addition to form

Complex A. The second step is decarbonylation to release a CO and form complex B (as mentioned before, N-Ni bond formation is confirmed to be possible). In the final step, two Complex B are involved and finally, complexes C and D, which are both Ni(II) complexes are formed.

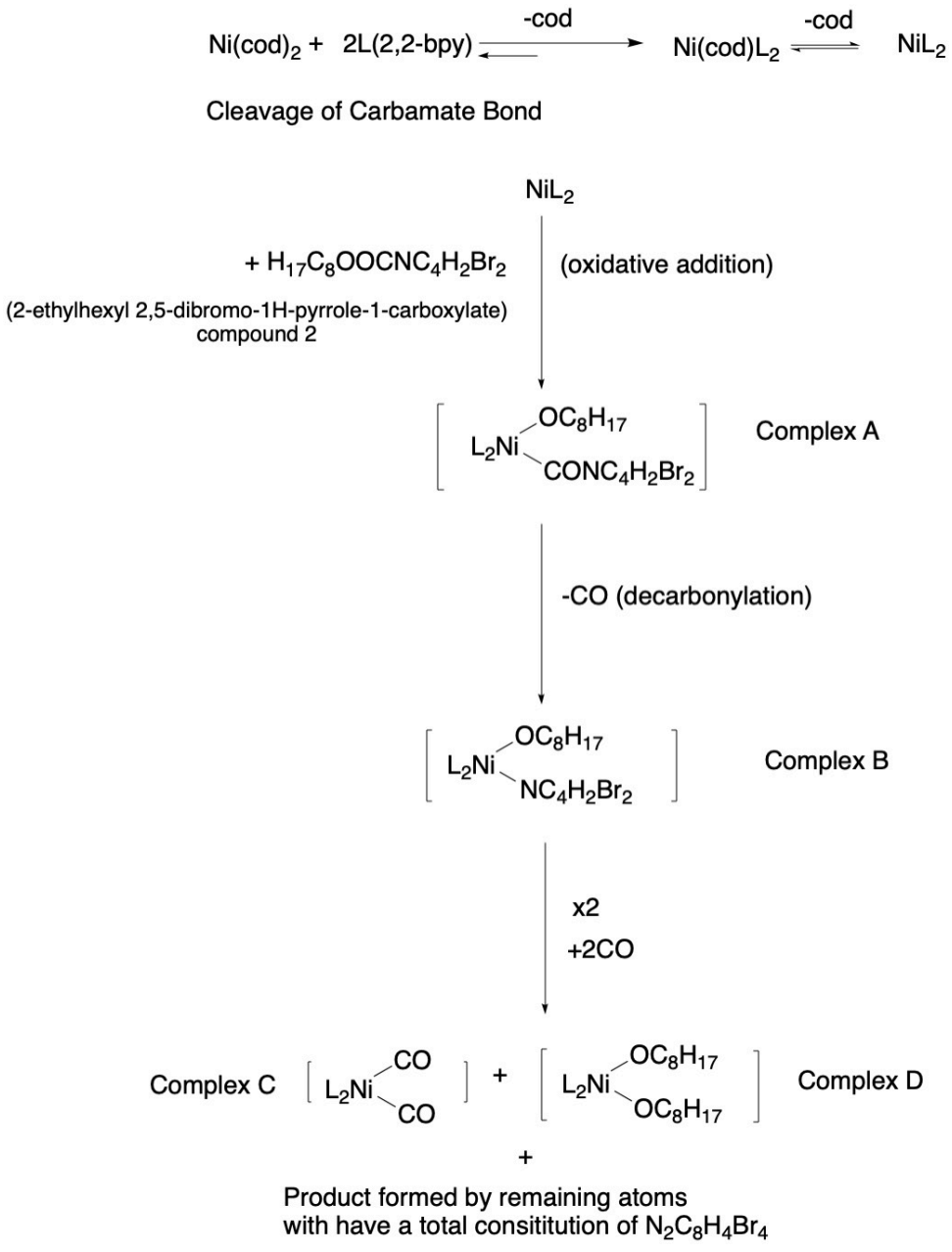

Scheme 3.5.

Due to limited research time, this mechanism has yet to be verified. In section 2.1.2.5, it was mentioned that Yamamoto et al. obtained an oligomer of (PPr(N-BOC)) up to five repeating units [90]. In contrast, a polymer of M_n = 9640 of the N-BOC-Poly(3-heptylpyrrole) (PPr(3-

Hep; N-BOC)) was also obtained. Yamamoto stated that the reason for the difference in the degree of polymerization between (PPr(3-Hep; N-BOC)) and (PPr(N-BOC)) could be the difference in the reactivity of the intermediate polymer-C-NiL_m due to the structural change caused by the 3-heptyl group [90]. The heptyl group may influence the relative reactivity of the bromo position and the CO-O position, resulting in Ni attacking CO-O more favorably than C-Br. This may be further evidence that the carbamate sidechain influences the proceeding of Yamamoto polycondensation.

3.2.3. Conclusion and Future Work

Through a comprehensive literature review and critical analysis, Yamamoto polycondensation was found to be one of the most suitable organometallic polymerization methods for this project. However, high molecular weight PEPC was not obtained through Yamamoto polymerization. Using a 2-ethylhexyl carbamate sidechain to improve the solubility of the monomer was not found to be helpful for the desired product synthesis, indicating that solubility was not the most crucial factor for a successful Yamamoto polycondensation in this project. Based on our knowledge, a presumption is raised that the bromo-aryl bond cleavage and the bromo-nickel-aryl bond formation may be competitive to the CO-O bond cleavage and the OC-Ni-O bond formation, therefore preventing the polymerization from proceeding to the end. Further study needs to be conducted to understand the whole process clearly. In conclusion, at this stage, Yamamoto polycondensation was not successfully applied to the synthesis of poly(2-ethylhexyl 1H-pyrrole-1-carboxylate). A better synthetic pathway would need to be developed to achieve the organometallic polymerization of PEPC.

3.2.4. Experimental Section

3.2.4.1. Materials

All the chemicals used in this project were purchased from Sigma-Aldrich, Fluka VWR, TCI, and Armstrong. Solvent used in the synthesis procedure were analytical grade and anhydrous or used as received. All column chromatography was conducted using silica gel (230-400 mesh) slurries purchased from the University of Waterloo.

3.2.4.2. Synthesis Procedures

Synthesis of 2-ethylhexyl 1*H*-pyrrole-1-carboxylate (1)

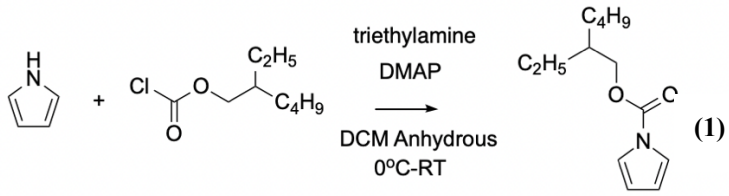

(1)

To a flask charged with pyrrole (0.5031g, 7.5 mmol), triethylamine (0.5692g, 5.6 mmol), and 4-(dimethylamino)pyridine (0.6872g, 5.6 mmol) was added anhydrous DCM (2.5 mL), and the resulting solution cooled to 0 °C, under N_2 atmosphere. 2-Ethylhexyl chloroformate (1.0838g, 5.6 mmol) was added slowly and the reaction mixture was then stirred at room temperature for 16 h. The reaction mixture was extracted with diethyl ether (3 × 5 mL), and the combined extracts were washed with aqueous potassium bisulfate, aqueous sodium bicarbonate and water. The organic phase was then dried over sodium sulfate and concentrated in vacuo, followed by column chromatography (eluent, pure hexane followed by hexane: DCM = 5:1 followed by hexane: ethyl acetate =10:1) to afford the product (transparent oil). ^{1}H NMR (300 MHz, chloroform-*d* δ/ppm): 7.25 (t, 2H), 6.23 (t,2H) 4.25 (m, 2H).

Synthesis of 2-ethylhexyl 2,5-dibromo-1H-pyrrole-1-carboxylate (2)

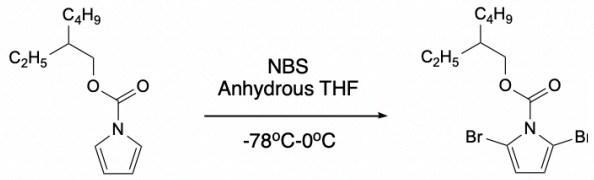

(2)

To a stirred solution of 2-ethylhexyl 1H-pyrrole-1-carboxylate (2 mmol, 0.4466 g) in 20mL of anhydrous THF at –78 °C, freshly recrystallized N-bromosuccinimide (4 mmol, 0.712 g) was added in portions. The reaction mixture was stirred at –78 °C for 1 h, after which it was warmed up to 0 °C and stirred for 18 h. Sodium sulfite (0.252 g) was added to the mixture, the solvent evaporated on a rotovap without any heat, and carbon tetrachloride (20 mL) added. The resulting precipitate was filtered off, and the solution was concentrated on a rotovap again without any heat, and subjected to column chromatography (silica gel, pure

hexane followed by hexane : DCM = 3:1). The product was a transparent, colorless oil. ^{1}H NMR (300 MHz, chloroform-*d* δ/ppm): 6.26 (m, 2H), 4.33 (d, 2H)

Synthesis of Poly(2-ethylhexyl 1*H*-pyrrole-1-carboxylate) (3) Approach A

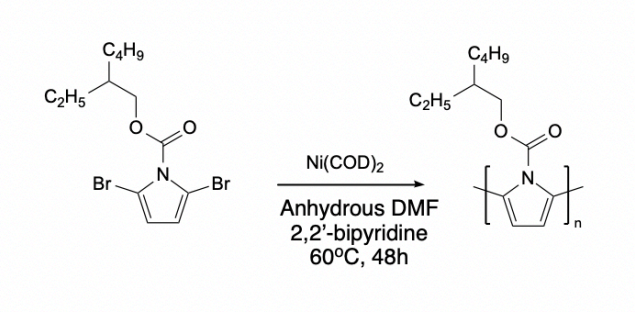

To a 25 mL RB flask with stir bar, 2-ethylhexyl 2,5-dibromo-1H-pyrrole-1-carboxylate (0.137 g, 0.3595 mmol) was added under Ar protection. A dry DMF (5mL) solution of 2,2'-Bipyridine (0.1129g, 0.72 mmol) was added at room temperature, followed by quickly adding the $Ni(cod)_2$ (0.1977 g, 0.72 mmol), (with minimized contraction of $Ni(cod)_2$ to air) and the mixture was stirred for 48 h at 60 °C. The reaction mixture was poured into methanol, stirred, and the precipitate was separated by filtration to obtain the crude product. The crude product was then stirred in methanol for 45 min which was followed by Soxhlet extraction.

Synthesis of Poly(2-ethylhexyl 1*H*-pyrrole-1-carboxylate) (3) Approach B

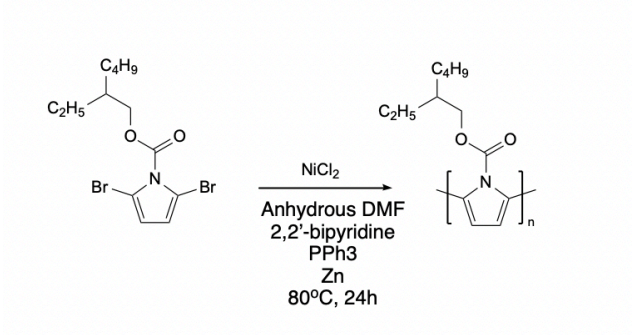

2-ethylhexyl 2,5-dibromo-1H-pyrrole-1-carboxylate, triphenylphosphine, zinc dust, dipyridyl, and nickel chloride were charged into a 25 ml RB-flask and purged with nitrogen. Anhydrous DMF (1.7 ml) was added via syringe, and the mixture was stirred at 80 °C for 24 h. The mixture was cooled and poured into 200 ml methanol, stirred, collected by filtration, and followed by Soxhlet extraction.

3.3. Synthesis of Poly(2-ethylhexyl 1H-pyrrole-1-carboxylate) (PEPC) Through Oxidative Polymerization

3.3.1. Synthesis of Poly(2-ethylhexyl 1*H*-pyrrole-1-carboxylate) with APS

3.3.1.1. Introduction

Ammonium persulfate (APS) is a commonly used oxidizing agent for synthesizing polypyrrole by oxidative polymerization (**Figure 3.1**). There have been many examples of the synthesis of polypyrrole with APS as the oxidizing agent with good yield, reasonable conductivity, and other beneficial properties [3].

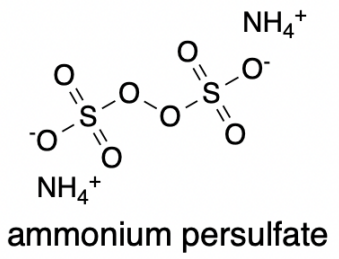

Figure 3.1. Structure of ammonium persulfate.

The half reaction of reduction of APS is:

$$S_2O_8^{2-} + 2H^+ + 2e^- \rightarrow 2HSO_4^- \quad E^0 = 2.12V \ (1)$$

and the whole oxidative reaction can be expressed as following:

$$S_2O_8^{2-} + 2H^+ + 2C_{13}H_{21}NO_2 \rightarrow 2HSO_4^- + 2C_{13}H_{21}NO_2^+ \ (2)$$

APS is not soluble in chloroform, and 2-ethylhexyl 1H-pyrrole-1-carboxylate is not soluble in water. Thus, a two-phase reaction system is designed to make the reaction happen. Surfactant is used to increase the interaction of the two phases. In addition, the surfactant can also be used as a dopant for the polymer to improve the electrical property of the polymer [77].

The synthetic route is shown in **Scheme 3.6**. The details of the reaction procedures are discussed in section 2.2.2.4. Briefly, in the first step, 2-ethylhexyl 1H-pyrrole-1-carboxylate (1) was synthesized using the same method as in step one of the synthetic routes for Yamamoto polycondensation. Then, (1) was dissolved in chloroform and mixed with APS or

APS-surfactant aqueous solution to initiate the oxidative polymerization under different conditions to synthesize the desired polymer (2). The surfactant used in all the experiments was sodium dodecyl sulfate. The reaction conditions are summarized in **Table 3.1**. The ratio of the monomer and APS was 1:1, and the ratio of water and chloroform as solvent was 1:1 for all the experiments.

Table 3.1. Reaction Conditions for Oxidative Polymerization of monomer (1) with APS as Oxidizing Agent

Experiment	Concentration of the Monomer Chloroform Solution (M)	Reaction Temperature (°C)	Surfactant Concentration (M)	Reaction Time (h)
1	0.1	25	0.0225	24
2	0.1	65	0.0225	24
3	0.1	65	0.0225	24
4	0.2	65	0.0225	24
5	0.5	65	0.0225	24
6	0.5	65	0.0225	24
7	0.5	65	0.0225	48
8	0.5	65	0.0225	72
9	0.5	65	0	48

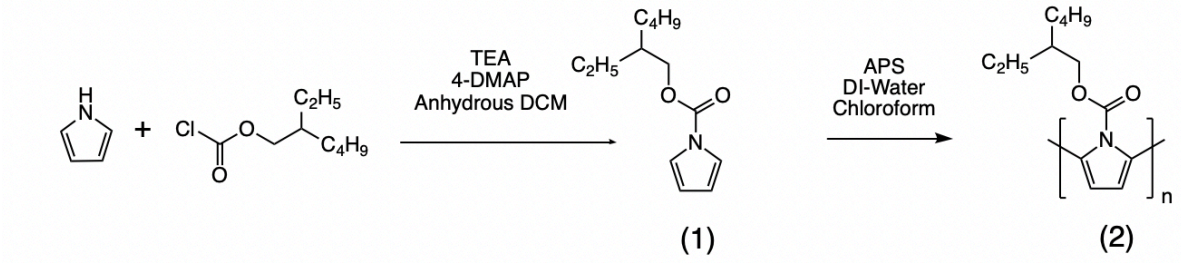

Scheme 3.6.

3.3.1.2. Result and Discussion

The influences of the temperature, starting material concentration, reaction time, and surfactant usage on the polymerization reaction were explored through experiments 1-9. Unfortunately, except for a yield of 5% (10 mg) of the solid product obtained from experiments 7 and 8, all the other experiments failed to obtain any precipitate after working

up the reaction with methanol. Except for experiment 1, all the methanol solutions had a yellow to brown colour after filtration, indicating some soluble oligomer may have been formed. The colour of the methanol solution after filtration tended to become darker with higher reaction temperature, higher concentration (although no significant difference was found between monomer concentrations of 0.2 M and 0.5 M), and longer reaction time (although 48 hours and 72 hours had no significant difference), indicating higher temperature, higher monomer concentration, and longer reaction time were beneficial for the formation of an oligomer with a higher number of repeating units. Adding surfactant had less influence on this reaction since no significant difference was observed between experiments 8 and 9. Eventually, the optimized reaction conditions were applied to experiment 8 with the reaction temperature of 65 ℃, 48 h reaction time, and the addition of 0.0225 M of surfactant, resulting in some black solid after filtration, indicating some higher molecular weight polymer formed. In addition, the obtained black solid was partially soluble in chloroform, indicating that part of the sidechain on the polymer backbone was broken. However, due to the very low yield of this reaction, the product obtained was not enough for further characterization.

Since the reaction is a two-phase reaction, the oxidizing agent $S_2O_8^{2-}$ may not sufficiently interact with the monomer which is only soluble in the chloroform phase. Thus, it may lead to the polymerization reaction proceeding reluctantly, resulting in a lower yield and molecular weight. In addition, the pK_b of the $S_2O_8^{2-}$ anion is 17.5 and the pK_b of HSO_4^- is 12.01. Therefore, the aqueous phase co-engaging $S_2O_8^{2-}$ and HSO_4^- is acidic. Moreover, in an aqueous solution, $S_2O_8^{2-}$ can also undergo a hydrolysis reaction, as shown in formula (3) [91]:

$$S_2O_8^{2-} + H_2O \rightarrow \frac{1}{2}O_2 + 2SO_4^{2-} + 2H^+ \quad (3)$$

which releases the strong acid H_2SO_4. This will increase the acidity of the aqueous phase, but the carbamate sidechain is sensitive to acidic conditions. Consequently, the acidic environment ruins the carbamate sidechain, as evidenced by the partial solubility of the obtained solid in chloroform. This likely explains the low yield of the reaction.

3.3.1.3. Conclusions

After our best efforts, the desired polymer was not able to be synthesized with an acceptable yield by using APS as the oxidizing agent. Insufficient interaction of the oxidizing agent and the acidic environment created by APS are believed to be the reasons for the unsuccessful polymerization. Other polymerization routes should be attempted to synthesize PEPC.

3.3.1.4. Experimental Section

Materials

All the chemicals used in this project were purchased from Sigma-Aldrich, Fluka VWR, TCI, and Armstrong. Solvent used in the synthesis procedure were analytical grade and anhydrous or used as received. All column chromatography was conducted using silica gel (230-400 mesh) slurries purchased from the University of Waterloo.

Synthesis of 2-ethylhexyl 1*H*-pyrrole-1-carboxylate (1)

To a flask charged with pyrrole (0.5031g, 7.5 mmol), triethylamine (0.5692g, 5.6 mmol), and 4-(dimethylamino)pyridine (0.6872g, 5.6 mmol) was added anhydrous DCM (2.5 mL), and the resulting solution cooled to 0 °C, under N_2 atmosphere. 2-Ethylhexyl chloroformate (1.0838g, 5.6 mmol) was added slowly and the reaction mixture was then stirred at room temperature for 16 h. The reaction mixture was extracted with diethyl ether (3 × 5 mL), and the combined extracts were washed with aqueous potassium bisulfate, aqueous sodium bicarbonate and water. The organic phase was then dried over sodium sulfate and concentrated in vacuo, followed by column chromatography (eluent, pure hexane followed by hexane: DCM = 5:1 followed by hexane:ethyl acetate =10:1) to afford the product (transparent oil). ^{1}H NMR (300 MHz, chloroform-*d* δ/ppm): 7.25 (t, 2H), 6.23 (t,2H) 4.25 (m, 2H)

Polymer Synthesis

Synthesis of Poly(2-ethylhexyl 1*H*-pyrrole-1-carboxylate)

2-ethylhexyl 1*H*-pyrrole-1-carboxylate monomer was dissolved in chloroform. An aqueous solution of APS and surfactant was then quickly added to the monomer solution under

vigorous magnetic stirring following the reaction conditions summarized in Table 2.2.3. The reaction mixture was cooled to room temperature and poured into 150 mL methanol and stirred, which was followed by filtration to afford the product as a black powder.

3.3.2. Synthesis of Poly(2-ethylhexyl 1*H*-pyrrole-1-carboxylate) with $FeCl_3$

3.3.2.1. Introduction

Ferric chloride is another commonly used oxidizing agent for synthesizing polypyrrole and its derivatives. Unlike APS which must be used in an aqueous medium, ferric chloride can be applied to an organic solution directly to achieve the polymerization. There are many examples of using $FeCl_3$ in pure organic solutions to polymerize pyrrole derivatives oxidatively. Several representative examples are shown in **Scheme 3.7** and **3.8**.

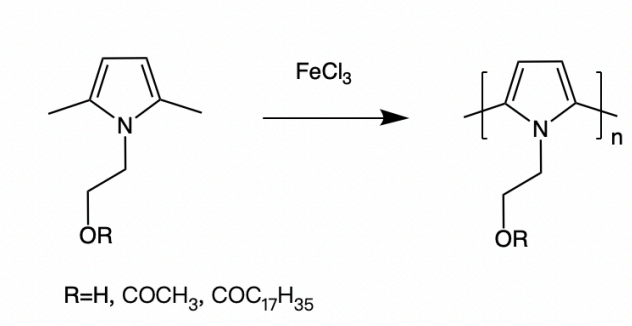

Scheme 3.7. Polymerization of N-Alkylpyrroles with Ferric Chloride. The solvent used was nitromethane [92].

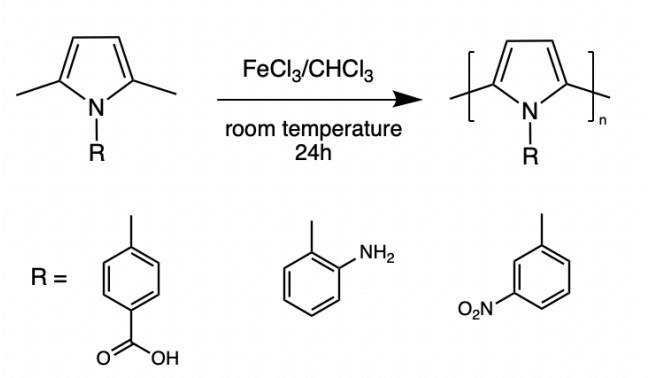

Scheme 3.8. Polymerization reactions of N-(p-benzoic acid) pyrrole (NpbPy), N-(o-aminophenyl) pyrrole (NoaPy) and N-(m- nitrophenyl) pyrrole (NmnPy) [93]. The solvent used was chloroform.

Applying $FeCl_3$ directly to the organic solution provides a possible way to address the problem that occurred with APS in that the two-phase polymerization did not permit sufficient interaction between the oxidizing agent and the monomer. In addition, since no water is involved in the reaction, using anhydrous $FeCl_3$ can minimize the potential of ruining the carbamate sidechain by an acidic environment generated in the polymerization process, which occurred in the reaction using APS. A synthetic route with $FeCl_3$ as the oxidizing agent was designed based on this knowledge. The synthetic route is shown in **Scheme 3.9**.

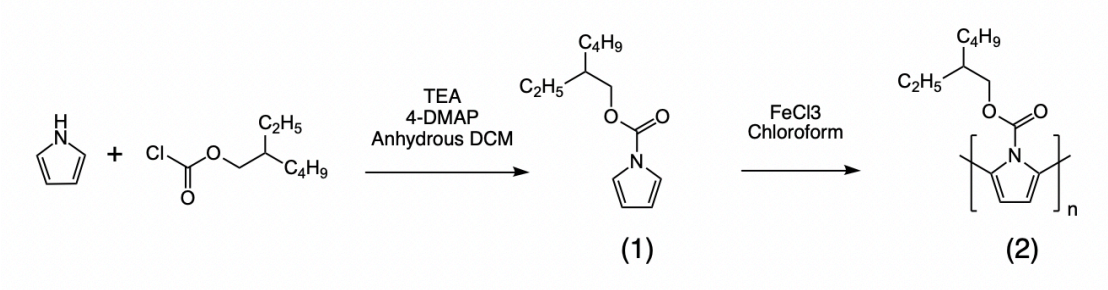

Scheme 3.9.

Briefly, (1) was synthesized using the same method described in section 2.2.2.4. Compound (1) was then dissolved in anhydrous chloroform under an N_2 atmosphere, and the anhydrous $FeCl_3$ powder was added to afford the desired polymer (2).

One item of interest in this approach is the purification procedure. When $FeCl_3$ is used as the oxidizing agent for the polymerization of pyrrole, it can also serve as a dopant to the polymer [77]. Thus, the crude polymer obtained through this method is already doped; therefore, a de-doping step is needed in the purification and isolation of the polymer. Herein, the influence of two types of de-doping agents, TEA, and aqueous ammonia, was also studied.

3.3.2.2 Results and Discussions

To optimize the yield of the product, different reaction conditions were explored. In addition, due to the carbamate sensitivity to acid, the effects of adding base as a neutralizing agent to trap the acid generated during the polymerization process was also studied. The base used was TEA.

a. Influence of reaction temperature, monomer concentration, and de-doping agent

Experiments 1-6 were conducted to evaluate the influence of reaction temperature, monomer concentration, and de-doping agent on product yield. Comparing experiments 1 and 2, the yield slightly increased with increasing monomer concentration. The temperature was raised to 70 ℃ in experiment 3, which was above the solvent's boiling point (chloroform), and the yield increased from 7% to 10% compared to 25 ℃ in experiment 2. Using aqueous ammonia to de-dope the crude polymer resulted in a higher yield than using TEA in experiment 4. In experiments 4 – 7, the monomer concentration increased in sequence from 0.02M to 0.09M. The highest yield of 45% was obtained from experiment 5 with a monomer concentration of 0.045 M. Higher or lower than this concentration resulted in a lower yield. This series of experiments showed that higher reaction temperature and using aqueous ammonia as a de-doping agent were beneficial for improving yield. The optimized monomer concentration was 0.045 M. Thus, an optimized reaction condition was determined as of experiment 5. The reaction conditions and yields are summarized in **Table 3.2**.

Table 3.2. Reaction Conditions for Oxidative Polymerization of Monomer (1) Using Ferric Chloride as Oxidizing Agent

Experiment	Concentration of the Monomer Chloroform Solution (M)	Reaction Temperature ℃	Reaction Time (h)	De-dope Reagent	Yield (%)
1	0.01	25	24	TEA	5
2	0.02	25	24	TEA	7
3	0.02	70	24	TEA	11
4	0.02	70	24	Aqueous Ammonia	13
5	0.045	70	24	Aqueous Ammonia	45
6	0.06	70	24	Aqueous Ammonia	35
7	0.09	70	24	Aqueous Ammonia	29

b. Influence of adding base as protecting agent

TEA was added at the beginning of the polymerization to trap any acid generated during the process. The reaction temperature and time, monomer concentration, and de-doping agent were kept the same as the optimized conditions in experiment 5. Other reaction conditions are summarized in **Table 3.3** Experiment 5 is included in **Table 3.3** as a reference.

Table 3.3. Summary of the Experiments Exploring the Influence of Adding Base

Experiment	Molar Ratio of TEA: HCl Generated in Theory	Yield (%)
5	0	45
7	1:1	5.3
8	4:1	0

Comparing experiments 5, 7, and 8, the yield significantly decreased with the increase of TEA concentration. This can be explained by the neutralization of $FeCl_3$ by TEA. According to Niemi et al., polymerization using $FeCl_3$ as oxidizing agent must occur when $FeCl_3$ exists as crystals [94]. The Fe(III) ions located on the surface of the crystal are the active sites for the polymerization (**Figure 2.12**). Each of the Fe(III) ions on the surface are only bonded with a chloride ion and have an empty orbital, permitting them to act as strong Lewis acids. TEA is a Lewis base that can donate electrons. Thus, it can bond with the surface Fe(III) ions, utilizing the free orbital, and consequently deactivating the active site. This explains the low yield when TEA was applied in the polymerization process.

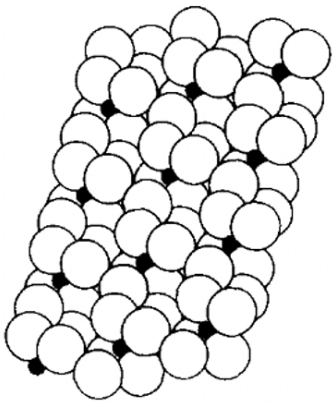

Figure 3.2. Crystals Structure of ferric chloride on the crystal surface [94].

c. Influence of solvents

From the results of experiment 1 – 3, it was found that the yield increased with increasing reaction temperature. The boiling point of chloroform is 61.2 ℃ under standard temperature and pressure. Thus, the highest temperature that can be applied to the reaction system is 61.2 ℃. To investigate if the yield could be further improved with evenhigher temperatures, dimethylformamide (DMF) was used as the solvent because it has a higher boiling point of 153 ℃. The reaction conditions are summarized in **Table 3.4**, and all the other reaction conditions except those listed in the table were the same as experiment 5.

Table 3.4. Summary of the Experiments Exploring the Influence of Solvents

Experiment	Solvent	Reaction Temperature ℃	Yield (%)
5	Chloroform	70	45
9	DMF	100	0

By using DMF as the solvent in an elevated temperature of 100℃, the yield dropped dramatically to zero, indicating the polymerization cannot proceed in DMF. This could result from the Fe(III) ion being deactivated. As mentioned previously, the Fe(III) ions

are only active on the surface of the $FeCl_3$ crystal for initiation of the polymerization. In chloroform, the $FeCl_3$ is partially soluble, and many $FeCl_3$ exist in crystal form; thus, the active Fe(III) ion is abundant. However, in DMF, $FeCl_3$ can form a $FeCl_3$-DMF complex; therefore it does not exist in the form of crystal $FeCl_3$ (**Scheme 3.10**) [95]. Thus, the active Fe (III) ions are insufficient, and the polymerization cannot be initiated.

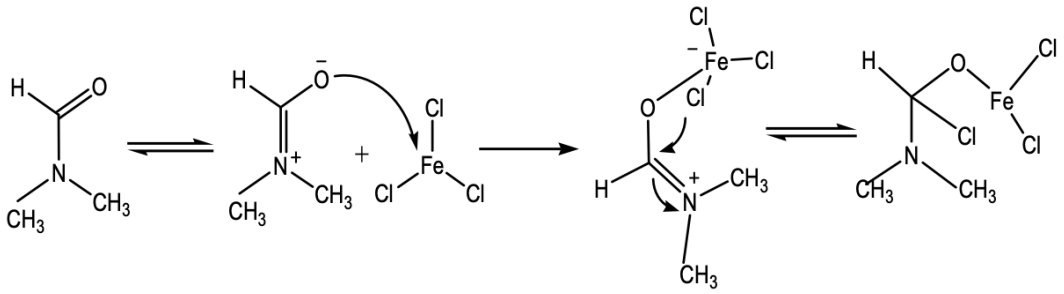

Scheme 3.10. Mechanism of formation of the $FeCl_3$-DMF complex [95].

3.3.2.3. Conclusions and Future Works

By using oxidative polymerization utilizing $FeCl_3$ as the oxidizing agent, the desired polymer, Poly(2-ethylhexyl 1H-pyrrole-1-carboxylate), was synthesized in a reasonable yield of 45%. The optimized reaction conditions were determined. Aqueous ammonia can be used as a de-doping agent to increase the yield. This synthetic method may be applied to synthesize other pyrrole-based polymers.

3.3.2.4. Experimental Sections

Materials

All the chemicals used in this project were purchased from Sigma-Aldrich, Fluka VWR, TCI, and Armstrong. Solvent used in the synthesis procedure were analytical grade and anhydrous or used as received. All column chromatography was conducted using silica gel (230-400 mesh) slurries purchased from the University of Waterloo.

Synthesis of 2-ethylhexyl 1*H*-pyrrole-1-carboxylate (2)

The synthesis procedure is same as described in section 2.2.2.4.

Polymer Synthesis

Synthesis of Poly(2-ethylhexyl 1*H*-pyrrole-1-carboxylate) (PEPC)

2-ethylhexyl 1*H*-pyrrole-1-carboxylate (0.2g) was dissolved in 20 mL $CHCl_3$. The solution was maintained in an inert N_2 atmosphere and under magnetic stirring. Anhydrous $FeCl_3$ (0.4 g) was quickly added into the solution upon stirring. After polymerization time of 24 h at 70 °C , the reaction mixture was cooled to room temperature and aqueous ammonia was added to the reaction mixture to de-dope the polymer. The precipitated polymer was then washed with methanol until the filtrate was colourless. Finally, the polymer was dried under vacuum environment.

3.4. Characterization of Poly(2-ethylhexyl 1*H*-pyrrole-1-carboxylate)

3.4.1. Solubility and Processability Test of PEPC

PEPC was found to be decently soluble in different organic solvents, including chloroform, acetone, and dichloromethane (DCM). A concentration of 25 mg/mL PEPC solution could be made using the solvents mentioned above, and by spin coating, a 50-60 nm PEPC film could be deposited on glass or SiO_2-Si wafer (will be discussed in detail later) substrate, which satisfies the conductivity requirements for sensor application [1,32].

3.4.2. Thermal Removal of Carbamate Sidechain

As stated previously, this project aims to synthesize a polypyrrole-based polymer with a thermally removable carbamate sidechain to make it more soluble for easy processability and be able to recover the high conductivity of PPy. Thus, the thermal properties of the PEPC were investigated.

The thermal properties of PEPC and the carbamate sidechain on the PEPC backbone were studied using thermogravimetric analysis (TGA). As previously stated, thermal decomposition can occur in the alkyl carbamate chain at a relatively mild temperature of around 100-250 ℃. In addition, doped polypyrrole may decompose starting at 150℃ if heated in air [96, 97]. Thus, inert gas can be introduced to reduce the decomposition. Based on this knowledge, experiments 1-3 were designed. The polymer was heated at a heating rate of

10 ℃ min^{-1} from 25℃ and held at 150℃ or 250℃ for 30 minutes, then heated at a rate of 10 ℃ min^{-1} to 600℃ under N_2 or air atmosphere. The measurement conditions are summarized in **Table 3.5**. The results are shown in **Figure 3.3**.

Table 3.5. Measuring Conditions for TGA

Experiment	Holding Temperature (℃)	Heating Environment
1	150	Air
2	250	N2
3	250	Air

(a)

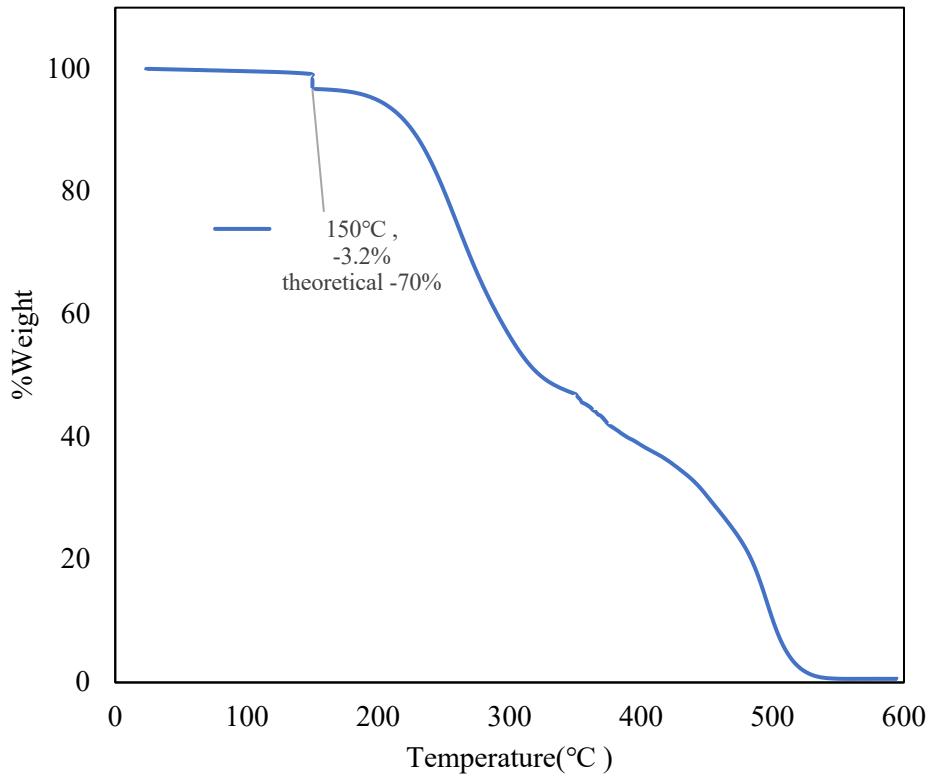

(b)

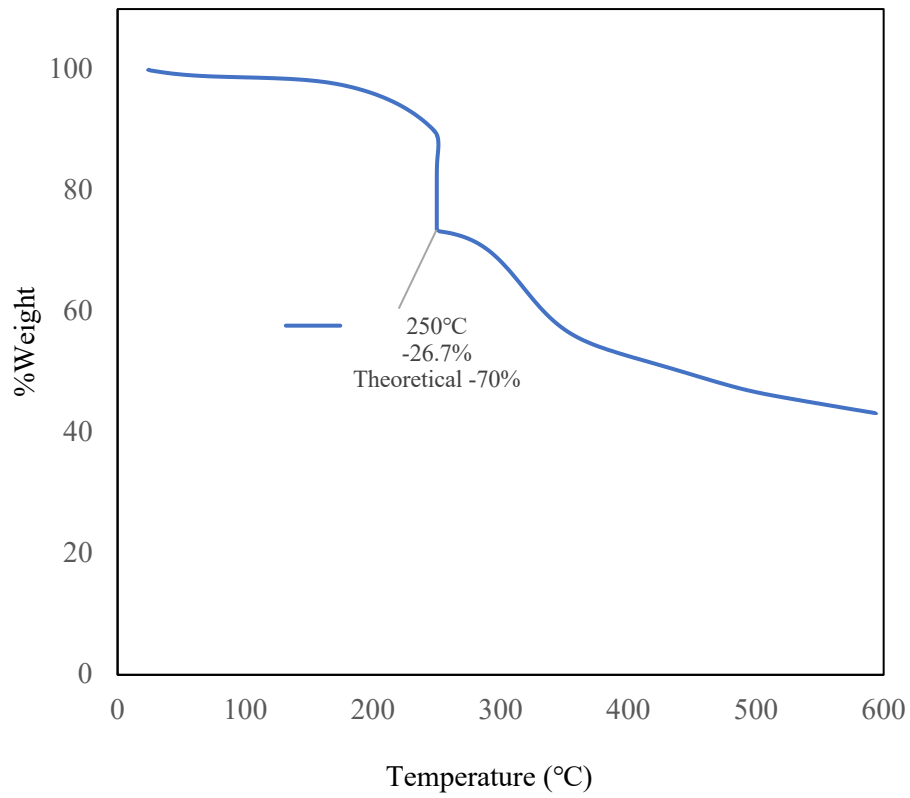
100
80
60
40
20
0
%Weight
0
100
200
300
400
500
600
Temperature (°C)
250°C
-26.7%
Theoretical -70%

(c)

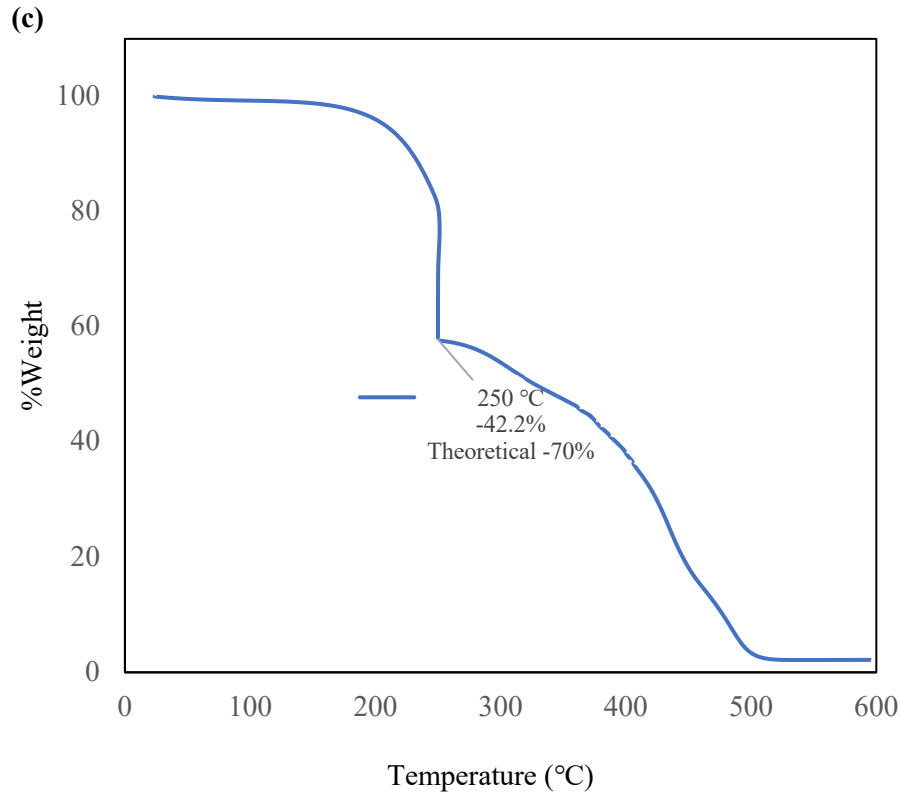
100
80
60
40
20
0
%Weight
0
100
200
300
400
500
600
Temperature (°C)
250 °C
-42.2%
Theoretical -70%

Figure 3.3. TGA diagram for **(a)** experiment 1, PEPC heated under air holding at 150℃ for 30 minutes **(b)** experiment 2, PEPC heated under N_2 holding at 250℃ for 30 minutes and **(c)** experiment 3, PEPC heated under air holding at 250℃ for 30 minutes.

As shown in **Figure 3.3 (a)**, 3.7% weight loss occurred at 150 ℃ during the 30 minute holding time, which was significantly lower than the theoretical weight loss of 70% if all the 2-ehthylhexyl carbamate sidechains were removed from the sample, indicating the thermal decomposition of the carbamate sidechain hardly occurred. When the holding temperature was raised to 250 ℃, under a nitrogen atmosphere, as shown in **Figure 3.3 (b)**, during the 30 minutes holding time, 26.7% weight loss occurred, which was still much lower than the theoretical 70% weight loss, indicating the carbamate sidechain was only partially removed from the sample. Finally, the sample was heated at 250℃ held for 30 minutes under an air environment. As shown in **Figure 3.3 (c)**, 42.2% weight loss occurred in the sample, which was still lower than the theoretical 70% weight loss, though it was higher than in experiments 1 and 2. TGA results suggested that the degree of thermal decomposition of the 2-ethylhexyl carbamate sidechains on PEPC increases with the elevated temperature and heating under air facilitates sidechain removal compared to heating under nitrogen. However, the carbamate sidechain was not totally removed even under heating at 250℃ in air.

FTIR spectroscopy was used to further evaluate the removal of the carbamate sidechain and the thermal stability of the PEPC polymer. **Figure 3.4 (a)** shows the whole FTIR spectrum of PEPC with the main characteristic peaks labeled on the diagram. The peaks at 730 cm^{-1}, 770 $cm^{-1,}$ and 1020 cm^{-1} correspond to pyrrole ring C-H out-of-plane bending [98–105]. The peaks at 1116 cm^{-1} and 1271 cm^{-1} represent the C-O stretching of the carbamate chain. The peak at 1407 cm^{-1} is attributed to the C-N bond stretching between the carbamate chain and the pyrrole ring nitrogen. Peaks at 1460 cm^{-1} and 1510 cm^{-1} correspond to the pyrrole ring [98–105]. The peak at 1460 cm^{-1} represents the pyrrole ring C-N stretching, C-C-N inter-ring and in-plane bending and the peak at 1510 cm^{-1} represents the pyrrole ring C=C-C in-ring stretching, C=C intra-ring stretching and C-C inter-ring stretching. The peaks at 1460 cm^{-1} and 1510 cm^{-1} show the conjugated structure of PEPC. The peak at 1720 cm^{-1} is a characteristic peak for the 2-ethylhexyl carbamate sidechain because it represents the C=O stretching and only the

carbamate sidechain contains the C=O group in PEPC. The peaks at 2864 cm^{-1},2929 cm^{-1}, and 2960 cm^{-1} correspond to aliphatic C-H stretching, which are also the characteristic peaks for the carbamate sidechain since only the sidechain in PEPC contains aliphatic C-H. The broad peak at 3375 cm^{-1} corresponds to N-H stretching, indicating part of the sidechain was removed in the polymerization process thus, some of the N-H bonds were exposed. The FTIR peak information is summarized in **Table 3.6.**

Table 3.6. FTIR Peaks of Assignments for PEPC

Peak Position (cm^{-1})	Description
3375	N-H Stretch
2864 2929 2960	Aliphatic C-H Stretch
1720	Carbamate C=O Stretch
1510	Py ring C=C-C in ring, including C=C intra-ring and C-C inter-ring stretch
1460	Py Ring C-N stretch C–C–N inter-ring in-plane bending
1407	O=C-N
1271 1116	C-O stretching
1020	C–H ring out-of-plane bending
770 730	C–H ring out-of-plane bending

Figure 3.4 (b)- (f) showed the FTIR spectra of PEPC before and after annealed comparison from experiment b-f. In each experiment, the same sample was used before and after annealing to quantitively determine the removal of carbamate sidechain. The annealed

conditions are summarized in **Table 3.7**. The annealing time for each of the experiments was 30 min.

Table 3.7. Annealing Conditions for FTIR Sample

Experiment	Anneal Temperature (℃)	Atmosphare
b	150	Air
c	150	Nitrogen
d	250	Nitrogen
e	250	Air
f	200	Air

The peaks at 1720 cm^{-1} and ~3000 cm^{-1} were used to evaluate the removal of the carbamate sidechain since these peaks are characteristic peaks of the sidechain and exclusive to the polypyrrole backbone of PEPC. As stated above, the peak at 1720 cm^{-1} is the carbonyl group peak of C=O of the carbamate chain, and the peaks at ~3000 cm^{-1} are the peaks of aliphatic C-H, which only originates from the sidechain. Here, peak areas were calculated by the integration of the peaks. As shown in **Figure 3.4 (b)**, the peak at 1720 cm^{-1} has a peak area of 31.2 and 26.3 before and after annealing, respectively, indicating that 15.7% of the sidechain was removed. The peaks at ~3000 cm^{-1} had peak areas of 68.9 and 67.1 before and after annealing, respectively, which corresponds to a 2.6% drop. The difference between the peak area drops of aliphatic C-H peaks and C=O peak is due to the product containing 2-ethylhexyl moieties from the thermolysis of carbamate chain, including 2-ethylhexanol, which were trapped in the sample, and the weight lost at this condition is largely due to the release of carbon dioxide. The weight loss was based on 15.7% sidechain removal and the correlated release of carbon dioxide was calculated to be 3.1%, which is well-matched with the TGA data (3.2%).

As shown in **Figure 3.4 (c)**, the peak at 1720 cm^{-1} has a peak area of 31.2 and 26.3 before and after annealing, respectively, indicating that 15.7% of the sidechain was removed. The peaks at ~3000 cm-1 had peak areas of 68.9 and 66.8 before and after annealing, respectively, which

corresponds to a 3.0% drop. As stated above, the difference in the peak area of C=O and aliphatic C-H peaks is due to the trapping of the thermolysis product(s). The results of experiment c were very close to those of experiment b, indicating no significant difference in the thermal decomposition of the 2-ethylhexyl carbamate sidechain of PEPC under nitrogen or air at 150 ℃. Moreover, under both conditions, only ~15% of the sidechain was removed, suggesting that 150 ℃ is inefficient for the thermal removal of the sidechain of PEPC.

A higher temperature was used to evaluate the thermal removal of the carbamate sidechain of PEPC. As shown in **Figure 3.4 (d)**, when annealed at 250 ℃ under nitrogen, the peak at 1720 cm^{-1} had a peak area of 308.4. The exact peak before annealing has a peak area of 406.9. By comparison, it can be determined that 33.1 % of the sidechain was removed under this condition. The peaks at ~3000 cm^{-1} had peak areas of 970.2 and 667.8 before and after annealing, respectively, corresponding to a 31.2% drop, which matches with the peak at 1720 cm^{-1}, indicating that under this condition, the thermolysis products were no longer trapped in the sample. The weight loss calculated based on 33.1% of sidechain removal is 23.3%, which matches with the TGA data (26.7%). From **Figure 3.4 (d)**, it can be observed that the peak area of the peak at 1510 cm^{-1}, which corresponds to the pyrrole ring C=C-C stretching, had a 55.5% drop from 33.9 to 15.1 after annealing, indicating the C=C-C bond was partially degraded, and the polypyrrole backbone had already started decomposing. This explains the slightly higher weight loss shown by the TGA data than the calculated value only based on sidechain removal.

The same experiment was conducted under air and the result is shown in **Figure 3.4 (e)**. It can be observed that the peak at 1720 cm^{-1} has a peak area drop of 46.3%, from 502.4 to 269.9, after annealing of 30 min under air at 250℃, indicating 46.3% of the sidechain was removed under this condition. The peaks at ~ 3000 cm^{-1} had peak areas of 1039.4 and 477.4 before and after annealing, respectively, corresponding to a 54.0% drop, which matches the peak area drop of the 1720 peak. The percent weight loss based on ~50% of sidechain removal is calculated to be 35%, lower than the TGA value of 42.2%. This is due to the thermal decomposition of the polypyrrole backbone at a high temperature and without nitrogen gas protection, which can be confirmed by the FTIR peak at 1510 cm^{-1}. It can be clearly observed that after annealing, the peak at 1510 cm^{-1} is missing, indicating the decomposition of the

pyrrole ring. The more severe damage of the pyrrole ring under air than under nitrogen indicates that nitrogen does protect the polypyrrole backbone at some level. However, thermal decomposition was still observed when annealing under nitrogen at 250 ℃.

Since 250 ℃ was so high a temperature that it may ruin the polypyrrole backbone, a lower temperature of 200 ℃ was used to further explore the thermal removal of the carbamate sidechain. As shown in **Figure 3.4 (f)**, the peak area of the peak at 1720 cm^{-1} drops 17.8% from 853.5 before annealing to 702.0 after annealing, indicating 17.8% of the sidechain was removed. The aliphatic C-H peaks had a peak area drop of 21.7%, matched with the C=O peak. It can be observed that the peak area of the peak at 1510 cm^{-1} also drops 21.9%, indicating the pyrrole ring was partially ruined even at 200℃.

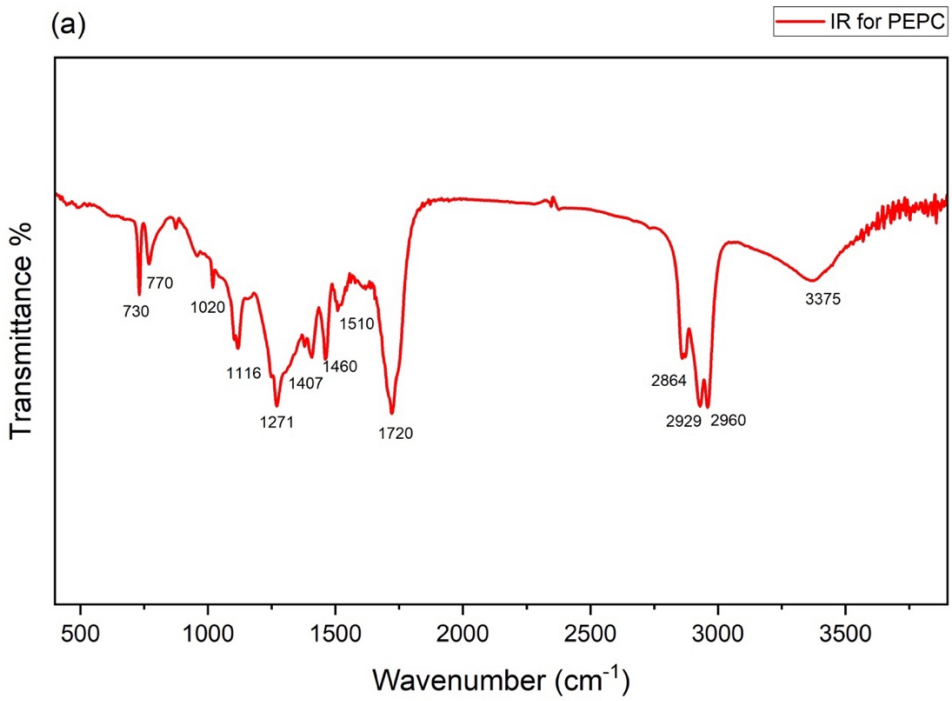

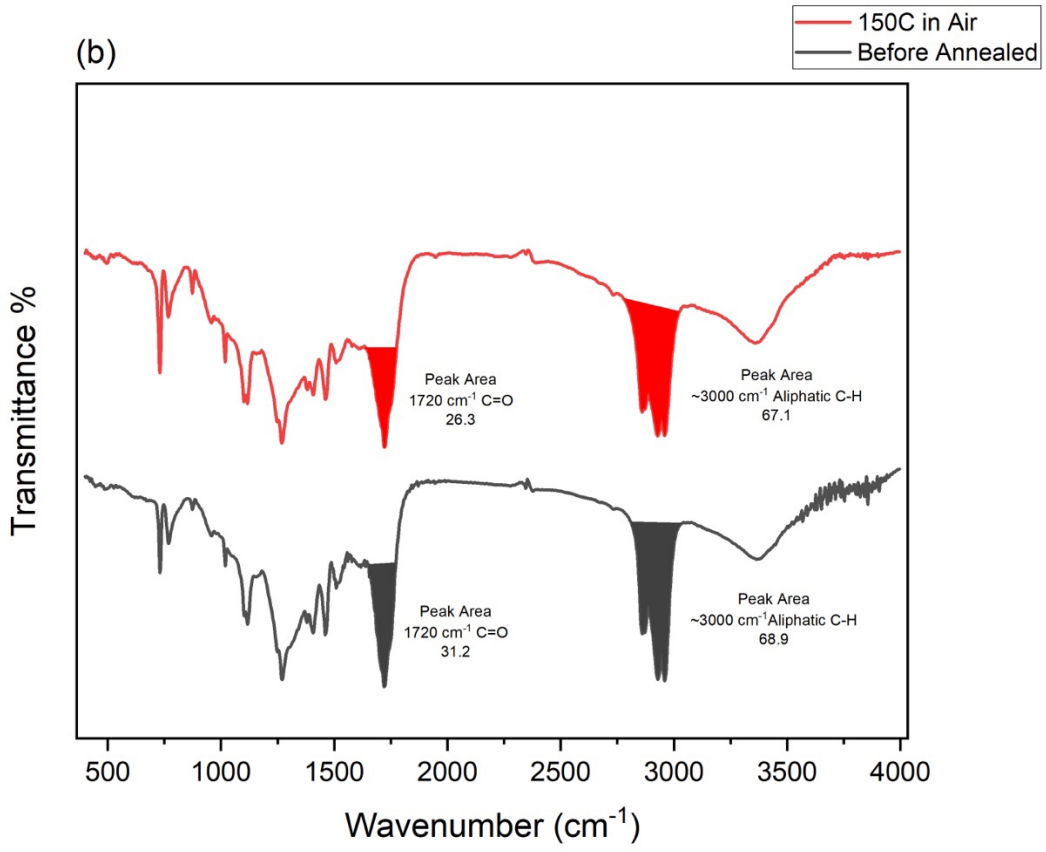
(b)
150C in Air
Before Annealed
Transmittance %
Peak Area
1720 cm-1 C=O
26.3
Peak Area
~3000 cm-1 Aliphatic C-H
67.1
Peak Area
1720 cm-1 C=O
31.2
Peak Area
~3000 cm-1Aliphatic C-H
68.9
500
1000
1500
2000
2500
3000
3500
4000
Wavenumber (cm-1)

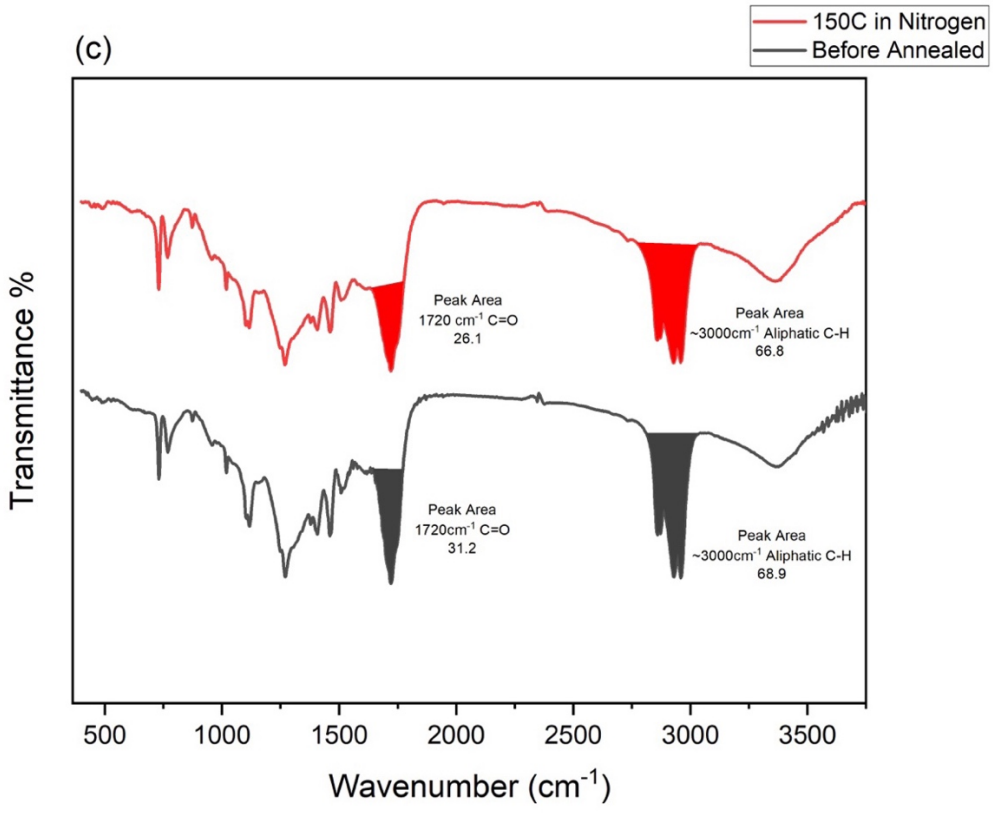
(c)
150C in Nitrogen
Before Annealed
Transmittance %
Peak Area
1720 cm-1 C=O
26.1
Peak Area
~3000cm-1 Aliphatic C-H
66.8
Peak Area
1720cm-1 C=O
31.2
Peak Area
~3000cm-1 Aliphatic C-H
68.9
500
1000
1500
2000
2500
3000
3500
Wavenumber (cm-1)

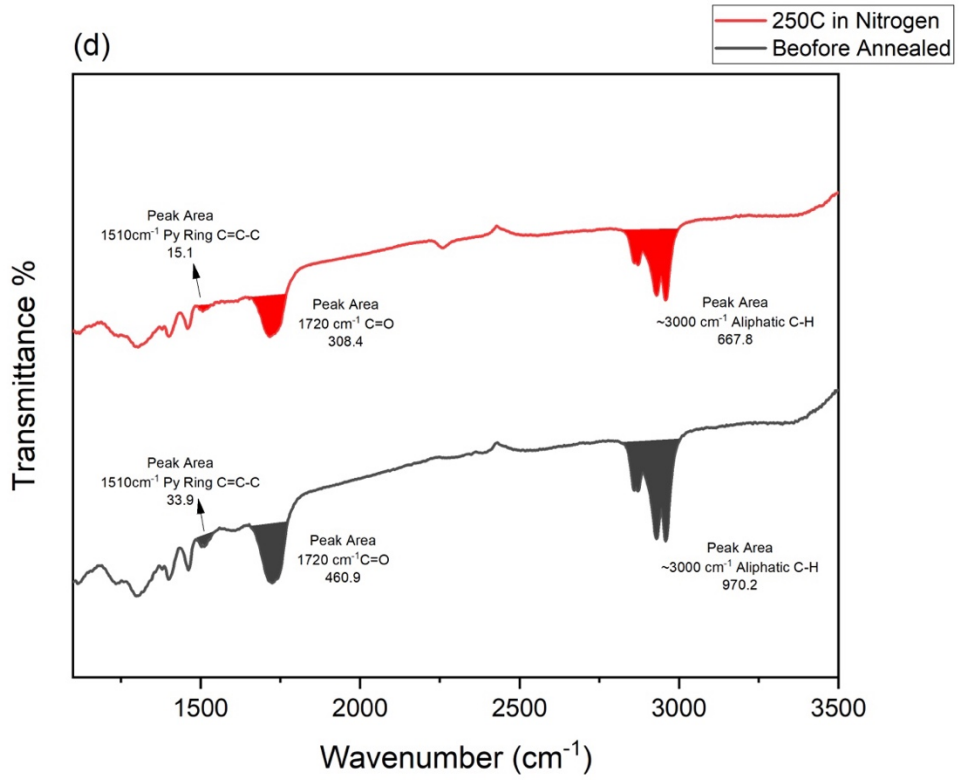
(d)
250C in Nitrogen
Beofore Annealed
Transmittance %
Peak Area
1510cm-1 Py Ring C=C-C
15.1
Peak Area
1720 cm-1 C=O
308.4
Peak Area
~3000 cm-1 Aliphatic C-H
667.8
Peak Area
1510cm-1 Py Ring C=C-C
33.9
Peak Area
1720 cm-1C=O
460.9
Peak Area
~3000 cm-1 Aliphatic C-H
970.2
1500
2000
2500
3000
3500
Wavenumber (cm-1)

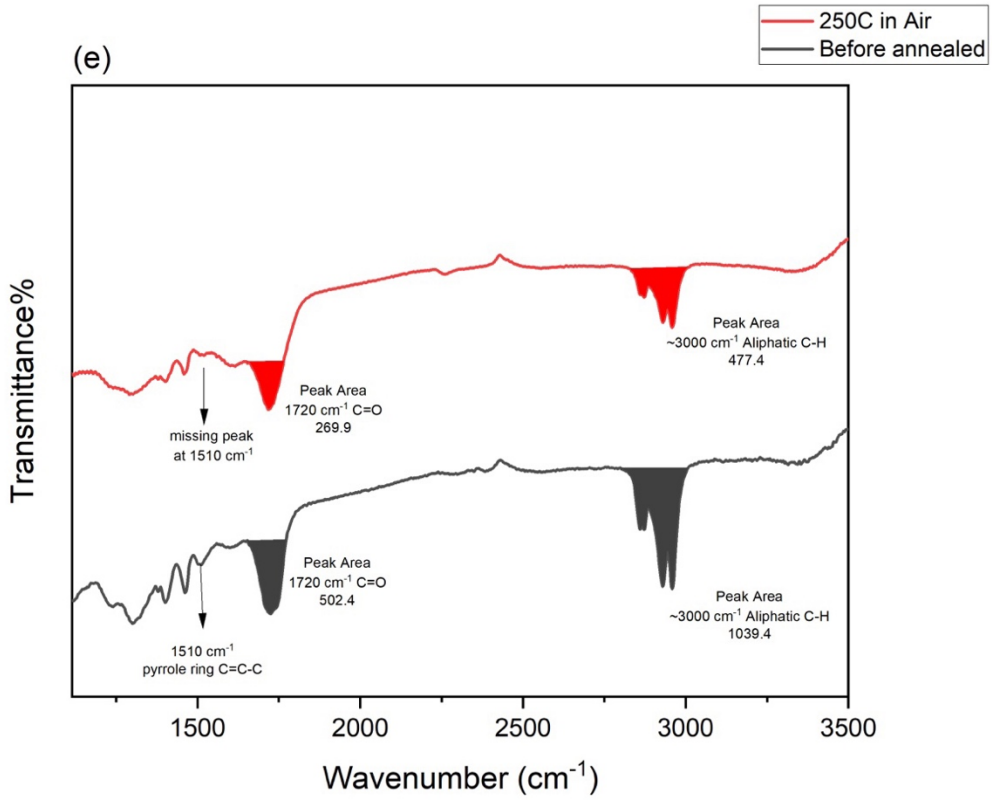
(e)
250C in Air
Before annealed
Transmittance%
Peak Area
~3000 cm-1 Aliphatic C-H
477.4
Peak Area
1720 cm-1 C=O
269.9
missing peak
at 1510 cm-1
Peak Area
1720 cm-1 C=O
502.4
Peak Area
~3000 cm-1 Aliphatic C-H
1039.4
1510 cm-1
pyrrole ring C=C-C
1500
2000
2500
3000
3500
Wavenumber (cm-1)

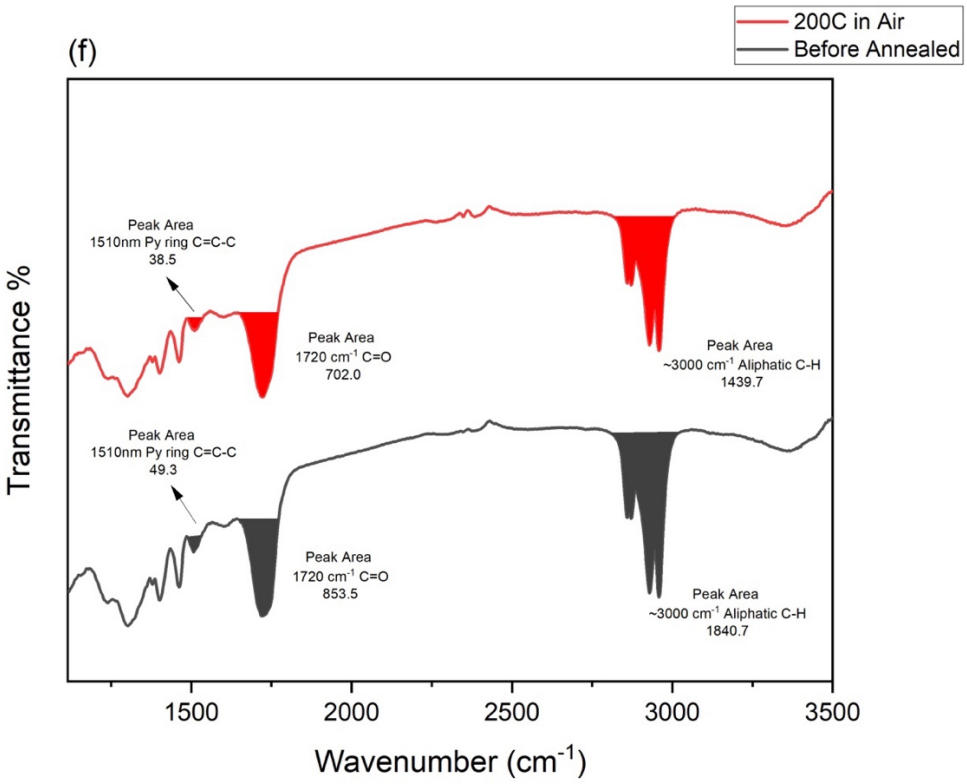

Figure 3.4. (a) PEPC FTIR Spectrum with peak assignments. **(b)** Comparison between before and after annealed at 150℃ in air. **(c)** Comparison between before and after annealed at 150℃ in nitrogen. **(d)** Comparison between before and after annealed at 250℃ in nitrogen. **(e)** Comparison between before and after annealed at 250℃ in air and **(f)** Comparison between before and after annealed at 200℃ in air.

Based on the TGA and FTIR results, it can be found that the carbamate sidechain of PEPC can be more readily removed at a higher temperature. However, a too-high temperature will damage the polypyrrole backbone and ruin the conjugated structure. Nitrogen can protect the polypyrrole backbone from decomposition to some extent; however, the sidechain is harder to remove in nitrogen as well. The decomposition of the polypyrrole backbone was significant even heated at 200 ℃ in air, and under this condition, the sidechain was only removed 17.8%. If annealed at 250 ℃ in air, the polypyrrole backbone was almost totally damaged; however, the sidechain was only half removed. Due to the trade-off relationship between the degree of sidechain removal and the degree of polymer backbone damage, the space to optimize the

annealing process is limited. Thermolysis does not appear to be an efficient method to remove sidechains from PEPC.

3.4.3. Acid Removal of the Carbamate Sidechain of PEPC

As previously stated, the alkyl carbamate chain is sensitive to acid. Thus, acid was applied to PEPC to study the carbamate sidechain removal under acidic condition. 2 mg of PEPC powder was stirred in 10 mL 5 M HCl methanol solution, under 50 ℃ for 2 hours, then washed with pure methanol and dried under vacuum for 24 hours. Another 2 mg of untreated PEPC was prepared. Both acid-treated and untreated PEPC powder was mixed with the same amount of dried KBr to make the FTIR sample pellet. The FTIR spectrum is shown in **Figure 3.5**.

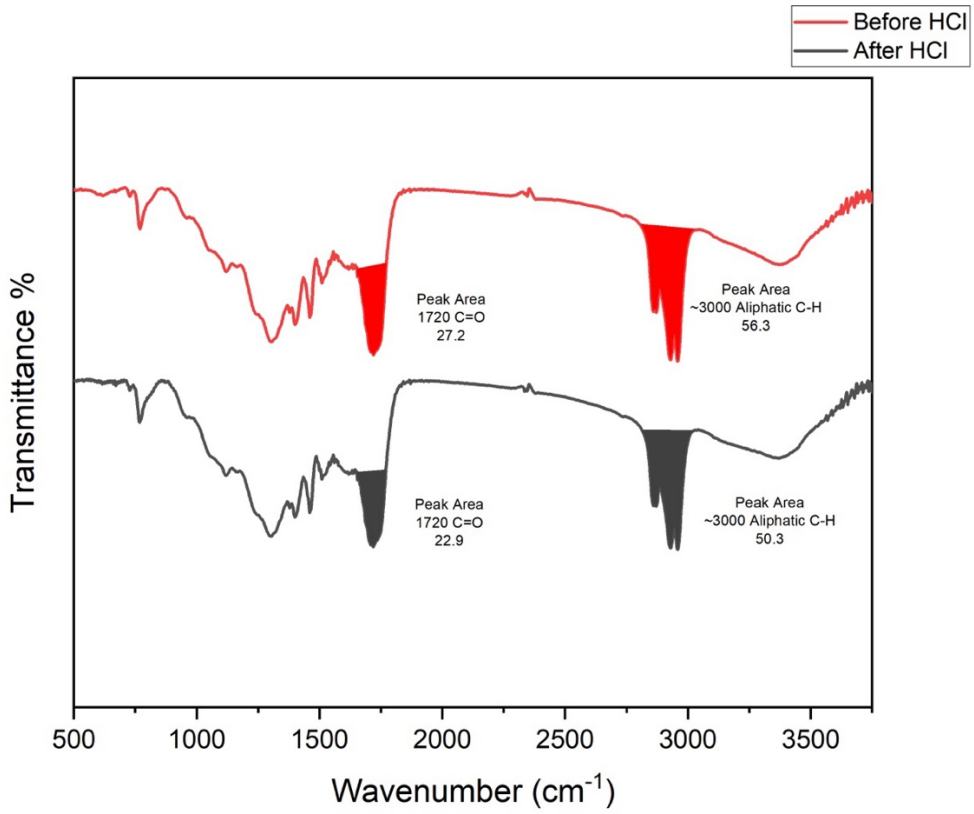

Figure 3.5. Comparison of the FTIR spectra for PEPC before and after treated with HCl.

As shown in **Figure 3.5**, the peak area of 1720 cm^{-1} peak is 27.2 and 22.9 before and after being treated with HCl, corresponding to a 15.8% removal of the carbamate sidechain after the acid was applied. The aliphatic C-H peak at ~3000 cm-1 had an 11% drop, from 56.3 to

50.3, after acid was applied, matching with the 1720 cm^{-1} peak area drop. To our surprise, based on the FTIR spectrum, it can be found that for PEPC, the carbamate sidechain was hard to remove even when acid was applied. It is known that the cleavage of a carbamate group under acidic conditions has a mechanism that involves the protonation of the carbamate oxygen, followed by a carbocation loss in the second step [30]. For the tert-butoxycarbonyl (Boc) group, tert-butyl carbocations will be generated under the acidic conditions, resulting in carbamic acid formation, and finally giving an amine by decarboxylation (**Figure 3.6**). The carbocation has a stability of 3°>2°>1°, and for the Boc group, the tert-butyl carbocation it releases has a tertiary structure; therefore, the acid cleavage of the Boc group readily occurs since tertiary carbocations are the most stable ones. 2-ethylhexyl, however, will release a primary carbocation if acid is applied. Compared with the Boc group, the acid cleavage of the 2-ethylhexyl carbamate will not be so feasible since the primary carbocation is less stable. This may explain why acid cleavage did not work well for PEPC.

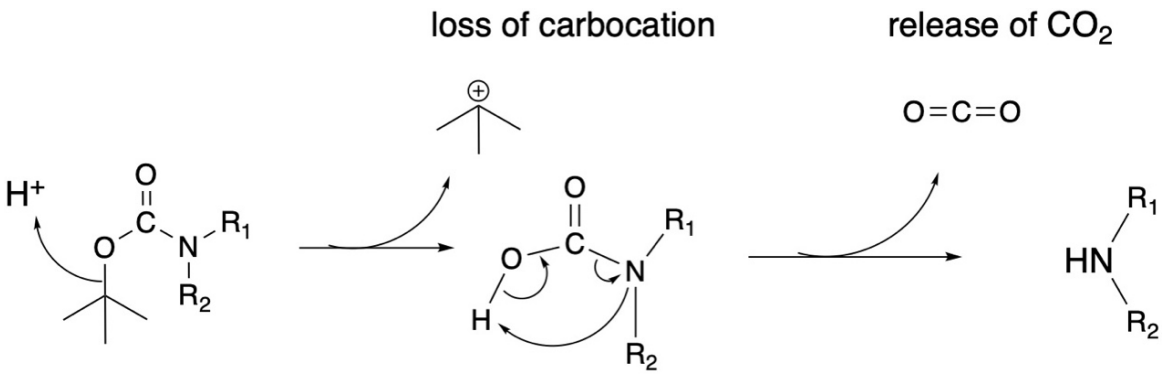

Figure 3.6. Mechanism of acid cleavage of Boc group.

3.4.4. Optical, Electrochemical Properties and Thin Film Crystallinity (UV, CV, XRD)

UV-Vis-Near-Infrared (NIR) spectroscopy was used to study the absorption properties of PEPC solution and thin films. The polymer thin films were fabricated through spin coating the 25 mg/ml solution in chloroform on a glass wafer. The optical properties of the thin films were investigated before and after annealing at 200 °C. As shown in **Figure 2.17**, the PEPC chloroform solution has a peak absorption (λ_{max}) of 242 nm and a broad absorption band with

an onset absorption (λ_{onset}) of 537 nm. PEPC thin films before and after annealing did not show an apparent peak absorption on the UV-vis-NIR spectra, probably because the peak absorption is below the measurement limit of the machine since noise started to show up below 240 nm. However, both films showed a broad absorption band. PEPC film before annealing had an onset absorption of 510 nm, and the film after annealing had a redshift onset absorption of 610 nm. The band gap (E_g) of PEPC film was calculated following the equation:

$$E_g = \frac{hc}{\lambda_{onset}}$$

where h is Planck's constant and c is the speed of light. The calculated band gap for PEPC thin film before and after annealing were 2.41 eV and 1.94 eV, respectively.

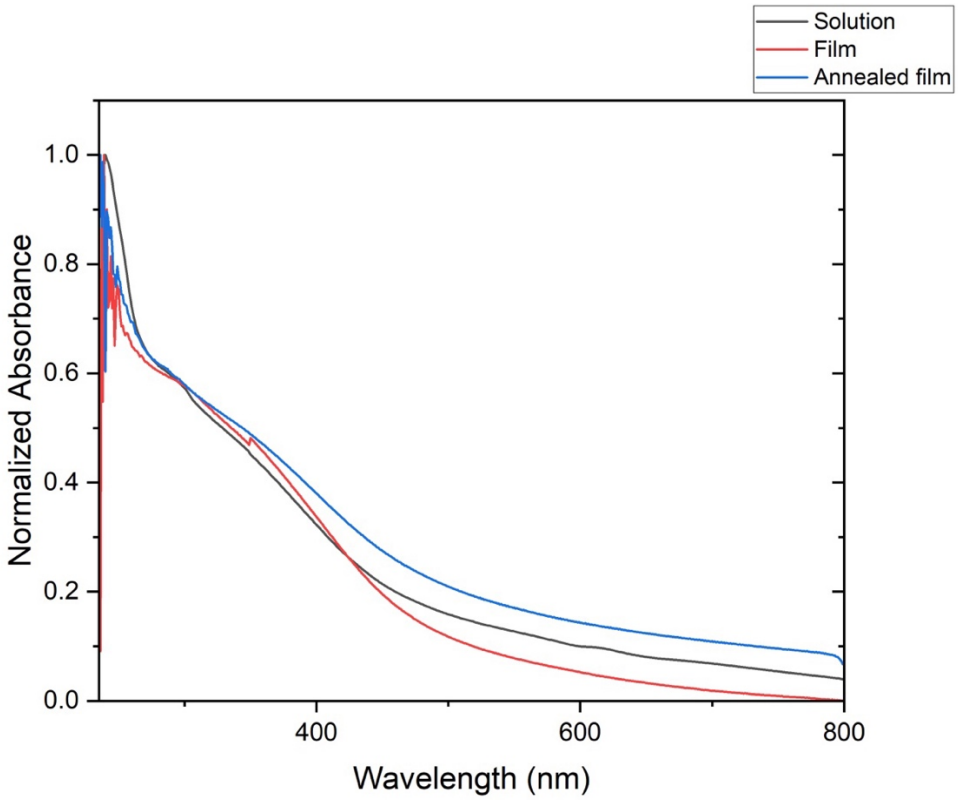

Figure 3.7. UV-vis-NIR spectra for PEPC solution (black line), film before annealed (red line) and film after annealed at 200℃ in air for 30 minutes (blue line).

The solvent resistance of PEPC film after annealing at 200℃ for 30 minutes in the air was evaluated by treating the polymer film with chloroform. Specifically, a ~60 nm PEPC film on a glass substrate was submerged in chloroform in a covered petri dish for 5 minutes. The glass

sample was then taken out, dried, and subjected to the UV-vis-NIR measurement. As shown in **Figure 3.8**, the absorption profile for untreated film and the chloroform-treated film was not superimposed, indicating the film did not have a good solvent resistance for chloroform. **Figure 3.9** compares the film before and after the solvent treatment, from which it can be clearly seen that the film was damaged after being soaked in chloroform. The insufficient solvent resistance was further evidence that the sidechain was not totally removed.

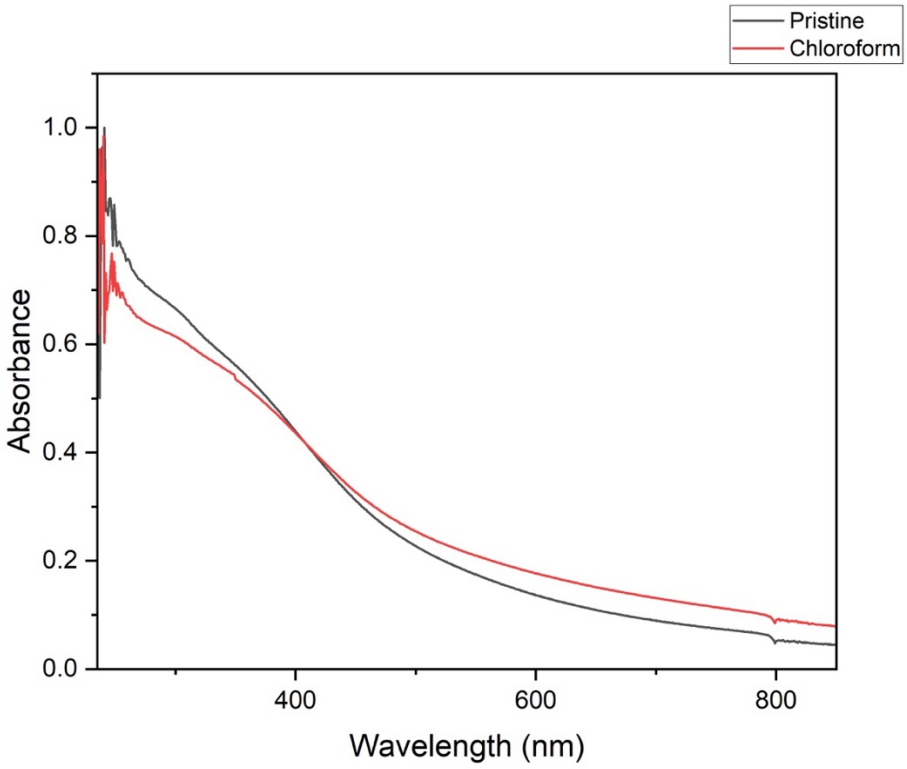

Figure 3.8. Solvent resistance test by UV-Vis-NIR spectra for annealed PEPC film before (black line) and after (red line) treated with chloroform.

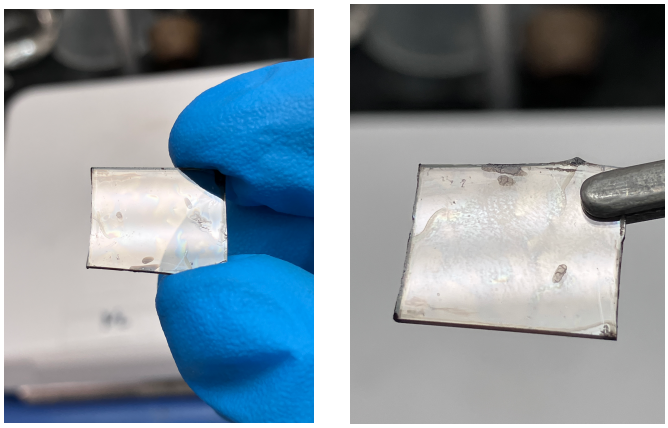

Figure 3.9. Film quality comparison before (left) and after (right) treated with chloroform.

Cyclic voltammetry (CV) measurements of PEPC thin film before and after annealing at 200℃ for 30 minutes in the air were conducted using transparent conductive indium tin oxide (ITO) glass as the substrate (**Figure 3.10**). PEPC exhibited a reversible oxidation process within the potential range from -1.20 to +1.20 V. The E_{HOMO} of PEPC was determined through CV measurement following the equation below, in which ferrocene with an E_{HOMO} of -4.8eV was used as the reference for the calculation [106] :

$$E_{HOMO} = -e\left[E_{ox}^{onset} - E_{\frac{FC}{FC^+}}\right] - 4.8eV$$

where e is the elementary charge and $E_{\frac{FC}{FC^+}}$ is the measured E_{ox}^{onset} of ferrocene from the same CV device. The E_{LUMO} was calculated through the difference between the E_g obtained from the UV-vis-NIR spectra and the calculated E_{HOMO} from CV. For PEPC before annealing, the onset oxidation potential was 0.70 V, corresponding to a HOMO level of -5.50 eV, and the calculated LUMO level was -3.10 eV. For PEPC after annealing, the onset oxidation potential was 0.25 V, corresponding to a HOMO level of -5.05 eV, and the calculated LUMO level was -3.11 eV. The optical and electrochemical properties of PEPC before and after annealing are summarized in **Table 3.7**.

Table 3.7. Optical and Electrochemical Properties of PEPC

Experiment Condition	λ_{max} (nm)	λ_{onset}	E_g(eV)	HOMO (eV)	LUMO (eV)
Before Annealed	242	510	2.41	-5.5	-3.1
After Annealed	N.A.	610	1.94	-5.05	-3.11

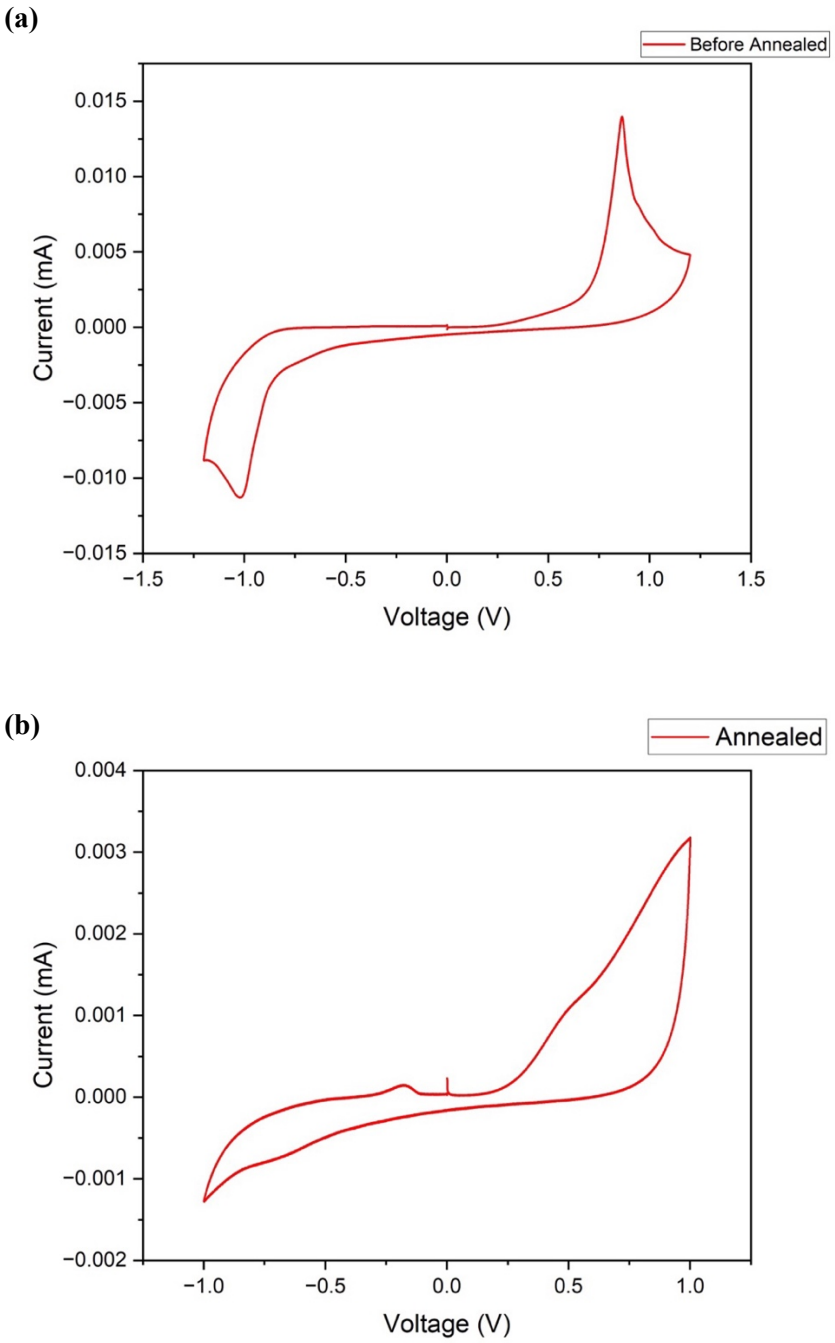

Figure 3.10. CV diagram for PEPC **(a)** before annealed and **(b)** after annealed.

The slightly higher HOMO energy level of the annealed PEPC can be attributed to the partial removal of the electron-withdrawing carbamate sidechain. However, both PEPC films before and after annealing showed a lower HOMO energy level than polypyrrole itself, which has an E_{HOMO} of ~-4.0 eV [107,108]. This can also be attributed to the electron-withdrawing carbamate

sidechain not being totally removed; therefore, the E_{HOMO} of annealed PEPC is still higher than that of PPy.

The two-dimensional grazing-incidence X-ray diffraction (XRD) spectroscopy was used to examine the crystallinity of PEPC films before and after annealing, and the results are shown in **Figure 3.11**. For the PEPC film before annealing, there was no significant peak in both in-plane (IP) and out-of-plane (OOP) directions, indicating the polymer chains were amorphous and disordered. Upon thermal annealing at 200°C, there was still no significant (100) lamellar peak shown up in both in-plane and out-of-plane direction, indicating the crystallinity for the film after annealing was still very low. This could be attributed to the long carbamate sidechain was not totally removed. However, a broad peak at 2θ=21.0° showed up in the XRD pattern of both in-plane and out-of-plane direction, corresponding to a d space of 4.23Å. This peak may consist of the amorphous halo. It may also be attributed to the main chain π-π stacking, indicating the partial removal of the sidechain did help with a better π-π stacking of PEPC.

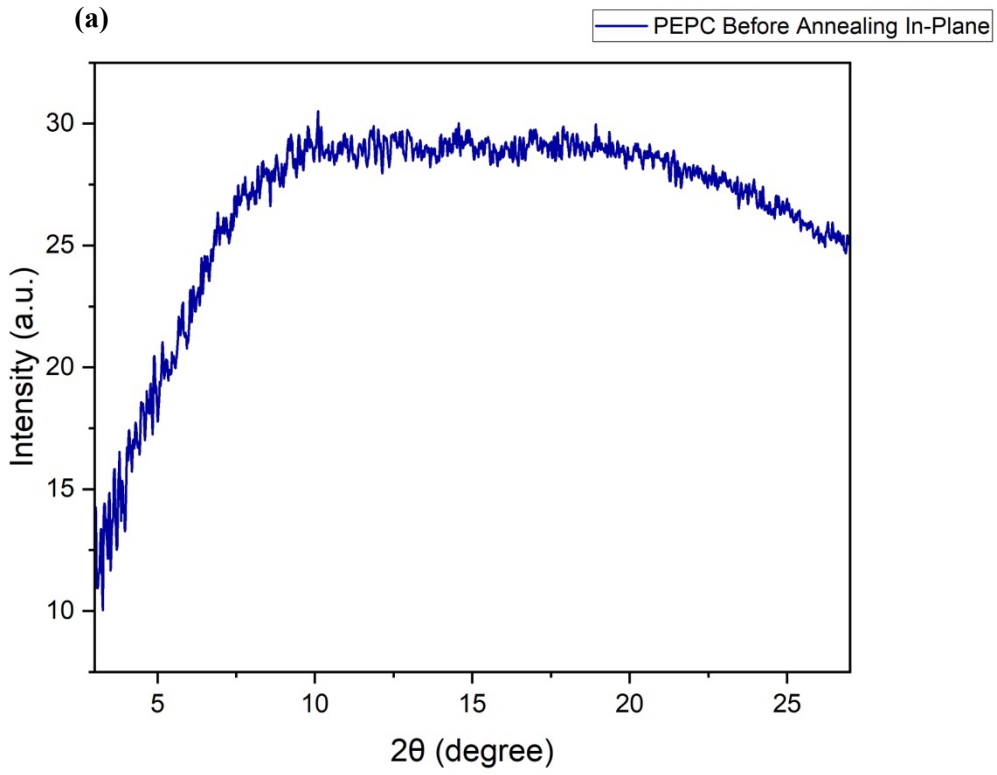

(b)

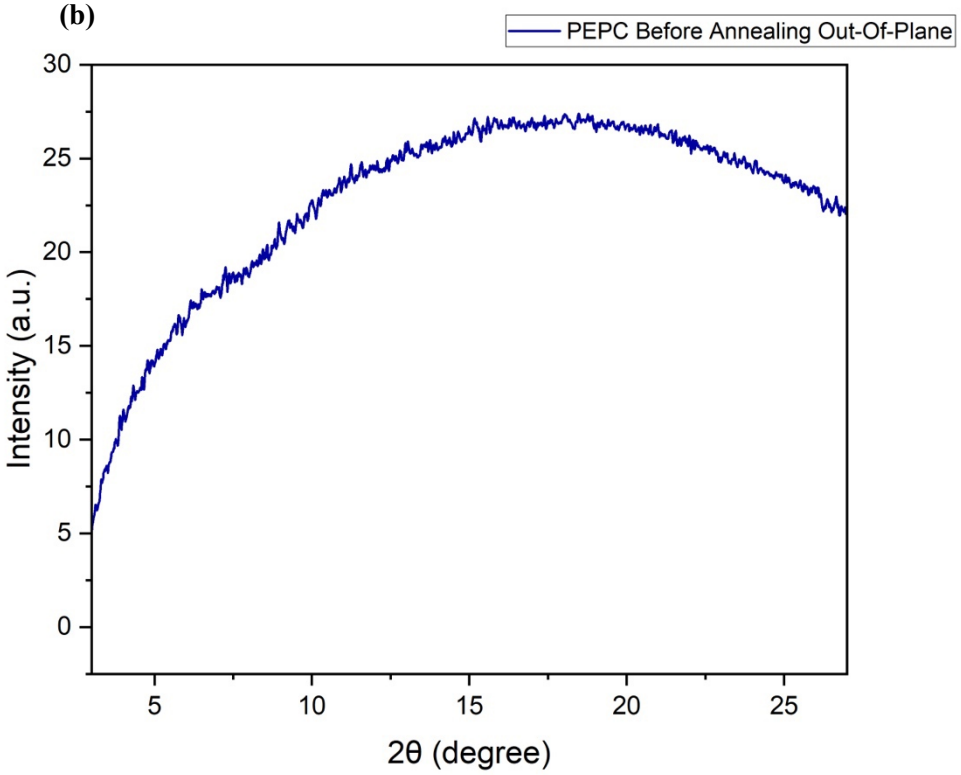
PEPC Before Annealing Out-Of-Plane
Intensity (a.u.)
2θ (degree)
0
5
10
15
20
25
30
5
10
15
20
25

(c)

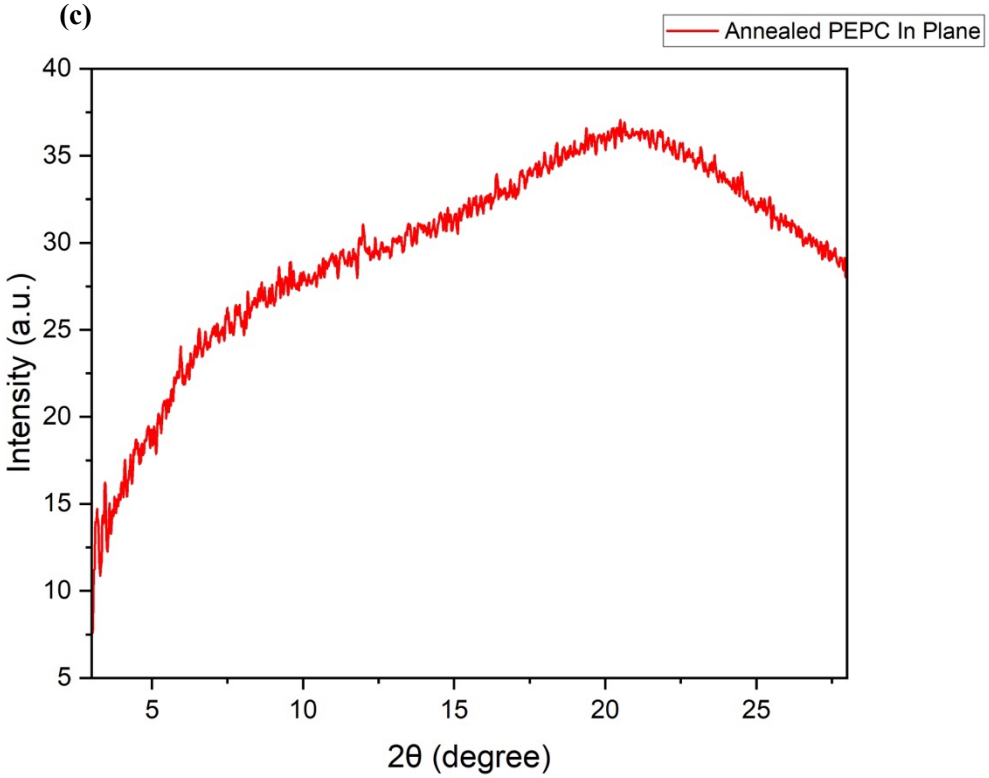
Annealed PEPC In Plane
Intensity (a.u.)
2θ (degree)
5
10
15
20
25
30
35
40
5
10
15
20
25

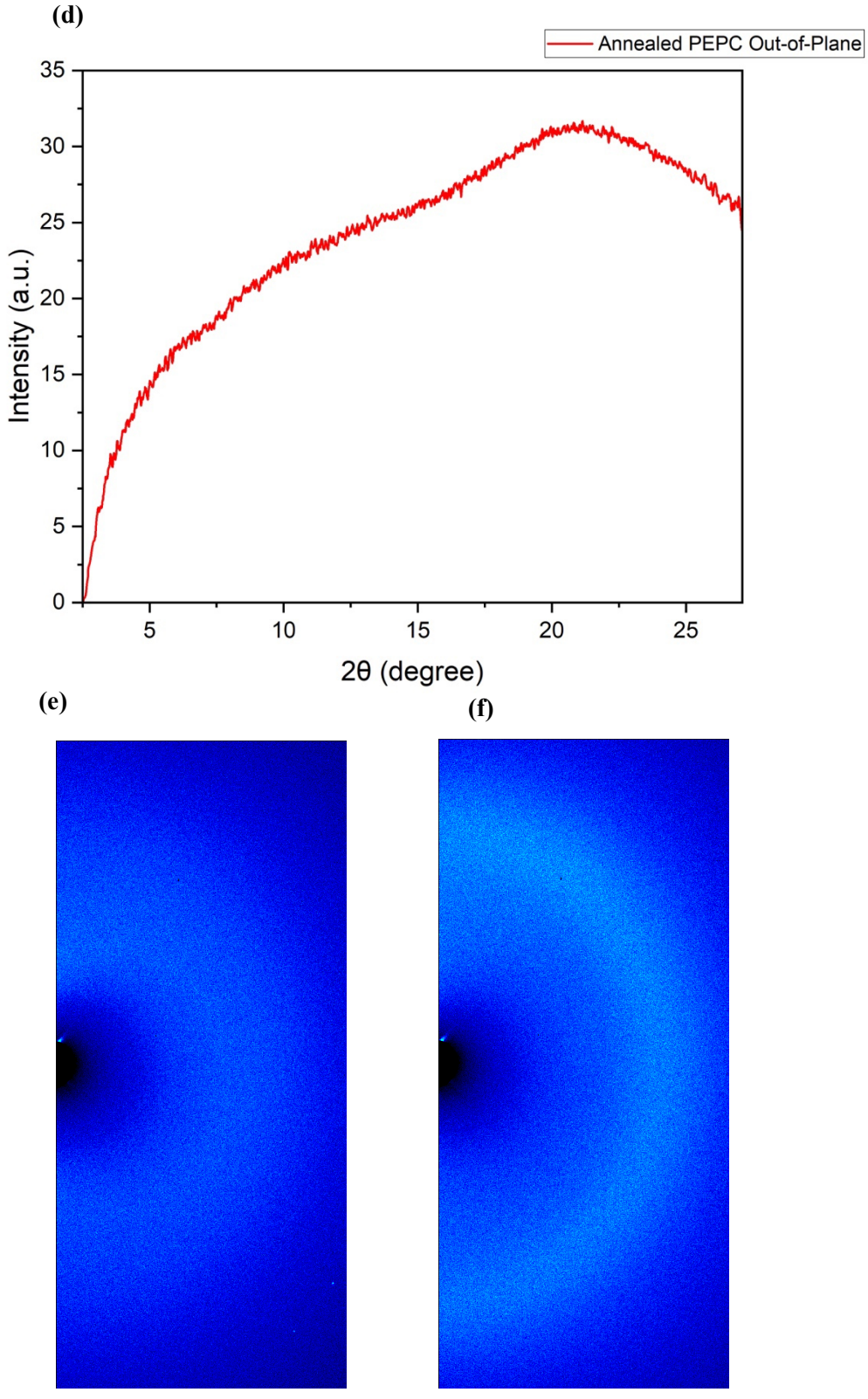

Figure 3.11. XRD spectra for PEPC film **(a)** before annealing in-plane cuts **(b)** before annealing out-of-plane cuts **(c)** after annealed in-plane cuts **(d)** after annealed out-of-plane cuts, **(e)** 2D Image before annealing and (f) 2D image after annealed.

3.4.5. Conductivity Measurement of PEPC Thin Film

The conductivity of PEPC film in different conditions was tested. Three common p-type ionic dopants for polypyrrole, including hydrochloric acid (HCl,5N), Ferric chloride ($FeCl_3$), and p-toluenesulfonic acid (p-TSA,5N) and molecular dopant 2,3,5,6-tetrafluoro-7,7,8,8-tetracyanoquinodimethane (F4TCNQ) were used to dope PEPC. The device for conductivity measurement was shown in **Figure 3.12**, which was an interdigitated two-electrode resistor. By conventional lithography and thermal evaporation, a silicon wafer substrate with a 300 nm thermally grown SiO_2 top layer was prepatterned, in which a pair of gold electrodes were interdigitated, each with a channel length (L) of 30 μm and a channel width (W) of 15.8 mm and a W/L ratio of 527. Firstly, a PEPC film was deposited on the substrate by spin coating a PEPC solution in chloroform, followed by thermal annealing at a certain condition if annealing was needed. The thickness of the films before and after annealing was in the range of 50-60 nm. After the film was prepared, the device was swept by changing the bias from -1 to +1 V to obtain an I-V curve. The doped polymer films were also measured for conductivity using the same procedure. The sample preparation conditions are summarized in **Table 3.8**.

Table 3.8. Summary of sample preparation conditions for conductivity measurement

Experiment	Annealing Temperature (℃)	Annealing Atmosphere	Annealing Time (mins)	Dopant
1	Not Annealed	N.A.	N.A	Non-doped
2	Not Annealed	N.A.	N.A	HCl
3	Not Annealed	N.A.	N.A	FeCl3
4	150	N2	30	HCl
5	150	Air	30	HCl
6	200	N2	30	HCl
7	200	Air	30	HCl
8	250	N2	30	HCl
9	250	Air	30	HCl
10	200	Air	30	FeCl3
11	200	Air	30	p-TSA
12	200	Air	30	F4TCNQ
13	200	N2	30	F4TCNQ
14	250	N2	30	F4TCNQ
15	100-150-200	Air	10min for each temperature	HCl
16	100-150-200	N2	10min for each temperature	HCl
17	100-150-200	Air	10min for each temperature	F4TCNQ

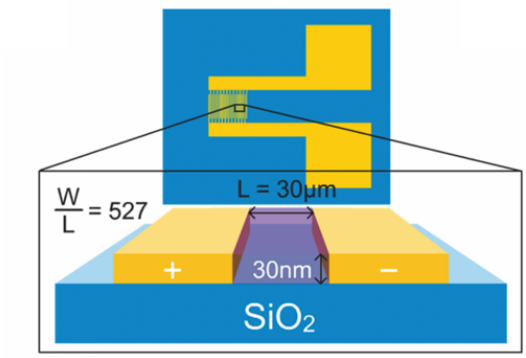

Figure 3.12. Illustration of the device for polymer thin film conductivity measurement [32].

Unfortunately, none of the PEPC films from experiments 1 to 17 showed significant conductivity. This could be explained by the low degree of sidechain removal and the damaged conjugated structure at the high annealing temperature. As stated in the previous section, at 150 ℃, only ~15% sidechain was removed, and at 200 ℃, the percentage was ~17%. Besides, at 200℃, the conjugated structure of PEPC had already been damaged, and it was more damaged at 250 ℃. As explained in chapter one, the bulky sidechain is detrimental to polypyrrole conductivity since it will reduce the conjugation length and make the polymer structure twisted. In addition, the sensitivity of PEPC to the high temperature also limits its conductivity. The ruined pyrrole ring of the PEPC backbone will significantly reduce the conjugation length, thus significantly influencing the conductivity.

3.5. Conclusions and Future Works

In this work, a soluble polypyrrole derivative PEPC was synthesized in 45% yield by oxidative polymerization using ferric chloride as the oxidizing agent. The thermal stability of the polymer was tested through TGA and FTIR. The 2-ethylhexyl carbamate sidechain in PEPC is relatively stable and could not be totally removed even at 250 ℃. In contrast, the PEPC backbone is relatively thermal unstable, and the conjugated structure will be ruined at a temperature higher than 150 ℃. In addition, the primary carbamate chain was relatively stable to acid. Thus, acid could not totally remove the sidechain either. Therefore, though the goal of making the polypyrrole soluble was achieved, another goal of removing the sidechain

to recover its conductivity could not be achieved. Due to the long and bulky carbamate sidechain, PEPC was found to be an insulator.

Though PEPC did not achieve the two goals simultaneously, it still paves a way to design new N-carbamate substituted polypyrroles. Since primary carbamates are hard to remove via either thermolysis or acid cleavage, long secondary or tertiary carbamates may be applied to be the sidechain of polypyrrole. Work done with N-Boc oligopyrroles showed that the Boc sidechain could be removed from the PPy backbone through thermolysis [31]. However, the Boc group is too short to achieve high solubility of polypyrrole when the molecular weight is high. If a longer secondary or tertiary carbamate could be applied as the sidechain to PPy, it could be more easily removed through thermolysis or acid lysis, subsequently recovering the polypyrrole backbone and achieving good conductivity.

3.6. Experiment Section

Material Characterization

The thermogravimetric analyses (TGA) were measured using TA Instruments SDT 2960 at scan rate of 10 ℃ /min, holding at 150 ℃ or 250 ℃ for 30 minutes under nitrogen and air. Cyclic Voltammetry (CV) was measured on a CHI600E electrochemical analyzer using Ag/AgCl as reference electrode, with two Pt disk electrodes as working electrode and counter electrode, in a 0.1 M tetrabutylammonium hexafluorophosphate acetonitrile solution at a scan rate of 100 mV/s. Ferrocene with a E_{HOMO} of -4.8 eV was used as reference system. Polymer films were deposited on the transparent conductive indium tin oxide (ITO) glass substrate for CV measurement. The UV-Vis spectra were obtained by Cary 7000 Universal Measurement Spectrophotometer. The NMR spectra were measured using a Bruker DPX 300 MHz spectrometer with chemical shifts relative to tetramethyl silane (TMS, 0 ppm). Two-dimensional grazing-incidence X-ray diffraction (XRD) patterns were measured by a Bruker D8 Discover power diffractometer with Cu Ra (Rigaku) X-ray source (λ = 0.15418 nm) in standard Bragg-Brentano geometry.

Doping of Polymer Films

A doped annealed PEPC film was prepared by submerging the annealed film on the SiO_2-Si substrate into a petri dish containing a 5 N acid solution in methanol of p-toluenesulfonic acid

(pTSA), hydrochloric acid (HCl) or 1.7 M $FeCl_3$ solution in methanol. The petri dish with the dopant solution and the substrate coated with film was heated at 50 ℃ for 30 minutes on a hotplate. The doped polymer film was then washed with deionized water (18MΩ) and dried in air.

Conductivity Calculation

The conductivity of the polymer film was calculated following the equation:

$$\sigma = G\frac{L}{A}$$

Where σ is the conductivity, G is the conductance (S), L is the length of the channel ($3\times 10^{-4} cm$) and A (cm^2) is area of the cross section of the polymer channel, which is the product of the film thickness (cm) and the channel width (1.581 cm) of the device.

Chapter 4. Study of the Synthesis of Poly[1-((2-ethylhexyl)oxy)-1*H*-pyrrole]

4.1. Introduction

As stated in chapter 1, introducing an alkyl sidechain to the polypyrrole backbone will lead to a twisted structure, which is detrimental to conductivity. Compared with the alkyl sidechain, alkoxy sidechains with the smaller oxygen atom will have less steric hindrance than the alkyl chain, thus leading to a less twisted structure and reducing the negative influence of the sidechain on the conductivity of polypyrrole. Alkoxy sidechains have been used for some other conjugated polymers by our research group [34–37]. To the best of our knowledge, no soluble N-substituted alkoxy polypyrrole has ever been synthesized. Herein, we explored the synthesis of soluble poly[1-((2-ethylhexyl)oxy)-1H-pyrrole] (PEOP) (**Figure 4.1**).

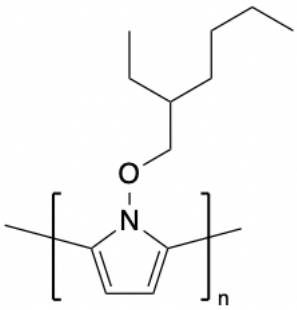

Figure 4.1. Structure of PEOP.

4.2. Polymer Simulation Based on Density Functional Theory

Density Functional Theory (DFT) simulations were conducted to estimate the sidechain's influence on the polymer backbone's planarity. The simulation was performed using Gaussian 09 with a B3LYP/6-31G(d) basis set. As shown in **Figure 4.2 (a**), the N-alkyl substituted pyrrole dimer had a dihedral angle of 67.2° between two pyrrole rings. In contrast, as shown in **Figure 4.2(b)**, the N-alkoxy substituted pyrrole dimer had a dihedral angle of 66.0°, which is smaller than the N-alkyl substituted one. Thus, based on the DFT simulations, it was determined that the alkoxy sidechain indeed had less steric hindrance than the alkyl chain, which is expected to be beneficial for polymer conductivity.

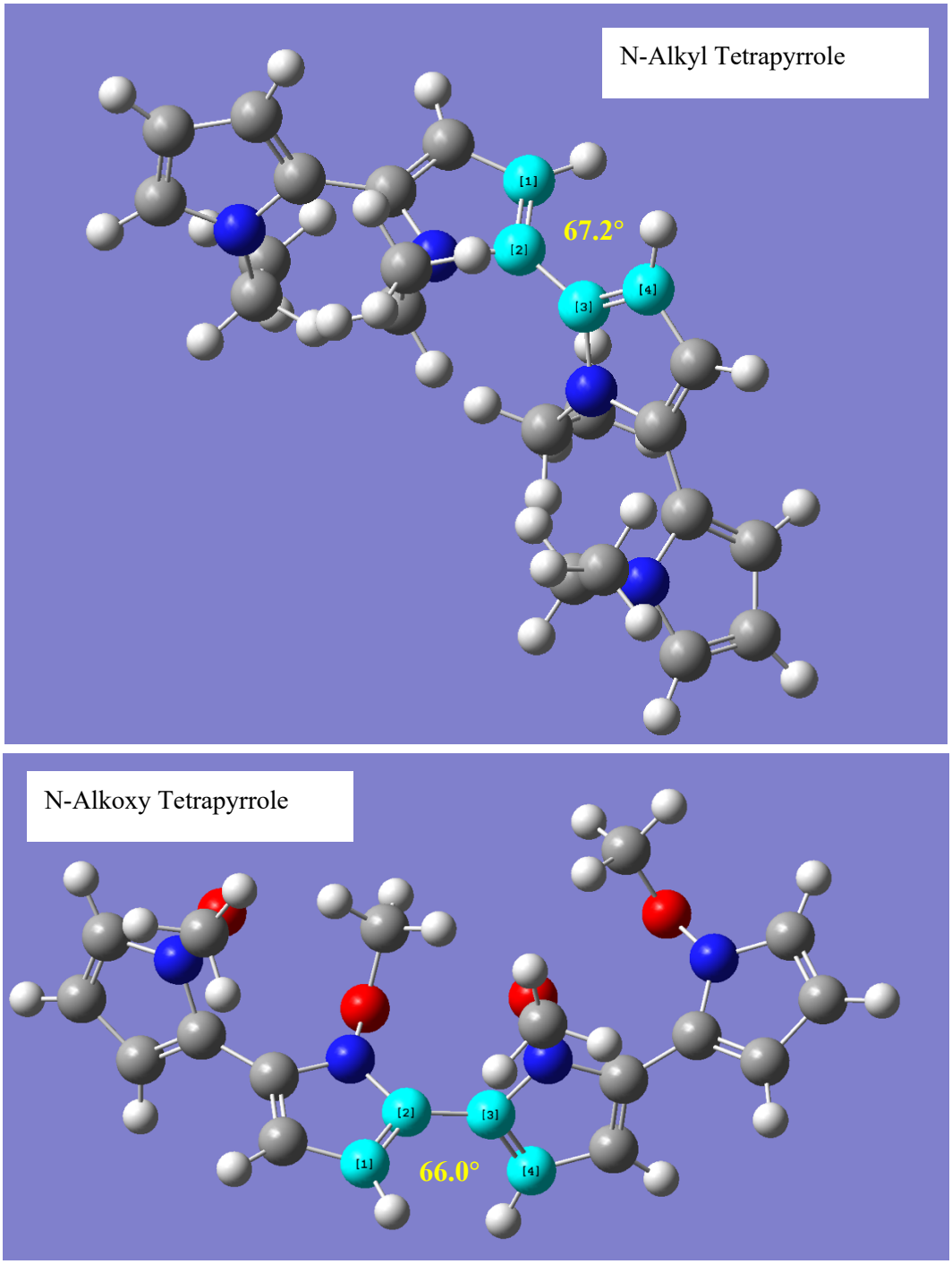

Figure 4.2. DFT Simulation of N-alkyl substituted tetrapyrrole and N-alkoxy substituted tetrapyrrole.

4.3. Monomer and Polymer Synthesis

The synthetic route to PEOP used in this work is shown in Scheme 3.1. The detailed synthetic procedure and the NMR data are listed in Chapter 4.6.

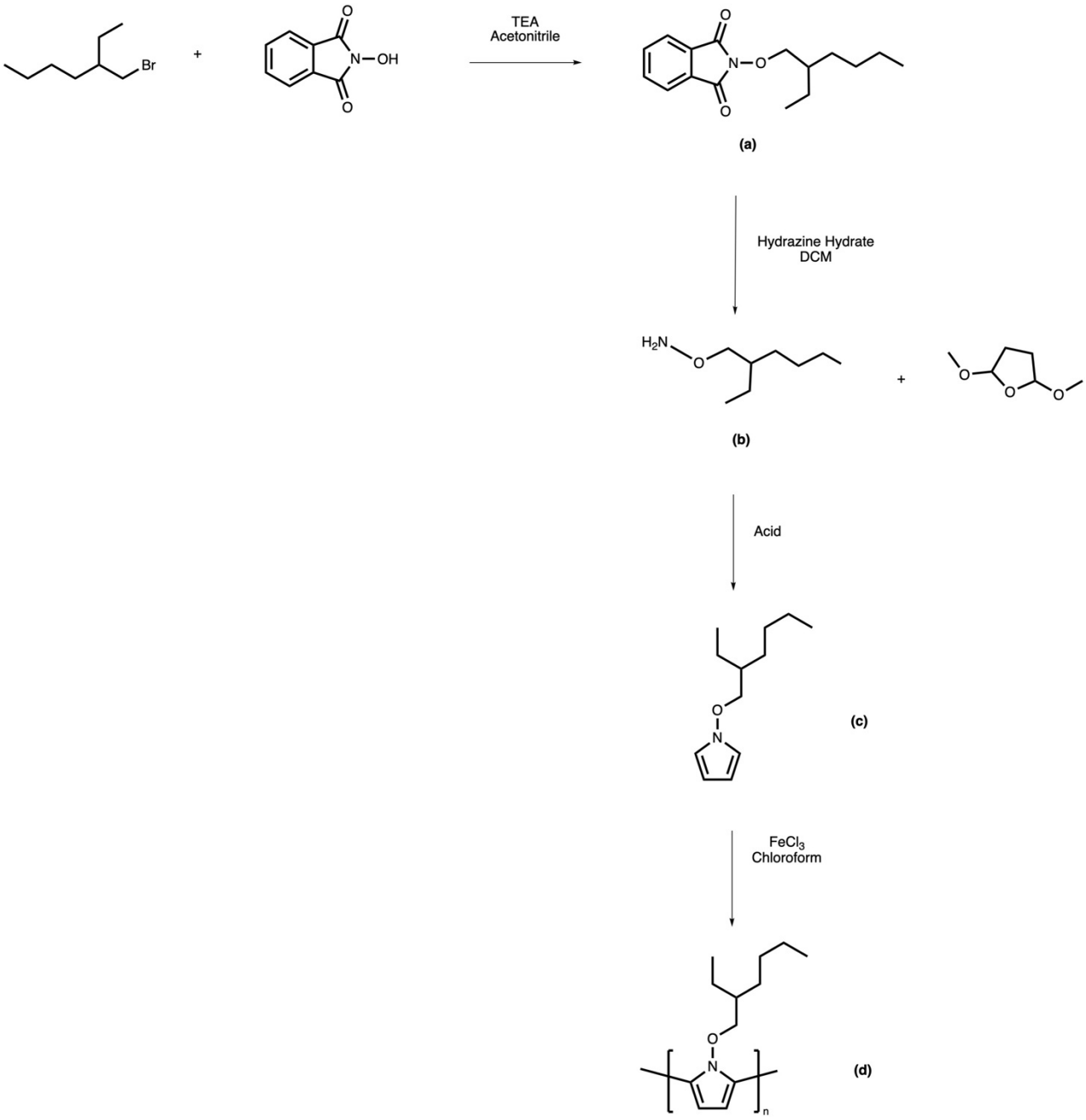

Scheme 4.1. Synthetic Route to PEOP

Briefly, 3-(bromomethyl)heptane and 2-hydroxyisoindoline-1,3-dione were mixed in acetonitrile with TEA as the base to obtain 2-((2-ethylhexyl)oxy)isoindoline-1,3-dione **(a)**. Subsequently, compound **(a)** was used to obtain O-(2-ethylhexyl)hydroxylamine (b) in the presence of hydrazine hydrate via Gabriel synthesis. The third step involved Clauson-Kass Pyrrole Synthesis, which combines a primary amine **(b)** and 2,5-dialkoxytetrahydrofuran to synthesize 1-((2-ethylhexyl)oxy)-1H-pyrrole (c) by condensation in the presence of acid.

Different methods for this step were tried and will be discussed in detail in section 3.4. Finally, compound **(c)** was used as the monomer to produce polymer **(d)** by oxidative polymerization with ferric chloride as the oxidizing agent.

4.4. Results and Discussions

Different reaction conditions were applied in step 3 to optimize the yield. The reaction conditions used are summarized in **Table 4.1**.

Table 4.1. Reaction Condition for Synthesis of Monomer (f)

Experiment	Reaction Conditions	Yield (%)
1	Sulfuric Acid/Silica 30mins	9.2
2	Sulfuric Acid/Silica 2hours	5.1
3	Sulfuric Acid/Silica 12hours	0
4	Pure ACOH	0
5	sodium acetate/water glacial acetic 75C 2.5h	7.5
6	sodium acetate/water glacial acetic 75C 12h	0
7	sodium acetate/water glacial acetic 75C 1h	12.5

Among all the experiments, the highest yield of compound **(c)** was 12%. This yield was thought to be due to many side reactions occurring, which was confirmed by TLC and NMR. In addition, due to the very similar polarity of the desired product and side products, the desired product could not be totally purified through column chromatography. Nevertheless, the polymerization was still conducted with the monomer containing unavoidable impurities

since if the impurity cannot be polymerized, it would be possible to remove them in the purification procedure of the obtained polymer.

The obtained polymer was characterized by FTIR spectroscopy first. As shown in **Figure 4.3**, the characteristic peak of polypyrrole derivative at ~1550 cm^{-1} was missing, indicating the conjugated C=C-C structure of the pyrrole ring did not exist in the obtained polymer [98–105]. Therefore, the desired PEOP was not obtained, which was thought to be because the impurities remaining in the crude monomer interfered with the oxidative polymerization and therefore ruined the conjugation structure of the polypyrrole backbone. However, from the FTIR spectra, it can be seen that the alkoxy sidechain indeed existed in the polymer, confirmed by the peaks at 1460 cm^{-1}, 1037 cm^{-1} and ~3000 cm^{-1} as the characteristic peaks for the alkoxy chain, which corresponds to the C-N, C-O stretching and aliphatic C-H stretching respectively [109]. The peak descriptions of the FTIR spectra are summarized in **Table 4.2**.

Table 4.2. Peak Assignments for FTIR

Peak Position	Description
736 771	C-H bending
1037	C-O Stretching
1380	C-N Stretching C-N Vibration
1460	C-N Stretching C–C–N Inter-ring In-plane Bending
1620	Non-aromatic C=C Stretching
2871 2923 2960	Aliphatic C-H

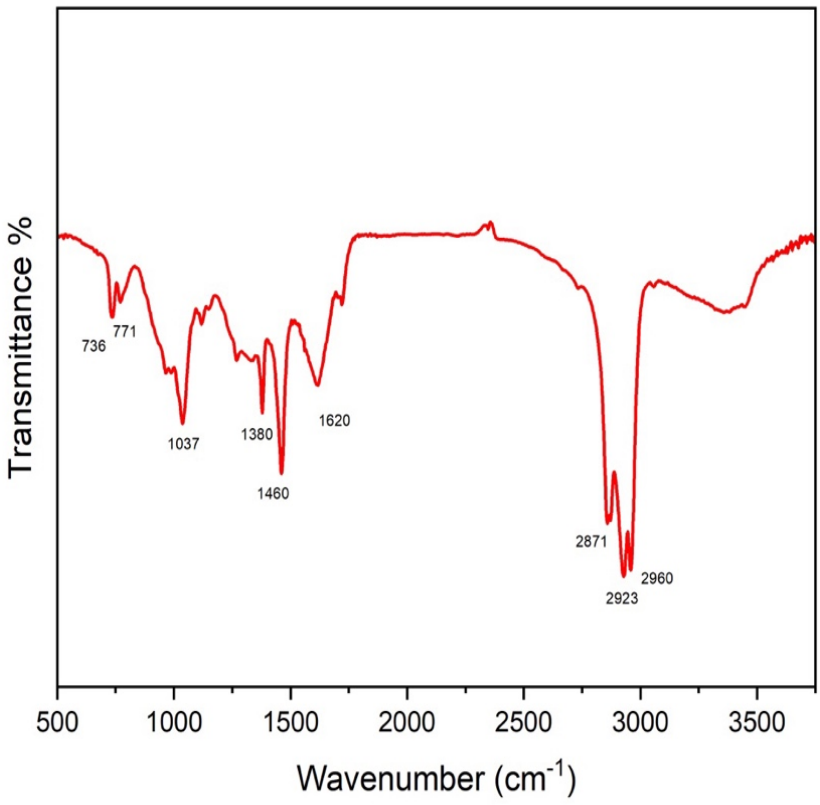

Figure 4.3. FTIR Spectrum of the Obtained Polymer.

The polymer was further characterized with FTIR spectra to explore the thermal stability of the sidechain. The polymer film was measured for FTIR before and after annealing at different temperatures for 30 min in different environments. The annealing conditions are summarized in **Table 4.3**.

Table 4.3. Annealing Conditions for FTIR Samples

Experiment	Annealing Temperature (°C)	Annealing Environment
1	150	Air
2	200	Air
3	250	N_2
4	250	Air

As shown in **Figure 4.4 (a)**, after annealing at 150 ℃ for 30 mins in air, the peak at ~3000 cm^{-1} had a peak area drop from 80.2 to 69.6, indicating the sidechain was removed by 13.2% since the only part in the polymer that contains aliphatic C-H bonds is the alkoxy sidechain. When the annealing temperature was elevated to 200 ℃, the peak area drop increased to 54.6%, as shown in **Figure 4.4 (b)**; further increasing of the annealing temperature to 250℃ led to a peak area drop of 75.2% and 95.5%, when annealed in nitrogen and air respectively, as shown in **Figure 4.4 (c)** and **(d)**. The results suggested that the degree of removal of the alkoxy sidechain increased with the increasing of the annealing temperature, and the air atmosphere facilitated the removal of the sidechain compared with the nitrogen atmosphere. More than half of the sidechain can be removed when annealed at 200 ℃, and it can almost be totally removed when annealed at 250 ℃. Based on the FTIR results, the alkoxy sidechain appears to undergo thermolysis at a high temperature.

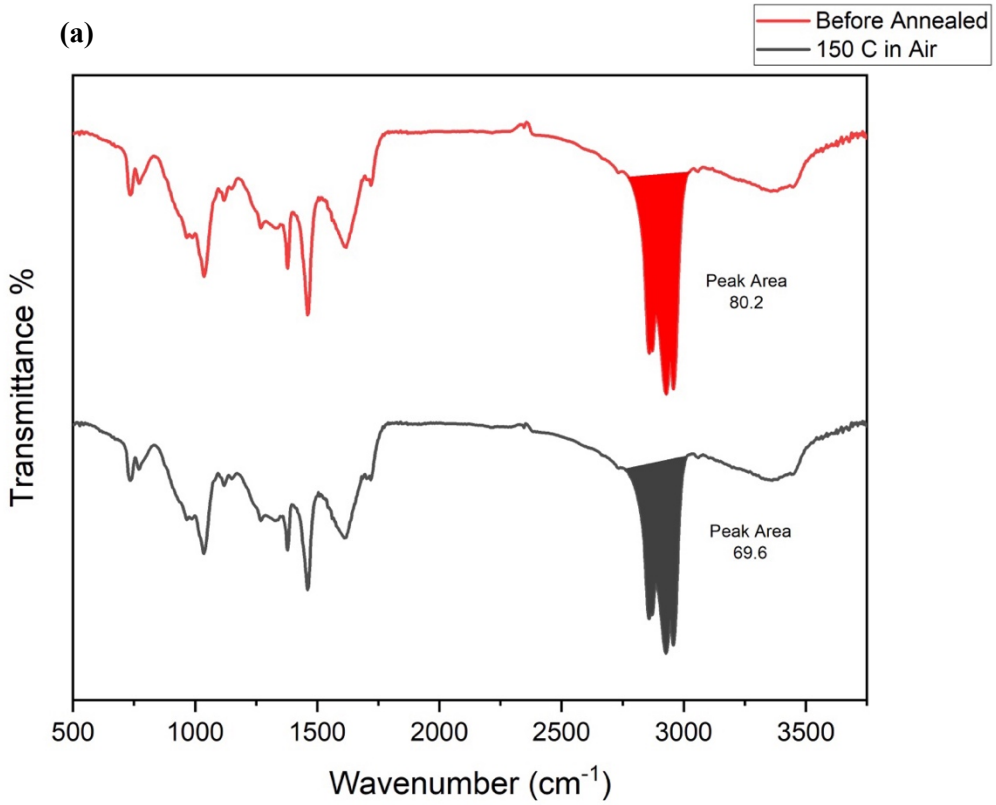

(b)

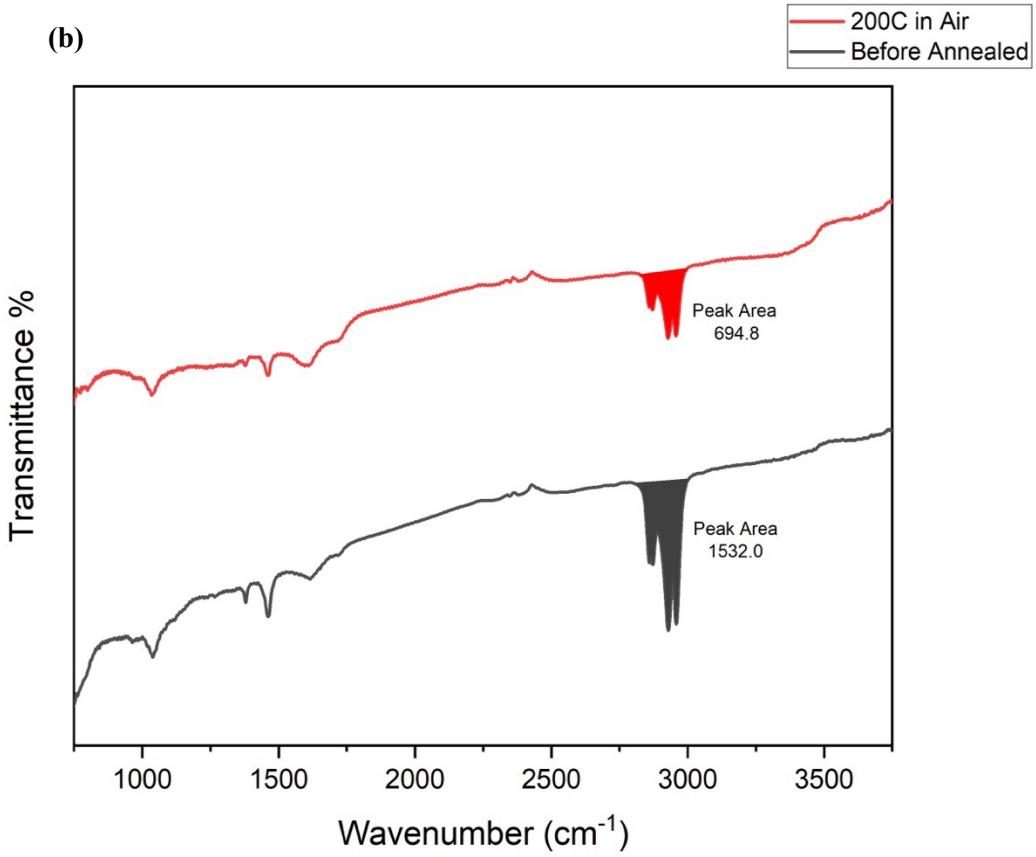
200C in Air
Before Annealed
Peak Area
694.8
Peak Area
1532.0
Transmittance %
1000
1500
2000
2500
3000
3500
Wavenumber (cm-1)

(c)

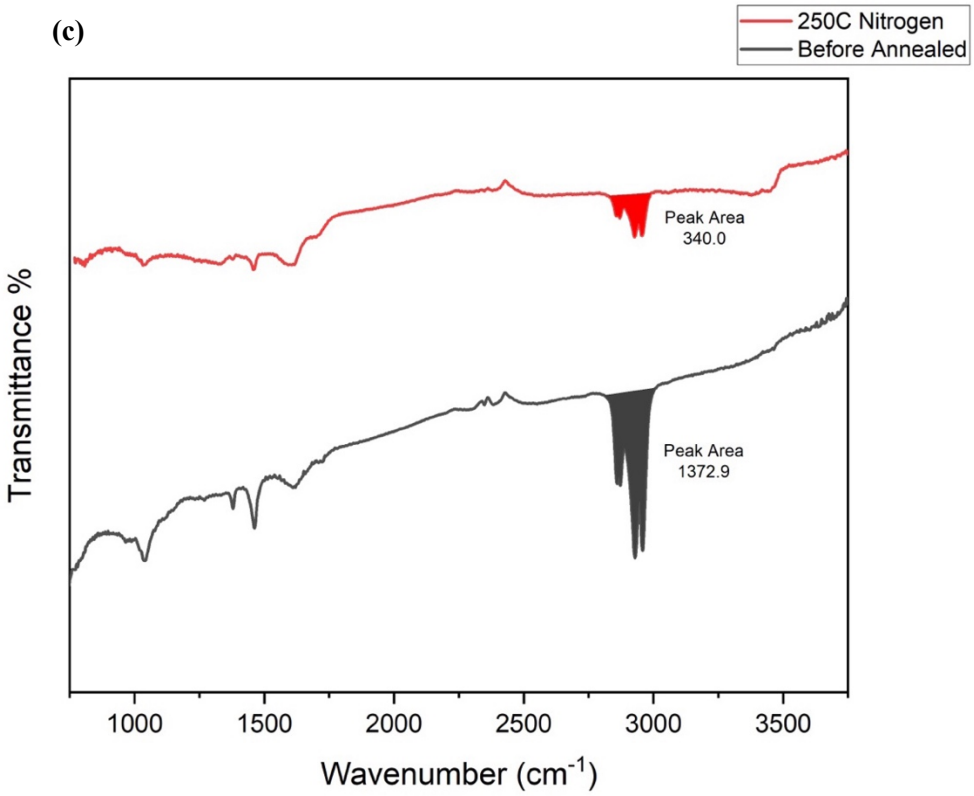
250C Nitrogen
Before Annealed
Peak Area
340.0
Peak Area
1372.9
Transmittance %
1000
1500
2000
2500
3000
3500
Wavenumber (cm-1)

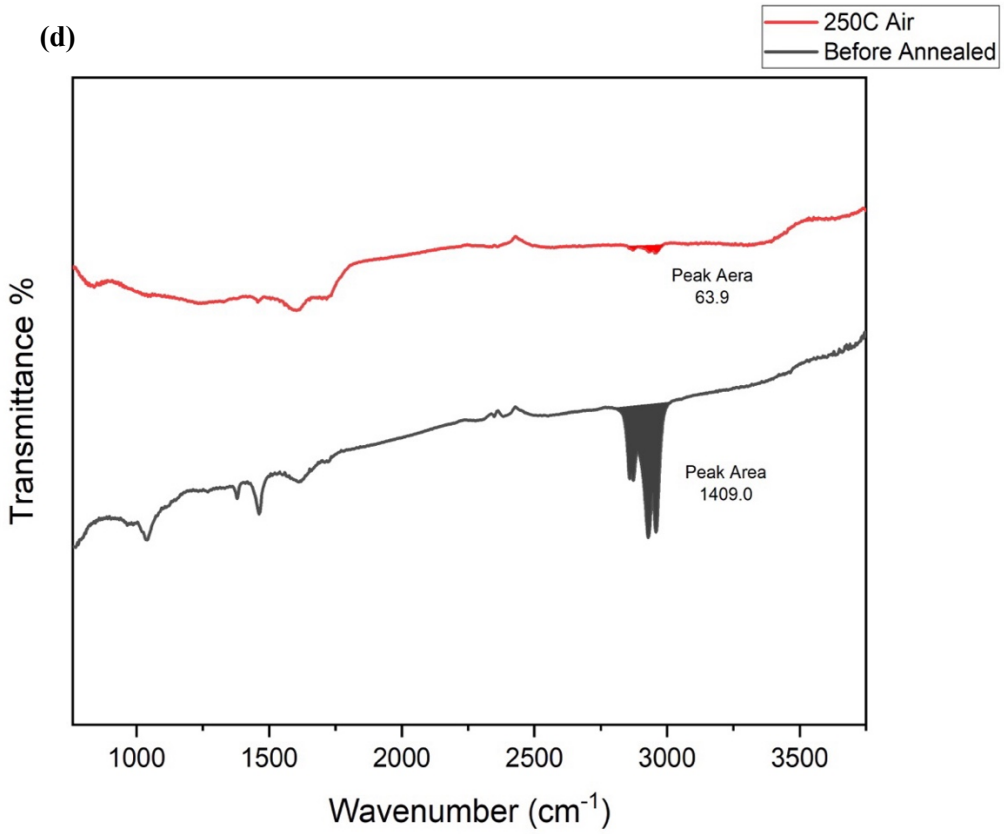

Figure 4.4. FTIR spectra for the polymer before and after annealing under different conditions.

TGA measurements were also conducted on the polymer to further explore its thermal properties. The polymer was heated at a heating rate of 10 °C min^{-1} from 25°C and held at 150 °C or 250 °C for 30 minutes, then heated at a rate of 10 °C min^{-1} to 600 °C under N_2 or air atmosphere. The measurement conditions are summarized in **Table 4.4.**

The results are shown in **Figure 4.5 (a)**, **(b)**, and **(c)**, which correspond to experiments 1, 2, and 3, respectively. As shown in **Figure 4.5**, the weight loss after holding at a specific temperature for 30 minutes for experiments 1, 2, and 3 were 12.9%, 44.0%, and 44.3%, respectively. Since the structure of the polymer was challenging to determine, quantitively comparing the FTIR data and the TGA data was not practical. However, the trend of the weight loss shown on the TGA diagram matches with the FTIR data, that higher temperature corresponds to a higher degree of sidechain removal. The weight was reduced starting at a temperature as low as 100 °C (**Figure 4.5 (c)**), indicating that the sidechain might start thermolysis at as low as 100 °C.

Table 4.4. TGA Measuring Conditions

Experiment	Holding Temperature (℃)	Heating Environment
1	150	Air
2	250	N_2
3	250	Air

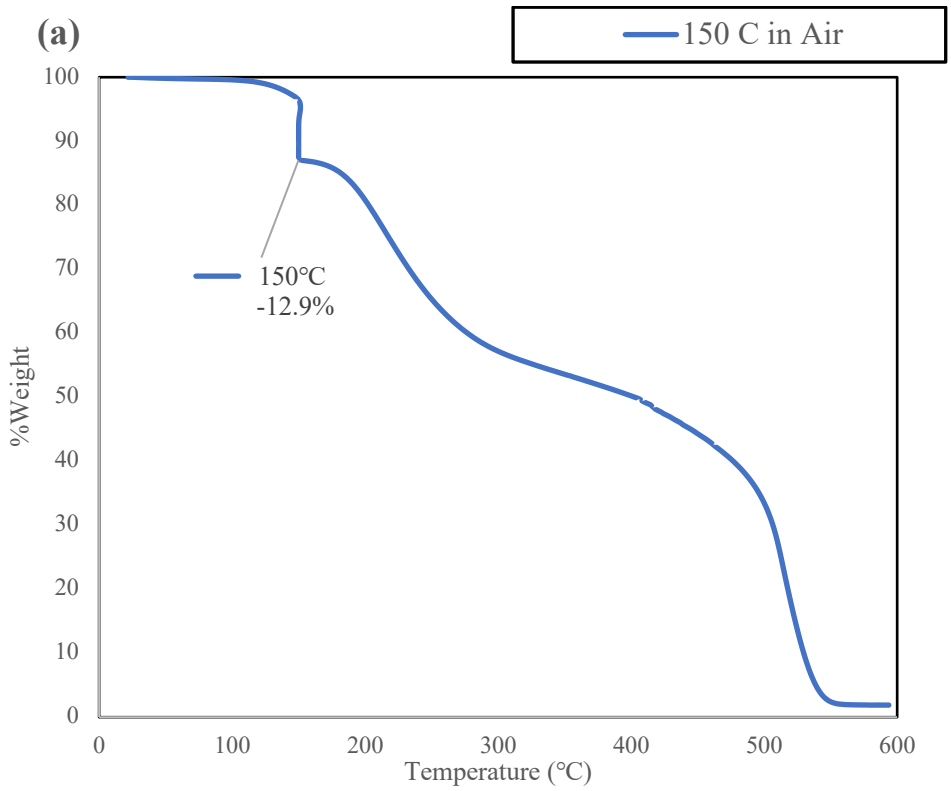

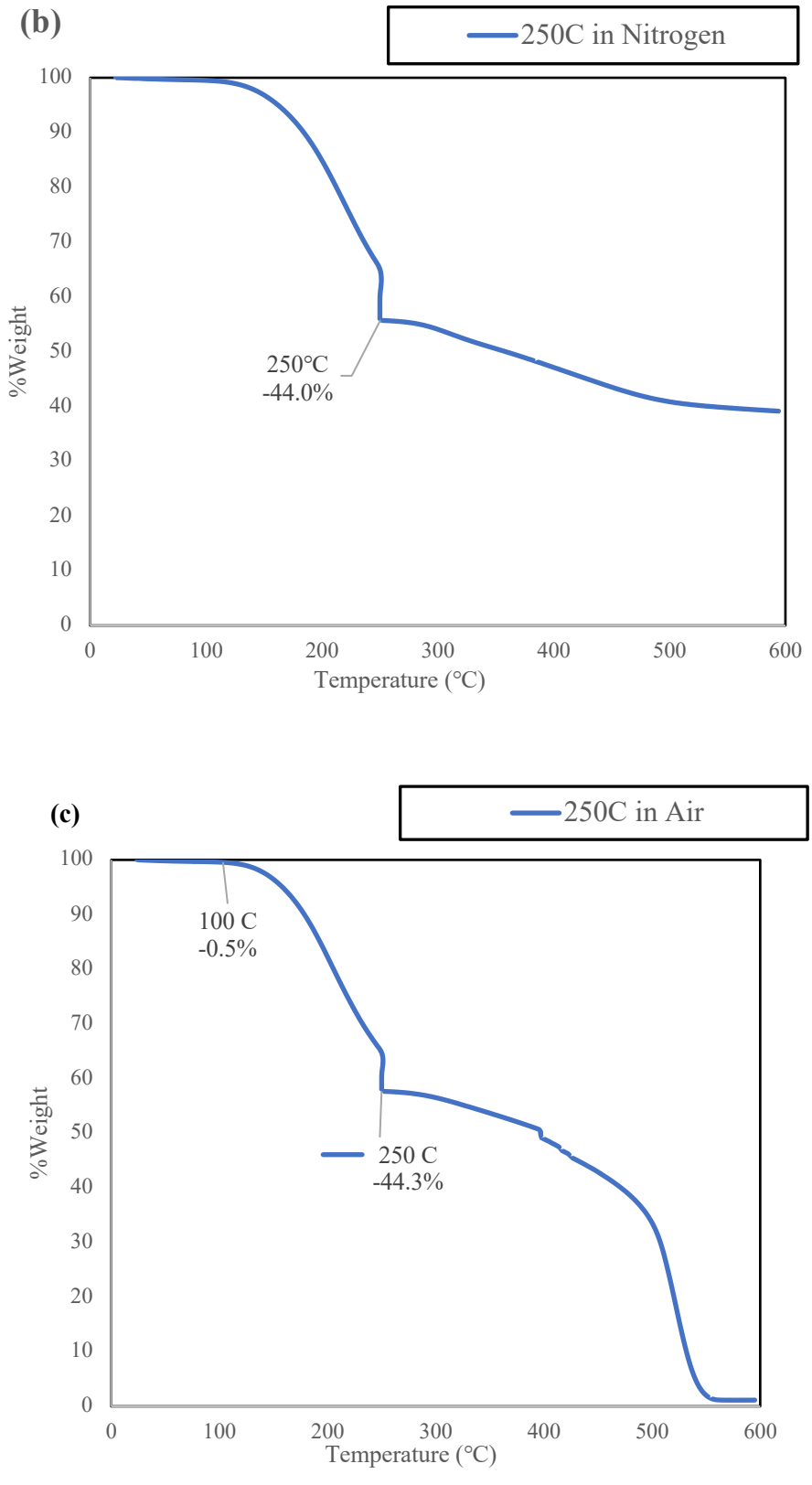

Figure 4.5. Polymer TGA diagram for **(a)** annealed at 150℃ in air, **(b)** annealed at 250℃ in nitrogen and **(c)** annealed at 250℃ in air.

Solubility and processability were tested for the polymer. It was confirmed to have good solubility in different organic solvents, including chloroform, acetone, and dichloromethane (DCM). A concentration of 25 mg/mL polymer solution could be made using the solvents mentioned above, and by spin coating using the 25 mg/mL polymer solution, a 50-60 nm polymer film was deposited on glass or SiO_2-Si wafer substrate, which satisfies the conductivity requirements for sensor application.

XRD was performed to evaluate the crystallinity of the polymer films before and after annealing, and the results are shown in **Figure 4.6.** As shown in **Figure 4.6 (a)** and **(b)**, there is no significant peak for the polymer film before and after annealing in both in-plane and out-of-plane directions, indicating the polymer chains were amorphous and disordered. The missing peak at 2θ=~20-25° indicates there is no π-π stacking in the polymer, which could be attributed to the non-conjugated structure of the polymer backbone.

(a)

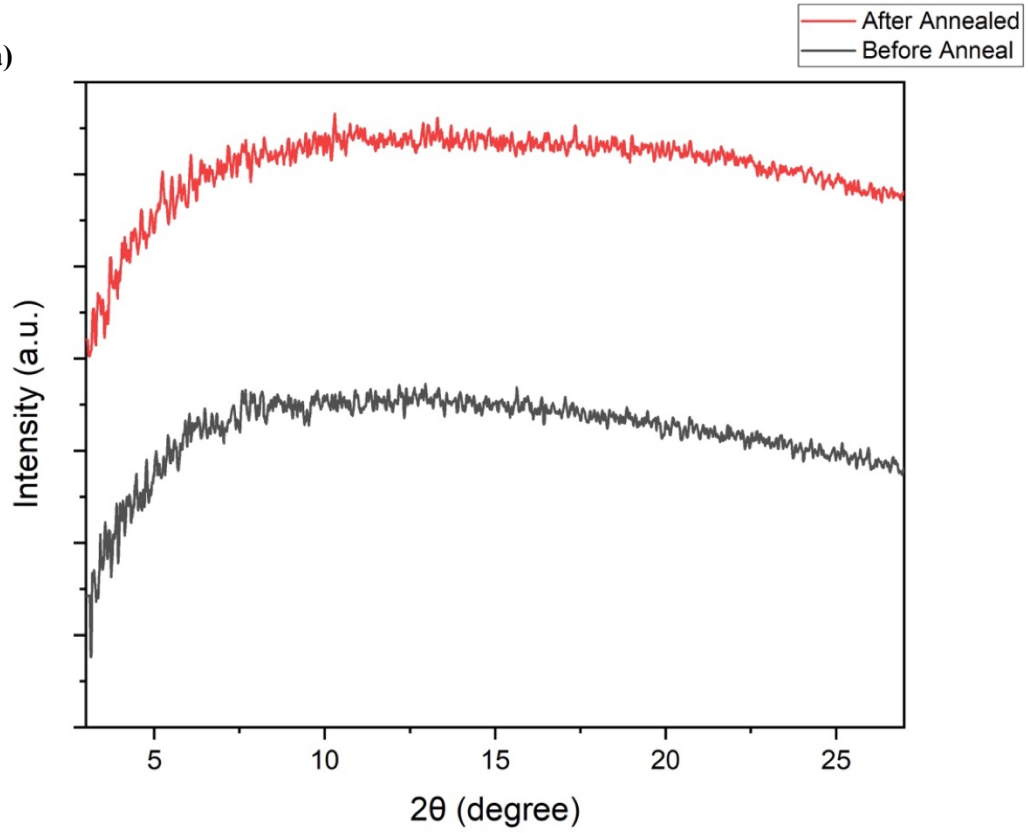

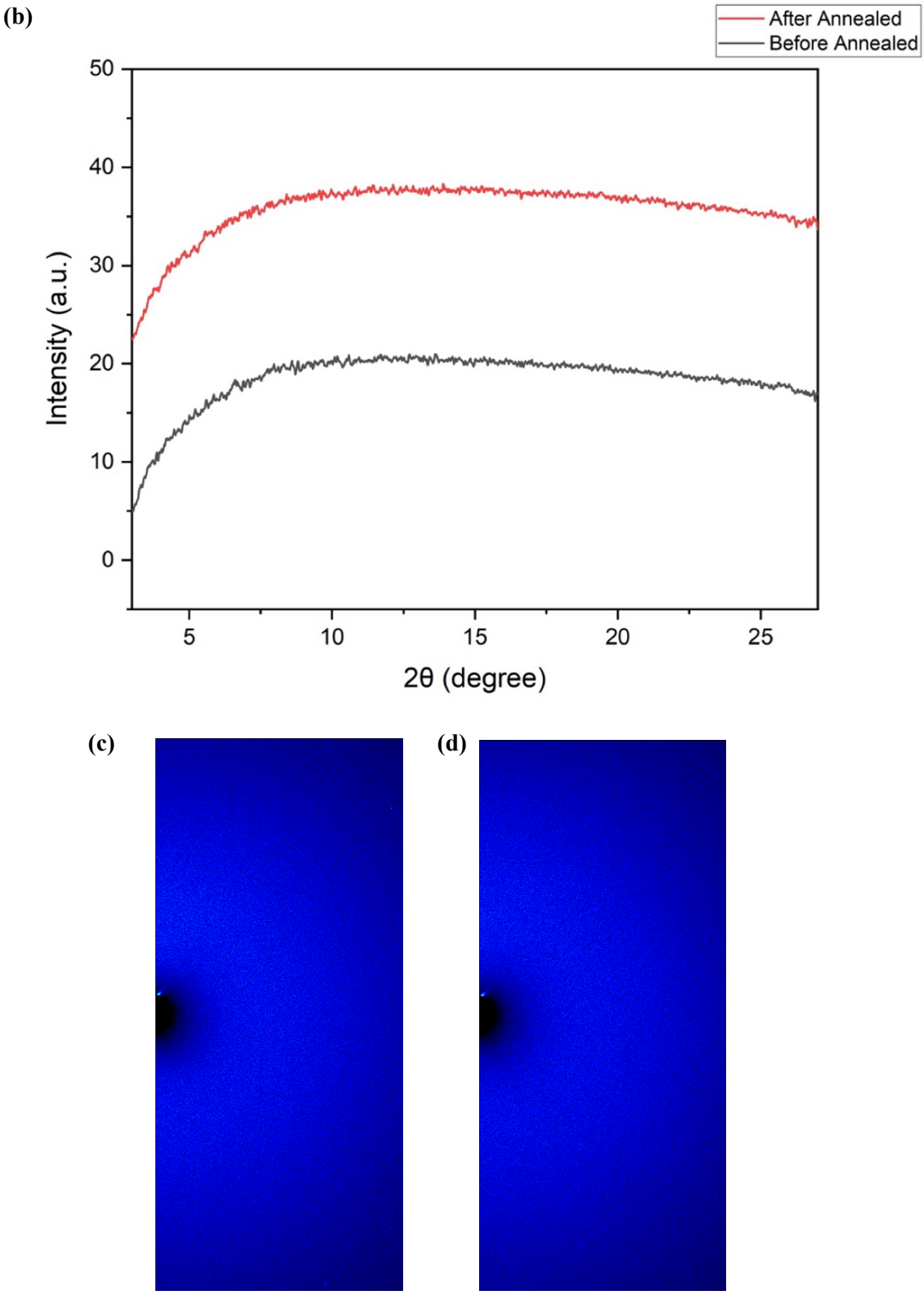

Figure 4.6. Polymer thin film XRD spectra for **(a)** before and after annealing in-plane cuts, **(b)** before and after annealing out-of-plane cuts, **(c)** 2D image before annealing and (d) 2D image after annealing

Finally, the conductivity of the polymer film was measured using the same procedure and under the same conditions as PEPC (**Table 3.9**). Unfortunately, no significant conductivity was observed, which was presumed to be the result of the desired polypyrrole-based polymer not being obtained and a lack of the conjugation of the polymer, which was corroborated with the FTIR spectra.

4.5. Conclusions and Future Works

In this work, the desired polymer was not obtained due to the difficulties of purifying the monomer. The impure monomer led to an unsuccessful polymerization, and the obtained polymer did not have a polypyrrole backbone. However, the TGA and FTIR results suggest that the alkoxy sidechain did exist in the obtained polymer, and it could successfully be removed through thermolysis at a relatively mild temperature. Compared with the carbamate sidechain used in chapter 2, the alkoxy sidechain seems more suitable to be thermally removed because it can be almost totally removed at 250 ℃ and had started to decompose at a temperature as low as 100 ℃.

In the future, a new synthetic method may be explored to get a higher yield of the pure monomer. If the N-alkoxy-substituted polypyrrole is successfully synthesized, due to the good thermal instability of the sidechain, polypyrrole may be recovered by thermal removal of the alkoxy sidechain at a mild temperature without ruining the conjugation structure of polypyrrole backbone, which was the issue that led to PEPC behaving as an insulator. This could be a good way to make polypyrrole soluble and, at the same time, maintain excellent conductivity.

4.6. Experimental Section

Materials and Characterization

All the chemicals used in this project were purchased from Sigma-Aldrich, Fluka VWR, TCI, and Armstrong. Solvents used in the synthesis procedure were analytical grade and anhydrous or used as received. All column chromatography was conducted using silica gel (230-400 mesh).

The density function theory (DFT) simulations were conducted using Gaussian 09 software with a B3LYP/6-31G (d) basis set. TGA, FTIR NMR and conductivity data were obtained using the same conditions as illustrated in chapter 2.6.

Monomer Synthesis

Synthesis of 2-((2-ethylhexyl)oxy)isoindoline-1,3-dione (a)

N-hydroxyphthalimide (3.3 grams, 20 mmol), 2-Ethylhexyl bromide (3.3 grams, 10 mmol), triethylamine (3 mL, 40 mmol), and acetonitrile (50 mL) were charged to a 250 mL round-bottom flask connected to a water-cooled condenser. The solution turned a deep red color upon addition of triethylamine indicating formation of the N-hydroxyphthalimide anion. The solution was stirred at reflux for 12 hours. After cooling, solvent was removed via rotary evaporator. The solution was then dissolved in ethyl acetate, washed three times with 50 mL water and three times with 50 mL brine, and dried with anhydrous sodium sulfate. Solvent was removed via rotary evaporator to yield a fluffy yellow solid (Rf = 0.55, 4:1 hexane:ethyl acetate). Yield: 2.56 grams (95%). NMR data is not available due to the product not being soluble in $CDCl_3$.

Synthesis of *O*-(3-ethylheptyl)hydroxylamine

2-((2-ethylhexyl)oxy)isoindoline-1,3-dione (2.56 grams, 9.3 mmol) was dissolved in dichloromethane (50 mL). Hydrazine hydrate (2 mL, 40 mmol) was added dropwise to the solution under vigorous stirring. After approximately 10 minutes, a fluffy white precipitate formed. Reaction progress was analyzed via TLC by monitoring disappearance of the starting material; no starting material was observed after 45 minutes. The reaction was stirred for an additional 4 hours and subsequently washed three times with 50 mL water and one time with 50 mL brine, and dried with anhydrous sodium sulfate. Solvent was removed via rotary evaporator yielding a yellow oil. 0.82g. yield: 61%. ^{1}H NMR (300 MHz, chloroform-*d* δ/ppm): 3.53 (d, 2H)

Synthesis of 1-((2-ethylhexyl)oxy)-1*H*-pyrrole (b) Using Sulfuric Acid Support with Silica (SSA) (Experiment 1, 2 and 3 in Table 3.1)

a. **Preparation of the catalyst $H_2SO_4 \cdot SiO_2$.**

To a slurry of silica gel (10 g) in dry diethyl ether (50 mL), concentrated H_2SO_4 (3 mL) was added upon shaking for 5 min. The solvent was evaporated under reduced pressure, and the catalyst was dried at 120°C for 3 h.

b. Synthesis procedure for SSA catalyzed Clauson– Kaas reaction.

To the mixture of SSA (125 mg) with silica gel (875 mg), 2,5-dimethoxytetrahydrofuran (DMTHF) (2 mmol) and *O*-(3-ethylheptyl)hydroxylamine (b) (2 mmol) were added. The mixture was grinded in a glass mortar with a pestle for 30 min, then left at room temperature for 30 minutes (experiment 1), 2 hours (experiment 2) and 12 hours (experiment 3). Progress of the reaction was monitored by TLC. After completion of the reaction, the mixture was dissolved in diethyl ether, then filtrated. The filtrate was dried under vacuum. The corresponding crude product was purified by column chromatography on silica gel with n-hexane and ethyl acetate as eluents.

Synthesis of 1-((2-ethylhexyl)oxy)-1*H*-pyrrole (b) Using Pure Acetic Acid as Solvent and Catalyst

Dimethoxytetrahydrofurane (DMTHF) (1.32 g, 10 mmol, 1 equiv.), *O*-(3-ethylheptyl)hydroxylamine (b) (1.4525, 10 mmol, 1 equiv.) were put into AcOH (7.93 ml) and refluxed (80 ℃) for 45 min. The system was cooled and AcOH was evaporated. Water (30 mL) was added and extracted with petroleum ether (3 *30 mL). The organic layer was washed with water (3 *100 mL), dried over anhydrous sodium sulphate and evaporated. The resulting residue was purified by column chromatography.

Synthesis of 1-((2-ethylhexyl)oxy)-1*H*-pyrrole (b) Using Acetic Acid and Water

Sodium acetate (20 mmol) was dissolved, under stirring, in water (40 mL) at room temperature. To this solution, *O*-(3-ethylheptyl)hydroxylamine (b) (20.6 mmol) was added followed by glacial acetic acid (10 mL). The reaction mixture was heated at 75 ℃ for about 10 minutes followed by addition of 2, 5-dimethoxytetrahydrofuran (DMT) (20.6 mmol) in a

drop wise manner into the vigorously stirred reaction mixture. The reaction mixture was allowed to stir at this temperature (75 ℃) for 1h. After cooling to room temperature, the reaction mixture was extracted with dichloromethane (50 mL), washed with brine, dried with anhydrous sodium sulphate and evaporated under reduced pressure. The crude compound was purified on silica gel using ethyl acetate: hexane as eluent. (12.5%). The desired product could not be fully isolated through column chromatography.

Polymer Synthesis

Synthesis of Poly-1-((2-ethylhexyl)oxy)-1H-pyrrole (d)

1-((2-ethylhexyl)oxy)-1*H*-pyrrole (0.2 g) was dissolved in 10 mL $CHCl_3$. The solution was maintained in an inert N_2 atmosphere and under magnetic stirring. Anhydrous $FeCl_3$ (0.4g) was quickly added to the solution upon stirring. After a polymerization time of 24 h, aqueous ammonia was added to the reaction mixture to de-dope the polymer obtained. The polymer precipitated as a black powder and was then washed with methanol until the filtrate was colourless. Finally, the crude polymer was dried under vacuum environment.

Chapter 5. Summary and Future Directions

In this thesis, two polypyrrole-based polymers were designed and synthesized to explore a way to address polypyrrole's solubility issues without sacrificing its conductivity. The first design was to introduce a thermal removable carbamate sidechain to the N position of the polypyrrole backbone to achieve solubility and by removing the sidechain to achieve good conductivity. The second design was to introduce a low steric hindrance alkoxy sidechain to the N position of the polypyrrole backbone to achieve solubility and higher backbone planarity. As a result, good conductivity was expected.

In Chapter 2, experimental methods, including polymer synthesis and characterization methods, were introduced and discussed. Through critical analysis of different organometallic polycondensation methods, it was found that the Yamamoto polycondensation was the most proper method to synthesize the poly(2-ethylhexyl 1H-pyrrole-1-carboxylate) (PEPC). Oxidative polymerization was also discussed. In addition, the characterization methods used in this project were introduced, including NMR, UV-VIS-NIR, CV FTIR, TGA, and XRD.

In Chapter 3, a solution-processable polypyrrole-based polymer with a thermally removable sidechain, poly(2-ethylhexyl 1H-pyrrole-1-carboxylate) (PEPC), was designed. The synthesis of PEPC through Yamamoto polycondensation was studied. Synthesis of the high molecular weight of PEPC through Yamamoto polycondensation was unsuccessful. The possible reason could be that the carbamate sidechain reacts with the nickel catalyst competing with the bromo atom, and it still remains to be verified. PEPC was synthesized through oxidative polymerization, and the reaction condition was optimized to achieve the best yield. It was found that the 2-ethylhexyl carbamate side could only be ~20% removed when PEPC was annealed at 200 °C for 30 minutes in the air; however, the PPy backbone had already started to decompose under these conditions. Other methods to remove the sidechain were proven to either lead to less removal of the sidechain or more damage to the backbone. As a result, PEPC did not show significant conductivity due to the twisted structure caused by the unremovable sidechain.

In Chapter 4, the solution-processable polypyrrole-based polymer poly[1-((2-ethylhexyl)oxy)-1H-pyrrole] (PEOP) was designed, and the synthetic route of it was explored. Due to the

difficulties of purifying the monomer, we were not able to obtain the desired PEOP. However, it was found that the 2-(ethylhexyl)oxy chain could be removed through thermolysis at a milder temperature compared with the alkyl carbamate chain. At the annealing conditions of 250 ℃ and 30 minutes in air, the sidechain was more than 95% removed based on the FTIR data.

In the future, a carbamate sidechain with a secondary or tertiary structure of aliphatic chain may be introduced to the PPy backbone since it is more easily removed by thermolysis or acid cleavage compared to the 2-ethylhexyl carbamate sidechain, which has a primary aliphatic chain structure. Alternatively, a new synthetic route could be explored to synthesize the pure monomer of PEOP to obtain the desired polymer. The 2-(ethylhexyl)oxy sidechain may also be further explored for its thermally removable property and may be introduced to other conjugated polymers' backbones to achieve solubility and improve conductivity.

Bibliography

(1) Ngai, J. H. L.; Polena, J.; Afzal, D.; Gao, X.; Kapadia, M.; Li, Y. Green Solvent-Processed Hemi-Isoindigo Polymers for Stable Temperature Sensors. *Adv. Funct. Mater.* **2022**, *32* (17), 2110995. https://doi.org/10.1002/adfm.202110995.
(2) Chiang, C. K.; Druy, M. A.; Gau, S. C.; Heeger, A. J.; Louis, E. J.; MacDiarmid, A. G.; Park, Y. W.; Shirakawa, H. Synthesis of Highly Conducting Films of Derivatives of Polyacetylene, (CH)x. **1978**, 3.
(3) Pang, A. L.; Arsad, A.; Ahmadipour, M. Synthesis and Factor Affecting on the Conductivity of Polypyrrole: A Short Review. *Polym. Adv. Technol.* **2021**, *32* (4), 1428–1454. https://doi.org/10.1002/pat.5201.
(4) Mishra, A. K. Conducting Polymers: Concepts and Applications. *J. At. Mol. Condens. Nano Phys.* **2018**, *5* (2), 159–193. https://doi.org/10.26713/jamcnp.v5i2.842.
(5) Le, T.-H.; Kim, Y.; Yoon, H. Electrical and Electrochemical Properties of Conducting Polymers. *Polymers* **2017**, *9* (12), 150. https://doi.org/10.3390/polym9040150.
(6) MacDiarmid, A. G.; Mammone, R. J.; Kaner, R. B.; Porter, Lord; Pethig, R.; Heeger, A. J.; Rosseinsky, D. R.; Gillespie, R. J.; Day, P. The Concept of 'Doping' of Conducting Polymers: The Role of Reduction Potentials. *Philos. Trans. R. Soc. Lond. Ser. Math. Phys. Sci.* **1985**, *314* (1528), 3–15. https://doi.org/10.1098/rsta.1985.0004.
(7) *Handbook of Organic Conductive Molecules and Polymers*; Nalwa, H. S., Ed.; Wiley: Chichester ; New York, 1997.
(8) Street, G. B.; Clarke, T. C.; Geiss, R. H.; Lee, V. Y.; Nazzal, A.; Pfluger, P.; Scott, J. C. CHARACTERIZATION OF POLYPYRROLE. *J. Phys. Colloq.* **1983**, *44* (C3), C3-599-C3-606. https://doi.org/10.1051/jphyscol:19833120.
(9) Lanzani, G. Organic Electronics Meets Biology. *Nat. Mater.* **2014**, *13* (8), 775–776. https://doi.org/10.1038/nmat4021.
(10) Kim, D.-H.; Abidian, M.; Martin, D. C. Conducting Polymers Grown in Hydrogel Scaffolds Coated on Neural Prosthetic Devices. *J. Biomed. Mater. Res. A* **2004**, *71A* (4), 577–585. https://doi.org/10.1002/jbm.a.30124.
(11) Fontana, M. T.; Stanfield, D. A.; Scholes, D. T.; Winchell, K. J.; Tolbert, S. H.; Schwartz, B. J. Evaporation vs Solution Sequential Doping of Conjugated Polymers: F $_4$ TCNQ Doping of Micrometer-Thick P3HT Films for Thermoelectrics. *J. Phys. Chem. C* **2019**, *123* (37), 22711–22724. https://doi.org/10.1021/acs.jpcc.9b05069.
(12) Sasso, C.; Beneventi, D.; Zeno, E.; Chaussy, D.; Petit-Conil, M.; Belgacem, N. Polypyrrole and Polypyrrole/Wood-Derived Materials Conducting Composites: A Review. *BioResources* **2011**, *6* ((3)).
(13) Wang, N.; Yang, A.; Fu, Y.; Li, Y.; Yan, F. Functionalized Organic Thin Film Transistors for Biosensing. *Acc. Chem. Res.* **2019**, *52* (2), 277–287. https://doi.org/10.1021/acs.accounts.8b00448.
(14) John, J.; Saheeda, P.; Sabeera, K.; Jayalekshmi, S. Doped Polypyrrole with Good Solubility and Film Forming Properties Suitable for Device Applications. *Mater. Today Proc.* **2018**, *5* (10), 21140–21146. https://doi.org/10.1016/j.matpr.2018.06.512.

(15) Lee, J. Y.; Song, K. T.; Kim, S. Y.; Kim, Y. C.; Kim, D. Y.; Kim, C. Y. Synthesis and Characterization of Soluble Polypyrrole. *Synth. Met.* **1997**, *84* (1), 137–140. https://doi.org/10.1016/S0379-6779(97)80683-2.
(16) Song, K. T.; Lee, J. Y.; Kim, H. D.; Kim, D. Y.; Kim, S. Y.; Kim, C. Y. Solvent Effects on the Characteristics of Soluble Polypyrrole. *Synth. Met.* **2000**, *110* (1), 57–63. https://doi.org/10.1016/S0379-6779(99)00267-2.
(17) Oh, E. J.; Jang, K. S.; MacDiarmid, A. G. High Molecular Weight Soluble Polypyrrole. *Synth. Met.* **2001**, *125* (3), 267–272. https://doi.org/10.1016/S0379-6779(01)00384-8.
(18) Lim, H. K.; Lee, S. O.; Song, K. J.; Kim, S. G.; Kim, K. H. Synthesis and Properties of Soluble Polypyrrole Doped with Dodecylbenzenesulfonate and Combined with Polymeric Additive Poly(Ethylene Glycol). *J. Appl. Polym. Sci.* **2005**, *97* (3), 1170–1175. https://doi.org/10.1002/app.21824.
(19) Lee, G. J.; Lee, S. H.; Ahn, K. S.; Kim, K. H. Synthesis and Characterization of Soluble Polypyrrole with Improved Electrical Conductivity. *J. Appl. Polym. Sci.* **2002**, *84* (14), 2583–2590. https://doi.org/10.1002/app.10281.
(20) John, J.; Saheeda, P.; Sabeera, K.; Jayalekshmi, S. Doped Polypyrrole with Good Solubility and Film Forming Properties Suitable for Device Applications. *Mater. Today Proc.* **2018**, *5* (10, Part 1), 21140–21146. https://doi.org/10.1016/j.matpr.2018.06.512.
(21) Kou, C.-T.; Liou, T.-R. Characterization of Metal—Oxide—Semiconductor Field-Effect Transistor (MOSFET) for Polypyrrole and Poly (N-Alkylpyrrole)s Prepared by Electrochemical Synthesis. *Synth. Met.* **1996**, *82* (3), 167–173. https://doi.org/10.1016/S0379-6779(96)03773-3.
(22) Aradilla, D.; Estrany, F.; Armelin, E.; Oliver, R.; Iribarren, J. I.; Alemán, C. Characterization and Properties of Poly[N-(2-Cyanoethyl)Pyrrole]. *Macromol. Chem. Phys.* **2010**, *211* (15), 1663–1672. https://doi.org/10.1002/macp.201000015.
(23) Massoumi, B.; Isfahani, N. S.; Saraei, M.; Entezami, A. Investigation of the Electroactivity, Conductivity, and Morphology of Poly(Pyrrole-Co-N-Alkyl Pyrrole) Prepared via Electrochemical Nanopolymerization and Chemical Polymerization. *J. Appl. Polym. Sci.* **2012**, *124* (5), 3956–3962. https://doi.org/10.1002/app.33649.
(24) Reynolds, J. R.; Poropatic, P. A.; Toyooka, R. L. Electrochemical Copolymerization of Pyrrole with N-Substituted Pyrroles. Effect of Composition on Electrical Conductivity. *Macromolecules* **1987**, *20* (5), 958–961. https://doi.org/10.1021/ma00171a011.
(25) Jarosz, T.; Ledwon, P. Electrochemically Produced Copolymers of Pyrrole and Its Derivatives: A Plentitude of Material Properties Using “Simple” Heterocyclic Co-Monomers. *Materials* **2021**, *14* (2), 281. https://doi.org/10.3390/ma14020281.
(26) Foitzik, R. C.; Kaynak, A.; Beckmann, J.; Pfeffer, F. M. Soluble Poly-3-Alkylpyrrole Polymers on Films and Fabrics. *Synth. Met.* **2005**, *155* (1), 185–190. https://doi.org/10.1016/j.synthmet.2005.08.001.
(27) Zotti, G.; Zecchin, S.; Schiavon, G.; Vercelli, B.; Berlin, A.; Dalcanale, E.; Groenendaal, L. “Bert.” Potential-Driven Conductivity of Polypyrroles, Poly- *N* -Alkylpyrroles, and Polythiophenes: Role of the Pyrrole NH Moiety in the Doping-

Charge Dependence of Conductivity. *Chem. Mater.* **2003**, *15* (24), 4642–4650. https://doi.org/10.1021/cm030336i.
(28) Ponder, J. F.; Gregory, S. A.; Atassi, A.; Menon, A. K.; Lang, A. W.; Savagian, L. R.; Reynolds, J. R.; Yee, S. K. Significant Enhancement of the Electrical Conductivity of Conjugated Polymers by Post-Processing Side Chain Removal. *J. Am. Chem. Soc.* **2022**, *144* (3), 1351–1360. https://doi.org/10.1021/jacs.1c11558.
(29) Kanazawa, K. K.; Diaz, A. F.; Krounbi, M. T.; Street, G. B. Electrical Properties of Pyrrole and Its Copolymers. *Synth. Met.* **1981**, *4* (2), 119–130. https://doi.org/10.1016/0379-6779(81)90027-8.
(30) Kocienski, P. J. *Protecting Groups*, 3rd Edition.; Thieme: Germany, 2004.
(31) Groenendaal, L. *The Chemistry of Oligopyrroles: Design, Synthesis and Characterization of Well-Defined and Functional α,α-Linked Oligomers*; 1996.
(32) Ngai, J. H. L.; Gao, X.; Kumar, P.; Polena, J.; Li, Y. A Highly Stable Diketopyrrolopyrrole (DPP) Polymer for Chemiresistive Sensors. *Adv. Electron. Mater.* **2021**, *7* (3), 2000935. https://doi.org/10.1002/aelm.202000935.
(33) Polena, J. Hemi-Isoindigo Polymers and Oligomers for Temperature Sensing Applications. Master Thesis, University of Waterloo, 2022.
(34) He, K.; Kumar, P.; Abd-Ellah, M.; Liu, H.; Li, X.; Zhang, Z.; Wang, J.; Li, Y. Alkyloxime Side Chain Enabled Polythiophene Donors for Efficient Organic Solar Cells. *Macromolecules* **2020**, *53* (20), 8796–8808. https://doi.org/10.1021/acs.macromol.0c01548.
(35) He, K.; Kumar, P.; Yuan, Y.; Zhang, Z.; Li, X.; Liu, H.; Wang, J.; Li, Y. A Wide Bandgap Polymer Donor Composed of Benzodithiophene and Oxime-Substituted Thiophene for High-Performance Organic Solar Cells. *ACS Appl. Mater. Interfaces* **2021**, *13* (22), 26441–26450. https://doi.org/10.1021/acsami.1c02442.
(36) He, Y.; Li, X.; Liu, H.; Meng, H.; Wang, G. Y.; Cui, B.; Wang, J.; Li, Y. A New N-Type Polymer Based on *N* , *N* ′-Dialkoxynaphthalenediimide (NDIO) for Organic Thin-Film Transistors and All-Polymer Solar Cells. *J. Mater. Chem. C* **2018**, *6* (6), 1349–1352. https://doi.org/10.1039/C7TC05145J.
(37) Jiang, Y.; Liu, H.; Li, X.; Yuan, Y.; Wang, J.; Cui, B.; Li, Y. Alkyloxime-Substituted Thiophene-Based Wide-Band-Gap Polymer Donor Achieving a High Short Circuit Current Density of 30 MA Cm–2 in Organic Solar Cells. *Chem. Mater.* **2022**, *34* (9), 4232–4241. https://doi.org/10.1021/acs.chemmater.2c00929.
(38) Yamamoto, T.; Koizumi, T. Synthesis of π-Conjugated Polymers Bearing Electronic and Optical Functionalities by Organometallic Polycondensations and Their Chemical Properties. *Polymer* **2007**, *48* (19), 5449–5472. https://doi.org/10.1016/j.polymer.2007.07.051.
(39) R. Murad, A.; Iraqi, A.; Aziz, S. B.; N. Abdullah, S.; Brza, M. A. Conducting Polymers for Optoelectronic Devices and Organic Solar Cells: A Review. *Polymers* **2020**, *12* (11), 2627. https://doi.org/10.3390/polym12112627.
(40) Yamamoto, T. π-Conjugated Polymers with Electronic and Optical Functionalities: Preparation by Organometallic Polycondensation, Properties, and Applications. *Macromol. Rapid Commun.* **2002**, *23* (10–11), 583.

https://doi.org/10.1002/1521-3927(20020701)23:10/11<583::AID-MARC583>3.0.CO;2-I.
(41) Street, G. B.; Clarke, T. C.; Geiss, R. H.; Lee, V. Y.; Nazzal, A.; Pfluger, P.; Scott, J. C. CHARACTERIZATION OF POLYPYRROLE. *J. Phys. Colloq.* **1983**, *44* (C3), C3-599-C3-606. https://doi.org/10.1051/jphyscol:19833120.
(42) Kumada, M. Nickel and Palladium Complex Catalyzed Cross-Coupling Reactions of Organometallic Reagents with Organic Halides. *Pure Appl. Chem.* **1980**, *52* (3), 669–679. https://doi.org/10.1351/pac198052030669.
(43) Tamao, K.; Kodama, S.; Nakajima, I.; Kumada, M.; Minato, A.; Suzuki, K. Nickel-Phosphine Complex-Catalyzed Grignard Coupling—II: Grignard Coupling of Heterocyclic Compounds. *Tetrahedron* **1982**, *38* (22), 3347–3354. https://doi.org/10.1016/0040-4020(82)80117-8.
(44) Heravi, M. M.; Zadsirjan, V.; Hajiabbasi, P.; Hamidi, H. Advances in Kumada–Tamao–Corriu Cross-Coupling Reaction: An Update. *Monatshefte Für Chem. - Chem. Mon.* **2019**, *150* (4), 535–591. https://doi.org/10.1007/s00706-019-2364-6.
(45) Tamao, K.; Sumitani, K.; Kumada, M. Selective Carbon-Carbon Bond Formation by Cross-Coupling of Grignard Reagents with Organic Halides. Catalysis by Nickel-Phosphine Complexes. *J. Am. Chem. Soc.* **1972**, *94* (12), 4374–4376. https://doi.org/10.1021/ja00767a075.
(46) Jana, R.; Pathak, T. P.; Sigman, M. S. Advances in Transition Metal (Pd,Ni,Fe)-Catalyzed Cross-Coupling Reactions Using Alkyl-Organometallics as Reaction Partners. *Chem. Rev.* **2011**, *111* (3), 1417–1492. https://doi.org/10.1021/cr100327p.
(47) Yokoyama, A.; Kato, A.; Miyakoshi, R.; Yokozawa, T. Precision Synthesis of Poly(N-Hexylpyrrole) and Its Diblock Copolymer with Poly(p-Phenylene) via Catalyst-Transfer Polycondensation. *Macromolecules* **2008**, *41* (20), 7271–7273. https://doi.org/10.1021/ma8017124.
(48) Stefan, M. C.; Javier, A. E.; Osaka, I.; McCullough, R. D. Grignard Metathesis Method (GRIM): Toward a Universal Method for the Synthesis of Conjugated Polymers. *Macromolecules* **2009**, *42* (1), 30–32. https://doi.org/10.1021/ma8020823.
(49) Bulumulla, C.; Gunawardhana, R.; Gamage, P. L.; Miller, J. T.; Kularatne, R. N.; Biewer, M. C.; Stefan, M. C. Pyrrole-Containing Semiconducting Materials: Synthesis and Applications in Organic Photovoltaics and Organic Field-Effect Transistors. *ACS Appl. Mater. Interfaces* **2020**, *12* (29), 32209–32232. https://doi.org/10.1021/acsami.0c07161.
(50) Krasovskiy, A.; Knochel, P. A LiCl-Mediated Br/Mg Exchange Reaction for the Preparation of Functionalized Aryl- and Heteroarylmagnesium Compounds from Organic Bromides. *Angew. Chem. Int. Ed.* **2004**, *43* (25), 3333–3336. https://doi.org/10.1002/anie.200454084.
(51) Negishi, E. Palladium- or Nickel-Catalyzed Cross Coupling. A New Selective Method for Carbon-Carbon Bond Formation. *Acc. Chem. Res.* **1982**, *15* (11), 340–348. https://doi.org/10.1021/ar00083a001.
(52) Geoghegan, M.; Hadziioannou, G. *Polymer Electronics*, First edition.; Oxford master series in physics; Oxford University Press: Oxford, 2013.

(53) Wardell, J. L. Chapter 12. Organometallic Chemistry. Part (Ii) Main-Group Elements. *Annu. Rep. Sect. B Org. Chem.* **1981**, *78* (0), 281–298. https://doi.org/10.1039/OC9817800281.
(54) Zheng, T.; Schneider, A. M.; Yu, L. Stille Polycondensation: A Versatile Synthetic Approach to Functional Polymers. In *Synthetic Methods for Conjugated Polymers and Carbon Materials*; Leclerc, M., Morin, J.-F., Eds.; Wiley-VCH Verlag GmbH & Co. KGaA: Weinheim, Germany, 2017; pp 1–58. https://doi.org/10.1002/9783527695959.ch1.
(55) Azarian, D.; Dua, S. S.; Eaborn, C.; Walton, D. R. M. Reactions of Organic Halides with R3 MMR3 Compounds (M = Si, Ge, Sn) in the Presence of Tetrakis(Triarylphosphine)Palladium. *J. Organomet. Chem.* **1976**, *117* (3), C55–C57. https://doi.org/10.1016/S0022-328X(00)91902-8.
(56) Kosugi, M.; Shimizu, Y.; Migita, T. Reaction of Allyltin Compounds: II. Facile Preparation of Allyl Ketones via Allyltins. *J. Organomet. Chem.* **1977**, *129* (2), C36–C38. https://doi.org/10.1016/S0022-328X(00)92505-1.
(57) Milstein, D.; Stille, J. K. A General, Selective, and Facile Method for Ketone Synthesis from Acid Chlorides and Organotin Compounds Catalyzed by Palladium. *J. Am. Chem. Soc.* **1978**, 3.
(58) Milstein, D.; Stille, J. K. Palladium-Catalyzed Coupling of Tetraorganotin Compounds with Aryl and Benzyl Halides. Synthetic Utility and Mechanism. *J. Am. Chem. Soc.* **1979**, *101* (17), 4992–4998. https://doi.org/10.1021/ja00511a032.
(59) Stille, J. K. The Palladium-Catalyzed Cross-Coupling Reactions of Organotin Reagents with Organic Electrophiles [New Synthetic Methods (58)]. *Angew. Chem. Int. Ed. Engl.* **1986**, *25* (6), 508–524. https://doi.org/10.1002/anie.198605081.
(60) Espinet, P.; Echavarren, A. M. The Mechanisms of the Stille Reaction. *Angew. Chem. Int. Ed.* **2004**, *43* (36), 4704–4734. https://doi.org/10.1002/anie.200300638.
(61) L. Casado, A.; Espinet, P.; M. Gallego, A.; M. Martínez-Ilarduya, J. Snapshots of a Stille Reaction. *Chem. Commun.* **2001**, *0* (4), 339–340. https://doi.org/10.1039/B008811K.
(62) Nova, A.; Ujaque, G.; Maseras, F.; Lledós, A.; Espinet, P. A Critical Analysis of the Cyclic and Open Alternatives of the Transmetalation Step in the Stille Cross-Coupling Reaction. *J. Am. Chem. Soc.* **2006**, *128* (45), 14571–14578. https://doi.org/10.1021/ja0635736.
(63) Casado, A. L.; Espinet, P.; Gallego, A. M. Mechanism of the Stille Reaction. 2. Couplings of Aryl Triflates with Vinyltributyltin. Observation of Intermediates. A More Comprehensive Scheme. *J. Am. Chem. Soc.* **2000**, *122* (48), 11771–11782. https://doi.org/10.1021/ja001511o.
(64) Schlüter, A.-D.; Wegner, G. Palladium and Nickel Catalyzed Polycondensation - The Key to Structurally Defined Polyarylenes and Other Aromatic Polymers. *Acta Polym.* **1993**, *44* (2), 59–69. https://doi.org/10.1002/actp.1993.010440201.
(65) Kang, S.-K.; Namkoong, E.-Y.; Yamaguchi, T. Palladium-Catalyzed Homocoupling of Organostannanes. *Synth. Commun.* **1997**, *27* (4), 641–646. https://doi.org/10.1080/00397919708003337.

(66) Suzuki, A. Recent Advances in the Cross-Coupling Reactions of Organoboron Derivatives with Organic Electrophiles, 1995–1998. *J. Organomet. Chem.* **1999**, *576* (1–2), 147–168. https://doi.org/10.1016/S0022-328X(98)01055-9.
(67) Schlüter, A. D. The Tenth Anniversary of Suzuki Polycondensation (SPC). *J. Polym. Sci. Part Polym. Chem.* **2001**, *39* (10), 1533–1556. https://doi.org/10.1002/pola.1130.
(68) Martina, S.; Enkfjj, V.; Schlüter, A. D.; Wegner, G. Polypyrrole: Towards the Development of a Chemical Synthesis. *Synth. Met.* **1991**, *41* ((1-2)), 403–406.
(69) Asakura, H.; Shishido, T.; Tanaka, T. In Situ Time-Resolved XAFS Study of the Reaction Mechanism of Bromobenzene Homocoupling Mediated by [Ni(Cod)(Bpy)]. *J. Phys. Chem. A* **2012**, *116* (16), 4029–4034. https://doi.org/10.1021/jp211627v.
(70) Kanbara, T.; Kushida, T.; Saito, N.; Kuwajima, I.; Kubota, K.; Yamamoto, T. Preparation and Properties of Highly Electron-Accepting Poly(Pyrimidine-2,5-Diyl). *Chem. Lett.* **1992**, *21* ((4)), 583–586. https://doi.org/10.1246/cl.1992.583.
(71) Yamamoto, T.; Yamamoto, A. A Novel Type of Polycondensation of Polyhalogenated Organic Aromatic Compounds Producing Thermostable Polyphenylene Type Polymers Promoted by Nickel Complexes. *Chem. Lett.* **1977**, *6* ((4)), 353–356. https://doi.org/10.1246/cl.1977.353.
(72) Yamamoto, T.; Maruyama, T.; Zhou, Z.-H.; Ito, T.; Fukuda, T.; Yoneda, Y.; Begum, F.; Ikeda, T.; Sasaki, S. ..Pi.-Conjugated Poly(Pyridine-2,5-Diyl), Poly(2,2'-Bipyridine-5,5'-Diyl), and Their Alkyl Derivatives. Preparation, Linear Structure, Function as a Ligand to Form Their Transition Metal Complexes, Catalytic Reactions, n-Type Electrically Conducting Properties, Optical Properties, and Alignment on Substrates. *J. Am. Chem. Soc.* **1994**, *116* (11), 4832–4845. https://doi.org/10.1021/ja00090a031.
(73) Yamamoto, T.; Hayashi, Y.; Yamamoto, A. A Novel Type of Polycondensation Utilizing Transition Metal-Catalyzed C–C Coupling. I. Preparation of Thermostable Polyphenylene Type Polymers. *Bull. Chem. Soc. Jpn.* **1978**, *51* ((7)), 2091–2097. https://doi.org/10.1246/bcsj.51.2091.
(74) Yamamoto, T.; Ito, T.; Kubota, K. A Soluble Poly(Arylene) with Large Degree of Depolarization. Poly(2,5-Pyridinediyl) Prepared by Dehalogenation Polycondensation of 2,5-Dibromopyridine with Ni(0)-Complexes. *Chem. Lett.* **1988**, *17* ((1)), 153–154. https://doi.org/10.1246/cl.1988.153.
(75) Yamamoto, T.; Zhou, Z.; Ando, I.; Kikuchi, M. Preparation of Polypyrrole by Dehalogenation Polycondensation of 2,5-Dibromopyrrole with a Zero-Valent Nickel Complex, and IR and Solid-State 13C NMR Spectra of the Polymer. *Makromol. Chem. Rapid Commun.* **1993**, *14* (12), 833–839. https://doi.org/10.1002/marc.1993.030141216.
(76) Yamamoto, T.; Yoshizawa, M.; Mahmut, A.; Abe, M.; Kuroda, S.; Imase, T.; Sasaki, S. Preparation of New π-Conjugated Polypyrroles by Organometallic Polycondensations. Synthesis OfN-BOC (t-Butoxycarbonyl) AndN-Phenylethynyl Polymers, Thermal Deprotection of the BOC Group, and Packing Structure of TheN-Phenylethynyl Polymer. *J. Polym. Sci. Part Polym. Chem.* **2005**, *43* (24), 6223–6232. https://doi.org/10.1002/pola.21080.

(77) Pang, A. L.; Arsad, A.; Ahmadipour, M. Synthesis and Factor Affecting on the Conductivity of Polypyrrole: A Short Review. *Polym. Adv. Technol.* **2021**, *32* (4), 1428–1454. https://doi.org/10.1002/pat.5201.
(78) Posudievsky, O. Yu.; Kozarenko, O. A. Effect of Monomer/Oxidant Mole Ratio on Polymerization Mechanism, Conductivity and Spectral Characteristics of Mechanochemically Prepared Polypyrrole. *Polym Chem* **2011**, *2* (1), 216–220. https://doi.org/10.1039/C0PY00212G.
(79) Tan, Y.; Ghandi, K. Kinetics and Mechanism of Pyrrole Chemical Polymerization. *Synth. Met.* **2013**, *175*, 183–191. https://doi.org/10.1016/j.synthmet.2013.05.014.
(80) Zia, K.; Siddiqui, T.; Ali, S.; Farooq, I.; Zafar, M. S.; Khurshid, Z. Nuclear Magnetic Resonance Spectroscopy for Medical and Dental Applications: A Comprehensive Review. *Eur. J. Dent.* **2019**, *13* (1), 124–128. https://doi.org/10.1055/s-0039-1688654.
(81) Costa, J. C. S.; Taveira, R. J. S.; Lima, C. F. R. A. C.; Mendes, A.; Santos, L. M. N. B. F. Optical Band Gaps of Organic Semiconductor Materials. *Opt. Mater.* **2016**, *58*, 51–60. https://doi.org/10.1016/j.optmat.2016.03.041.
(82) Leonat, L.; Sbârcea, G.; Brânzoi, I. V. Cyclic Voltammetry for Energy Levels Estimation of Organic Materials. *UPB Sci Bull Ser B* **2013**, *75* ((3)), 111–118.
(83) Mohamed, M. A.; Jaafar, J.; Ismail, A. F.; Othman, M. H. D.; Rahman, M. A. Chapter 1 - Fourier Transform Infrared (FTIR) Spectroscopy. In *Membrane Characterization*; Hilal, N., Ismail, A. F., Matsuura, T., Oatley-Radcliffe, D., Eds.; Elsevier, 2017; pp 3–29. https://doi.org/10.1016/B978-0-444-63776-5.00001-2.
(84) Ng, H. M.; Saidi, N. M.; Omar, F. S.; Ramesh, K.; Ramesh, S.; Bashir, S. Thermogravimetric Analysis of Polymers. In *Encyclopedia of Polymer Science and Technology*; John Wiley & Sons, Ltd, 2018; pp 1–29. https://doi.org/10.1002/0471440264.pst667.
(85) Sherman, R. Chapter 3 - Carbon Dioxide Snow Cleaning Applications. In *Developments in Surface Contamination and Cleaning: Applications of Cleaning Techniques*; Kohli, R., Mittal, K. L., Eds.; Elsevier, 2019; pp 97–115. https://doi.org/10.1016/B978-0-12-815577-6.00003-7.
(86) Gilow, H. M.; Burton, D. E. Bromination and Chlorination of Pyrrole and Some Reactive 1-Substituted Pyrroles. *J. Org. Chem.* **1981**, *46* (11), 2221–2225. https://doi.org/10.1021/jo00324a005.
(87) Yamamoto, T.; Ishizu, J.; Kohara, T.; Komiya, S.; Yamamoto, A. Oxidative Addition of Aryl Carboxylates to Nickel(0) Complexes Involving Cleavage of the Acyl-Oxygen Bond. *J. Am. Chem. Soc.* **1980**, *102* (11), 3758–3764. https://doi.org/10.1021/ja00531a016.
(88) Ishizu, J.; Yamamoto, T.; Yamamoto, A. Selective Cleavage of c–o Bonds in Esters through Oxidative Addition to Nickel(0) Complexes. *Chem. Lett.* **1976**, *5* (10), 1091–1094. https://doi.org/10.1246/cl.1976.1091.
(89) Yamamoto, T.; Kohara, T.; Yamamoto, A. Preparation and Properties of Monoalkylnickel(II) Complexes NiR(NR1R2)L2 Having Imido, Imidazolato, or

Methyl Phenylcarbamato-N Ligand. *Bull. Chem. Soc. Jpn.* **1981**, *54* (6), 1720–1726. https://doi.org/10.1246/bcsj.54.1720.
(90) Yamamoto, T.; Yoshizawa, M.; Mahmut, A.; Abe, M.; Kuroda, S.; Imase, T.; Sasaki, S. Preparation of New π-Conjugated Polypyrroles by Organometallic Polycondensations. Synthesis OfN-BOC (t-Butoxycarbonyl) AndN-Phenylethynyl Polymers, Thermal Deprotection of the BOC Group, and Packing Structure of TheN-Phenylethynyl Polymer. *J. Polym. Sci. Part Polym. Chem.* **2005**, *43* (24), 6223–6232. https://doi.org/10.1002/pola.21080.
(91) FMC Corporation; CEFIC Persulfates Working Group. *Persulfates*; U.S. Environmental Protection Agency: Washington, 2005.
(92) Stanke, D.; Hallensleben, M. L.; Toppare, L. Oxidative Polymerization of Some N-Alkylpyrroles with Ferric Chloride. *Synth. Met.* **1995**, *73* (3), 267–272. https://doi.org/10.1016/0379-6779(95)80025-5.
(93) Gursoy, S. S.; Uygun (GOK), A.; Tilki, T. Synthesis and Characterization of Some N-Substituted Polypyrrole Derivatives: Towards Glucose Sensing Electrodes. *J. Macromol. Sci. Part A* **2010**, *47* (7), 681–688. https://doi.org/10.1080/10601325.2010.483376.
(94) Niemi, V. M.; Knuuttila, P.; Österholm, J.-E.; Korvola, J. Polymerization of 3-Alkylthiophenes with FeCl3. *Polymer* **1992**, *33* (7), 1559–1562. https://doi.org/10.1016/0032-3861(92)90138-M.
(95) Guenadil, F. FeCl3-DMF Complex as Efficient Catalyst for the Synthesis of 6-Acyl-2(3H)-Benzoxazolones and 6-Acyl-2(3H)-Benzothiazolones. *Bull. Chem. Soc. Ethiop.* **2019**, *33* (3), 579. https://doi.org/10.4314/bcse.v33i3.18.
(96) Jakab, E.; Mészáros, E.; Omastová, M. Thermal Decomposition of Polypyrroles. *J. Therm. Anal. Calorim.* **2007**, *88* (2), 515–521. https://doi.org/10.1007/s10973-006-8241-7.
(97) Uyar, T.; Toppare, L.; Hacaloğlu, J. Characterization of Electrochemically Synthesized P-Toluene Sulfonic Acid Doped Polypyrrole by Direct Insertion Probe Pyrolysis Mass Spectrometry. *J. Anal. Appl. Pyrolysis* **2002**, *64* (1), 1–13. https://doi.org/10.1016/S0165-2370(01)00166-8.
(98) Fabrication of a Novel Flexible Room Temperature Hydrogen Sulfide (H2S) Gas Sensor Based on Polypyrrole Films. *Int. J. Sci. Res. IJSR* **2016**, *5* (3), 106–111. https://doi.org/10.21275/v5i3.NOV161786.
(99) Cui, Z.; Coletta, C.; Dazzi, A.; Lefrançois, P.; Gervais, M.; Néron, S.; Remita, S. Radiolytic Method as a Novel Approach for the Synthesis of Nanostructured Conducting Polypyrrole. *Langmuir* **2014**, *30* (46), 14086–14094. https://doi.org/10.1021/la5037844.
(100) Fu, Y.; Su, Y.-S.; Manthiram, A. Sulfur-Polypyrrole Composite Cathodes for Lithium-Sulfur Batteries. *J. Electrochem. Soc.* **2012**, *159* (9), A1420–A1424. https://doi.org/10.1149/2.027209jes.
(101) Yussuf, A.; Al-Saleh, M.; Al-Enezi, S.; Abraham, G. Synthesis and Characterization of Conductive Polypyrrole: The Influence of the Oxidants and Monomer on the Electrical, Thermal, and Morphological Properties. *Int. J. Polym. Sci.* **2018**, *2018*, 1–8. https://doi.org/10.1155/2018/4191747.

(102) Chougule, M. A.; Pawar, S. G.; Godse, P. R.; Mulik, R. N.; Sen, S.; Patil, V. B. Synthesis and Characterization of Polypyrrole (PPy) Thin Films. *Soft Nanosci. Lett.* **2011**, *01* (01), 6–10. https://doi.org/10.4236/snl.2011.11002.
(103) Ahmad, Z.; Choudhary, M. A.; Mehmood, A.; Wakeel, R.; Akhtar, T.; Rafiq, M. A. Synthesis of Polypyrrole Nano/Microspheres Using Cobalt(III) as an Oxidizing Agent and Its Ammonia Sensing Behavior. *Macromol. Res.* **2016**, *24* (7), 596–601. https://doi.org/10.1007/s13233-016-4081-x.
(104) Kostić, R.; Raković, D.; Stepanyan, S. A.; Davidova, I. E.; Gribov, L. A. Vibrational Spectroscopy of Polypyrrole, Theoretical Study. *J. Chem. Phys.* **1995**, *102* (8), 3104–3109. https://doi.org/10.1063/1.468620.
(105) Ju, M.; Gong, F.; Cheng, S.; Gao, Y. Fast and Convenient Synthesis of Amine-Terminated Polylactide as a Macroinitiator for ω -Benzyloxycarbonyl-L-Lysine- *N* -Carboxyanhydrides. *Int. J. Polym. Sci.* **2011**, *2011*, 1–7. https://doi.org/10.1155/2011/381076.
(106) Pommerehne, J.; Vestweber, H.; Guss, W.; Mahrt, R. F.; Bässler, H.; Porsch, M.; Daub, J. Efficient Two Layer Leds on a Polymer Blend Basis. *Adv. Mater.* **1995**, *7* (6), 551–554. https://doi.org/10.1002/adma.19950070608.
(107) Miliaieva, D.; Matunova, P.; Cermak, J.; Stehlik, S.; Cernescu, A.; Remes, Z.; Stenclova, P.; Muller, M.; Rezek, B. Nanodiamond Surface Chemistry Controls Assembly of Polypyrrole and Generation of Photovoltage. *Sci. Rep.* **2021**, *11* (1), 590. https://doi.org/10.1038/s41598-020-80438-3.
(108) Toufik, H.; Bouzzine, S. M.; Ninis, O.; Lamchouri, F.; Aberkane, M.; Hamidi, M.; Bouachrine, M. Opto-Electronic Properties and Molecular Design of New Materials Based on Pyrrole Studied by DFT. *Res. Chem. Intermed.* **2012**, *38* (7), 1375–1388. https://doi.org/10.1007/s11164-011-0469-6.
(109) Kostić, R.; Raković, D.; Stepanyan, S. A.; Davidova, I. E.; Gribov, L. A. Vibrational Spectroscopy of Polypyrrole, Theoretical Study. *J. Chem. Phys.* **1995**, *102* (8), 3104–3109. https://doi.org/10.1063/1.468620.

Appendix A

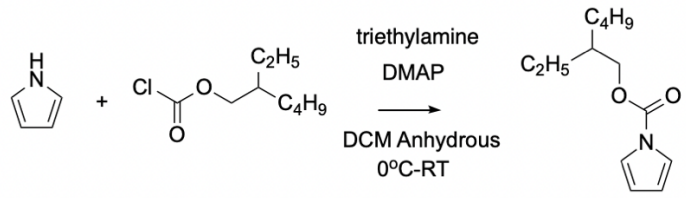

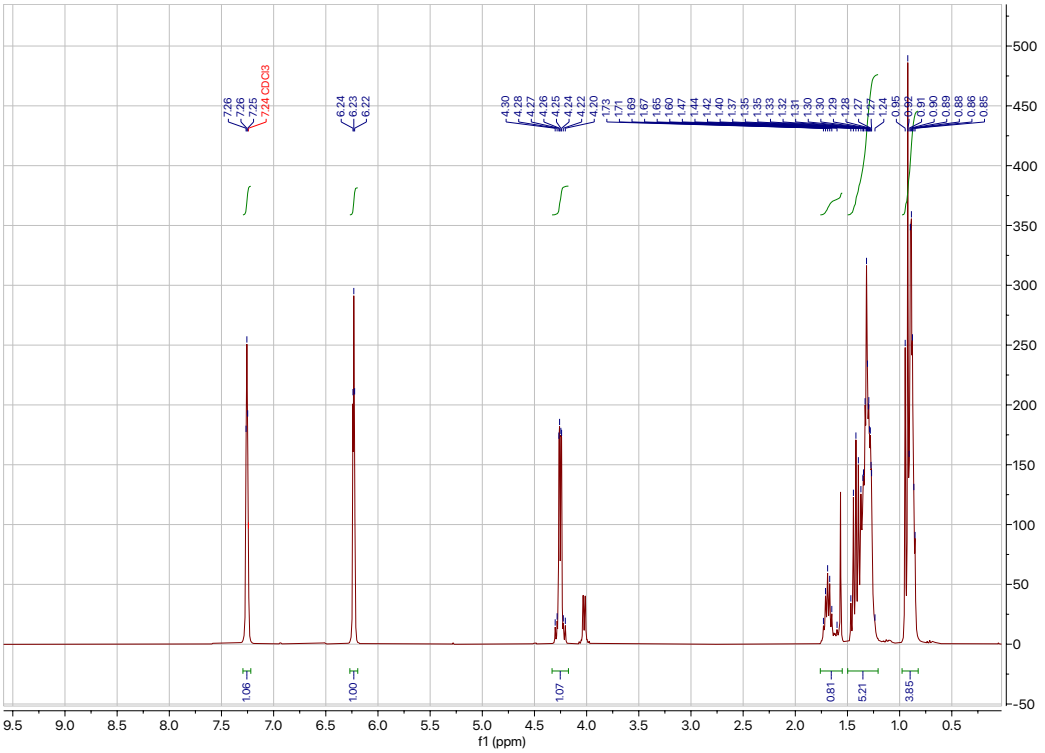

Appendix A-1: ^{1}H NMR Spectrum for the **2-ethylhexyl 1*H*-pyrrole-1-carboxylate** in chloroform-d

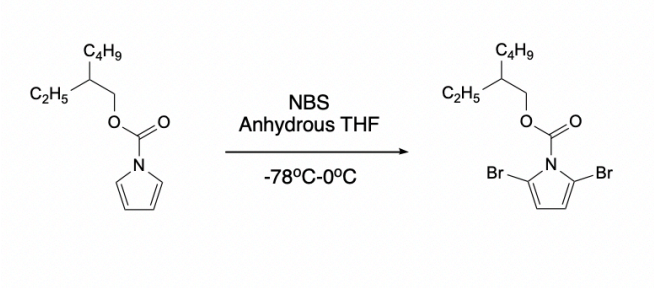

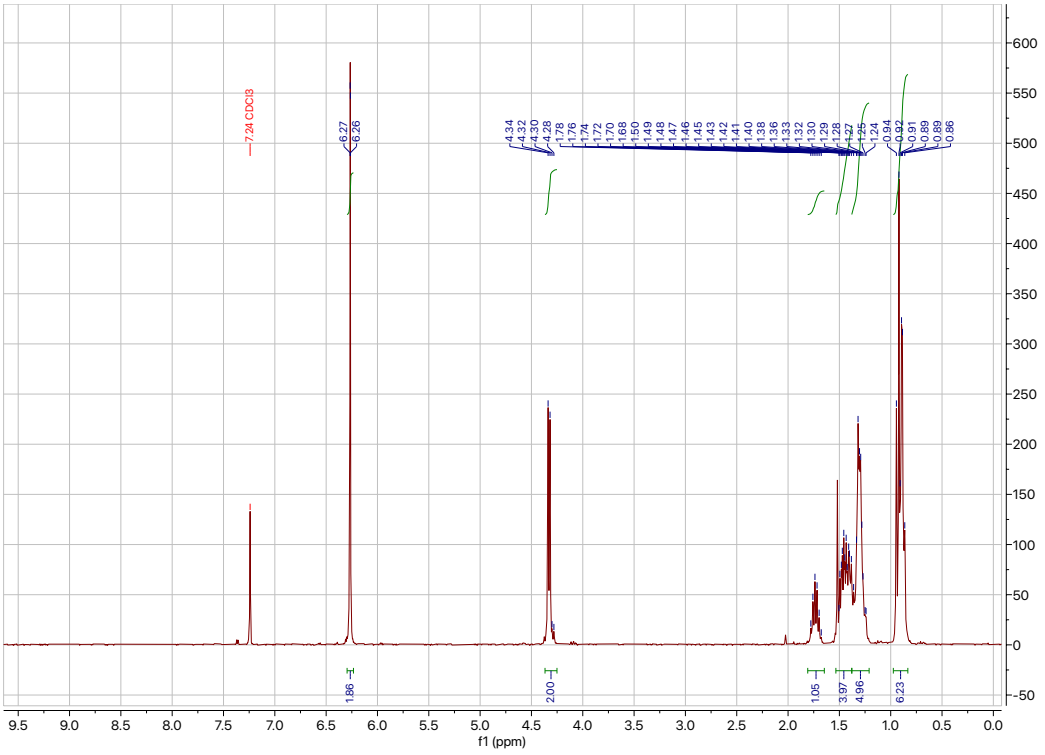

Appendix A-2: ^{1}H NMR Spectrum for the **2-ethylhexyl 2,5-dibromo-1H-pyrrole-1-carboxylate** in chloroform-d

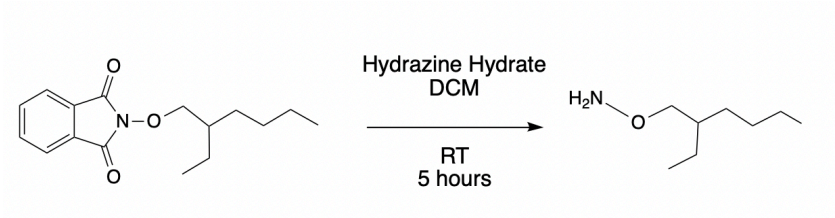

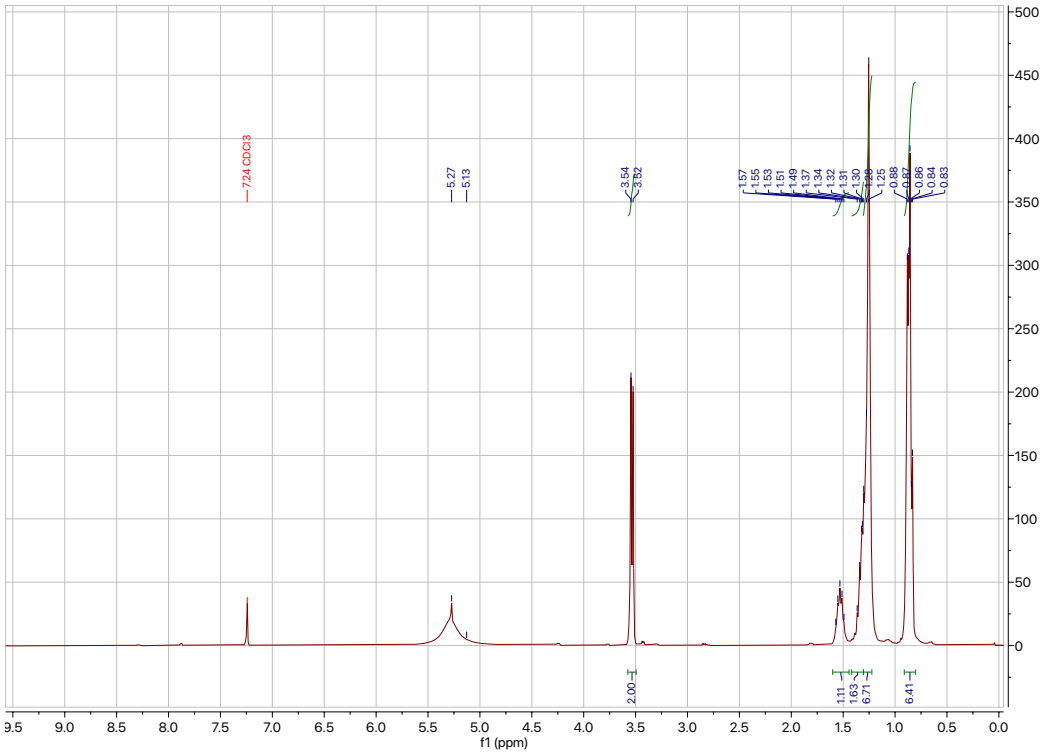

Appendix A-3: ^{1}H NMR Spectrum for the ***O*-(3-ethylheptyl)hydroxylamine** in chloroform-d